C-BAND POLARIMETRIC RADAR IDENTIFICATION OF HAIL: AN OBSERVATION AND MODELING STUDY

by

MATTHEW E. ANDERSON

A THESIS

Submitted in partial fulfillment of the requirements
for the degree of Master of Science
in
The Department of Atmospheric Sciences
to
The School of Graduate Studies
of
The University of Alabama in Huntsville

HUNTSVILLE, ALABAMA

2010

UMI Number: 1487682

UMI®

Dissertation Publishing

ProQuest®

In presenting this thesis in partial fulfillment of the requirements for a master's degree from The University of Alabama in Huntsville, I agree that the Library of this University shall make it freely available for inspection. I further agree that permission for extensive copying for scholarly purposes may be granted by my advisor or, in his/her absence, by the Chair of the Department or by the Dean of the School of Graduate Studies. It is also understood that due recognition shall be given to me and to The University of Alabama in Huntsville in any scholarly use which may be made of any material in this thesis.

Matthew E. Anderson
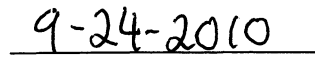
Date

THESIS APPROVAL FORM

Submitted by Matthew E. Anderson in partial fulfillment of the requirements for the degree of Master of Science in Atmospheric Science and accepted on behalf of the Faculty of the School of Graduate Studies by the thesis committee.

We, the undersigned members of the Graduate Faculty of The University of Alabama in Huntsville, certify that we have advised and/or supervised the candidate on the work described in this thesis. We further certify that we have reviewed the thesis manuscript and approve it in partial fulfillment of the requirements for the degree of Master of Science in Atmospheric Science.

Committee Chair

Department Chair

College Dean

Graduate Dean

ABSTRACT

School of Graduate Studies

The University of Alabama in Huntsville

Degree ____ Master of Science ____College/Dept. ____ Science/Atmospheric Science ____

Name of Candidate ___ Matthew E. Anderson _____

Title ____ C-band Polarimetric Radar Identification of Hail: An Observation _____

_____ and Modeling Study _____

Many studies have demonstrated that dual-polarimetric radar is an effective tool for hail detection. Studies employing radar at S-band frequencies have found that hail is characterized by high reflectivity ($Z_h > 50$ dBZ) and near zero differential reflectivity ($-1 < Z_{dr} < 1$ dB). Several studies have hypothesized that hail signatures observed by higher frequency radars, such as C-band, should be similar. To test the hypothesis, the dual-polarimetric radar signatures of nine hail events are carefully documented using C-band observations from the Advanced Radar for Meteorological and Operational Research (ARMOR). Unlike previous results at the S-band, this study shows that hail is characterized by high Z_h (> 50 dBZ) and high Z_{dr} ($3 - 8$ dB) at the C-band. In addition, a radar model is used to investigate the physical nature of the C-band hail signature and a hydrometeor identification algorithm is tested to evaluate its ability to detect hail at the C-band.

Abstract Approval: Committee Chair   _Kevin Knupp_ 9/24/2010

(Date)

Department Chair   _Sundar A. C._ 9/27/1010

Graduate Dean   _Rhonda Kay Gaede_ 12/9/10

iv

ACKNOWLEDGMENTS

TABLE OF CONTENTS

LIST OF FIGURES

LIST OF TABLES

CHAPTER 1

INTRODUCTION

A severe thunderstorm is defined as a storm that produces large hail (> 1.9 cm), strong winds (> 26 m/s), or a tornado (National Weather Service (NWS) definition). The definition of severe hail recently changed on January 5, 2010 to hail larger than 2.5 cm. Severe storms are important to identify and forecast because of the significant damage and fatalities that they can cause. One large hail producing storm can cause 100's of millions of dollars of property damage to crops, livestock, homes, and automobiles (Hillaker et al. 1985, Changnon 1999). Large hail, in rare cases, can even cause bodily injury and even death (National Climate Data Center (NCDC)). For this reason, it is important to be able to identify and locate areas of hail so that lives and property can be protected. Meteorological instrumentation is the most common way to access the current state of the atmosphere and the potential impacts of hail. The two main instruments that have been used for hail identification are satellite (e.g., Adler et al. 1985, Auer 1994, Cecil 2009) and radar (e.g., Atlas and Ludlham 1961, Donaldson 1961, Greene and Clark 1972, Eccles and Atlas 1973, Mather et al. 1976, Aydin et al. 1986, Bringi et al. 1986, Herzegh and Jameson 1992, Edwards and Thompson 1998, Hubbert et al. 1998, Straka et al. 2000), but of the two, radar has been the most widely utilized.

Numerous studies have used radar to identify areas of hail within thunderstorms (e.g., Atlas and Ludlham 1961, Donaldson 1961, Greene and Clark 1972, Eccles and Atlas 1973, Mather et al. 1976, Aydin et al. 1986, Bringi et al. 1986, Herzegh and Jameson 1992, Edwards and Thompson 1998, Hubbert et al. 1998, Straka et al. 2000). A number of techniques using radar have been performed to identify areas of hail aloft and severe hail at the surface (e.g., Carbone et al. 1973, Aydin et al. 1986, Bringi et al. 1986). Of course most methods of hail identification have some weaknesses and potentially significant sources of error (Rinehart and Tuttle 1982). Yet despite the limitations of some hail identification techniques, numerous concrete example of identifying severe hail with radar have been shown in thunderstorms all over the globe (e.g., Mather et al. 1976, Carbone et al. 1973, Bringi et al. 1986, Hubbert et al. 1998).

One of the first noteworthy methods for hail identification used the vertical profile of reflectivity within a hail producing thunderstorm. Donaldson (1961) was one of the first to note the differences between the vertical structure of hail and non-hail producing thunderstorms. The study observed that the hail producing storm had much higher reflectivity in the upper half of the vertical storm structure. Later studies, Mather et al. (1976), discovered that the height of the 45 dBZ isosurface is important for the identification of hail. The study found that if the 45 dBZ isosurface exceeds 8 km in a thunderstorm then the chances of the storm not producing severe hail is only 3 %. The Mather et al. (1976) study was performed in South Africa and is specific to that region. However, it proved to be an effective method for the region and has been applied elsewhere (Witt et al. 1998). Concurrently, Atlas and Ludlam (1961) presented the idea of using two different radars at different wavelengths for identifying hail. The method

involves comparing reflectivity between the two radars usually between an S-band and X-band radar. The reflectivity of the S-band radar would fall into the Rayleigh regime when hail is present while the X-band radar would fall into the Mie regime. Because of the different scattering regimes, the reflectivity would be expected to differ between the two radars indicating the presence of hail. This method was found to work well to detect hail at the ground and aloft (Carbone et al. 1973). However, the method is impractical because it requires that the antenna beam pattern must match including side lobes (Rinehart and Tuttle 1982). In addition, the method is impractical because of the cost of two radars. Another method used to detect hail utilizes the Vertically Integrated Liquid (VIL). VIL is a measure of the liquid content in a column of precipitation and is typically estimated from the profile of radar reflectivity (Greene and Clark 1972). Studies have shown that VIL is useful in hail identification and that the average VIL increases as the average hail size increases (Edwards and Thompson 1998). However, the study finds that VIL cannot be used alone to detect hail because of the large error associated with the calculation of VIL and the skill scores using VIL for hail identification vary widely from region to region and season to season (Edwards and Thompson 1998). From the list of techniques, it is easy to see there have been a number of ways to detect hail, but they all have their drawbacks.

Currently, most operational radars around the world only provide information in one polarization (horizontal), but with the advent of dual-polarimetric radar, the meteorological community has access to data in both the horizontal and vertical polarization (Seliga and Bringi 1976). Dual-polarization radar provides the radar meteorologist extra variables and information that can be used to better determine the

hydrometeor type that is being observed. Studies for the classification of hydrometeors based on their polarimetric variables have been performed at both the S-band (e.g., Aydin et al. 1986, Bringi et al. 1986, Herzegh and Jameson 1992, Hubbert et al. 1998, Straka et al. 2000, and Kennedy et al. 2001) and C-band (Meischner et al. 1991, Höller et al. 1994, Keenan et al. 2003, Baldini et al. 2004, and Deierling et al. 2005). A few studies done at the C-band have noticed significant differences between the signatures at the S-band and C-band in hail producing storms (Meischner et al. 1991, Höller et al. 1994, Ryzhkov et al. 2007, Tabary et al. 2009).

There are numerous literature examples demonstrating the effectiveness of hail identification with S-band polarimetric radar. Differential Reflectivity (Z_{dr}) is the measure of the difference between horizontal and vertical polarization. Therefore, Z_{dr} is helpful in identifying the oblateness of a hydrometeor (e.g., rain drop). The larger the Z_{dr}, the more oblate the particle would be expected. The effect of oblateness for hail can be different than rain because of the random orientations associated with tumbling motions and lower dielectric for hail. As a result, hail can appear to the radar as an effective sphere. In this case, the value of Z_{dr} for hail would be expected to be near 0 dB associated with large reflectivity (Z_h). There are several examples in the literature that have found hail to be identified by low Z_{dr} (near 0 dB) and high Z_h (>50 dBz) at the S-Band (e.g., Aydin et al. 1986, Bringi et al. 1986, Herzegh and Jameson 1992, Hubbert et al. 1998, Kennedy et al. 2001). The signature has been termed the "Z_{dr} hole" (Wakimoto and Bringi 1988) or "hail hole" because of the low Z_{dr} (hail) surrounded by higher Z_{dr} (rain). Some authors suggest that this method can be directly transferred and

applied to lower wavelength radars such as the C-band (e.g., Vivekanandan et al. 1990, Aydin and Giridhar and 1992, Bringi and Chandrasekar 2001).

However, a few studies at the C-Band have not been as conclusive. Meischner et al. (1991) and Ryzhkov et al. (2007) have shown that near 0 dB is not necessarily what can always be expected in areas of hail at the C-Band. Meischner et al. (1991) attributes the anomalously high Z_{dr} (> 5 dB) to smaller melting hail and resonance effects due to the smaller wavelength. Smaller melting hail stones can appear to the radar as large wet raindrops and exhibit high Z_{dr}. Resonance begins to take place at the C-Band for rain and mostly melted hailstones larger than about 5 mm (Zrnic et al. 2000). Therefore, when large particles are present, Z_h and Z_{dr} can be significantly higher at the C-Band compared to the S-Band (Zrnic et al. 2000). Ryzhkov et al. (2007) suggest that the anomalously high Z_{dr} can be explained by large raindrops and small melting hail that dominate Z_h and Z_{dr} in melting hail shafts. Alternatively, Smyth et al. (1999) suggest that non-zero and even large positive (3-5 dB) values of Z_{dr} at the S-band (and assumedly the C-band) can be associated with large oblate hail that fall with symmetric orientation of the major axis in the horizontal (i.e., non-tumbling). All three studies indicate that the traditional S-band approach for hail identification with Z_h and Z_{dr} may not always work when trying to identify hail at the C-band. On the other hand, Bringi and Chandrasekar (2001) (p.451-452) and Ryzhkov et al. (2009) suggest that the hail hole (large Z_h > 50 dBZ and $|Z_{dr}|$ < 1.0 dB) should be observed at the C-band when hailstones are large and numerous enough to dominate the reflectivity and appear as effective spheres. In addition, Vivekanandan et al. (1990) through the modeling of melting hailstones, based on the wind tunnel results of melting hail from Rasmussen et al. (1984), suggest that hail above

12-15 mm will shed their melt water leading to the "hail hole" signature (Bringi et al. 1986). The polarimetric signatures of hail at the C-band must be better understood in order for hail to be properly classified and used in Nowcasting. The use of C-band polarimetric radars is becoming more common among the operational weather services of European and Asian countries and the private market (e.g., television stations) in the United States because of their affordability. Clearly, more radar cases are warranted to address this limitation in our developing knowledge of the polarimetric hail signature at the C-band.

The hypothesis that is being tested herein is that C-band polarimetric signatures of hail are routinely similar results to the "hail hole" signature of high Z_h (> 50 dBZ) and low Z_{dr} (-1 to 1 dB) observed at the S-band (e.g., Aydin et al. 1986, Bringi et al. 1986, Hubbert et al. 1998). This study hopes to thoroughly document the C-band polarimetric hail signatures through the use of high quality hail cases observed by the Advanced Radar for Meteorological and Operational Research (ARMOR) in Huntsville, Alabama. In addition, a radar modeling approach will be used to determine if the observed C-band polarimetric signatures can be reproduced. If they can be reproduced, it is important to know what assumptions have to be made about the modeled hydrometeors. The study also hopes to address the following questions:

- What do the C-band polarimetric signatures of hail look like both at the surface and aloft?

- Are the C-band hail signatures consistent with what have been observed at the S-band?

- If a "hail hole" signature exists at the C-band, is it due to hail or other factors?

- What factors may contribute to situations where the "hail hole" signature does not exist at the C-band?

- Can radar modeling of hydrometeors be used to reproduce the C-band polarimetric signatures of hail?

- If radar modeling can be used to reproduce the C-band polarimetric signatures of hail, what assumptions have to be made about the hydrometeor being modeled?

- Do current hydrometeor identification algorithms work well at identifying hail at the surface? If so, why? If not, what suggestions can be made for improvement in hail identification at the C-band?

The hail reports from these storms were carefully quality controlled in order to use the most reliable reports available. The dual empirical and modeling approach used in this radar study should be able to answer these questions and address the objectives of this study. Chapter 2 discusses background information about hail characteristic, hail detection, hydrometeor identification, and microphysical modeling important to this study. Chapter 3 overviews the methodology and instrumentation used in this study. Chapters 4 and 5 will contain results from observations and modeling of hailstones. Chapters 6 and 7 will contain discussion and conclusions about the study along with suggestions for future work in the area of hail detection with C-band polarimetric radars.

CHAPTER 2

BACKGROUND

In order to set the framework for this study, it is appropriate to review previous studies of hail, polarimetric radar, and the application of polarimetric data. This includes hail characteristic, polarimetric radar variables, hail detection techniques, and hydrometeor identification.

2.1 Hail Characteristics

In order to understand the polarimetric signatures of hail, it is important to understand the characteristics of hail. These characteristics are important because they lead to the production of the polarimetric signatures that are observed. Polarimetric signatures can vary greatly depending upon the fall mode, shape, and concentration of hailstones.

2.1.1 Hail Fall Mode

Hail stone fall mode has been highly debated in the literature depending upon the characteristics of the hailstone. Knight and Knight (1970) assessed the falling behavior of large oblate hailstones based on the examination of the structure of the hailstones and

performing experiments with modeled hailstones. Rasmussen and Heymsfield (1987a) and Aydin and Zhao (1990) suggest that if melting is occurring and a sufficient water torus exists, then the hailstone will fall relatively stable with little to no canting or tumbling acting like a large raindrop. The fall mode is then highly dependent upon the state of the hailstone.

One of the more common hailstone shapes observed has been the oblate spheroid (e.g., Knight 1986). Another key hail characteristic that needs to be addressed is whether hail tends to fall with it major axis vertical or horizontal. Zrnic et al. (1993) suggest through observations of negative Z_{dr} within hail producing cells that hail falls with its major axis vertical. The study speculates that hailstones with diameters larger than 2 cm would fall with their major axis vertical. List et al. (1973) suggest through wind tunnel experiments that hailstones tumble with their major axis horizontally oriented. While Matson and Huggons (1980) using stroboscopic photography of hailstones near the ground, found that hailstones continuously changed orientations due to their tumbling motions. Aydin and Zhao (1990) modeled the radar characteristics of hailstones and melting hailstones based on the hail melting model of Rasmussen and Heymsfield (1987a). In the study, they assumed that hailstones fell with their major axis vertical and tumbled, while melting hailstones fell with their major axis horizontal and were stable. From the literature, it is easy to see there are no concise conclusions about the fall behavior of hailstones.

2.1.2 Hailstone Shape

Knight (1986) documented hailstone shapes from a wide sample from Oklahoma and Colorado. This study was performed on spheroids and conical shaped hailstones only. Any hailstones that were irregularly shaped were not used in the study. The data in this study consists of photographs of the hailstones and measurements of their short and long dimensions. Axis ratio is defined as a/b, where a is the minor axis and b is the major axis. From these measurements, the axis ratios of the hailstone were calculated. The study found that the axis ratios were in the range of 0.6 – 1.0 with hailstone sizes ranging from 5 – 55 mm. The study found that in both Oklahoma and Colorado hailstones, the axis ratio tends to decrease as the size of the hailstones increases (Figure 2.1). The only noticeable difference between the two samples occurs for the smaller (~ 5 mm) hailstone sizes where Oklahoma hailstones are nearly spherical with axis ratios near 1 while Colorado hailstone are a bit more oblate with axis ratios of 0.9. These axis ratio values match those in other studies as well (Thwaites et al. 1977). Therefore, hailstone shapes have been fairly well documented as oblate spheroids.

2.1.3 Hailstone Size Distributions

Hailstones, along with other hydrometeors, tend to fall in certain size distributions. Those parametric size distributions can be expressed mathematically as monodisperse, exponential, or gamma. A monodisperse distribution is where all hydrometeors in a given volume are of the same size and shape (no variability of size or shape in given volume). Ulbrich (1983) mathematically defines the exponential distribution as
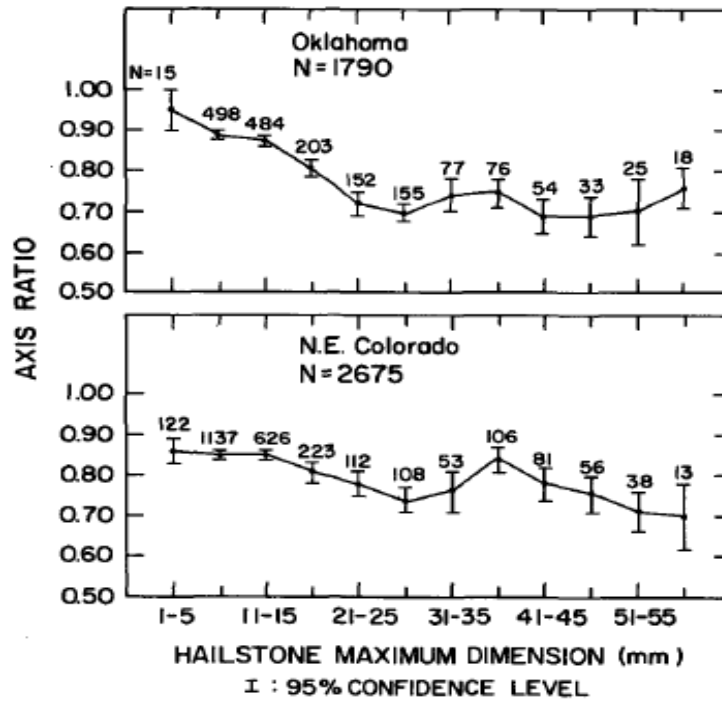
Figure 2.1: Adapted from Knight (1986). This figure shows axis ratio as a function of size for hailstones observed in Oklahoma and Colorado. The bars on the plot indicate the 95 % confidence level.

$$N(D) = N_0 e^{-\Lambda D} \quad (0 \le D \le D_{max}), \tag{2.1}$$

where $N(D)$ is the particle size distribution, N_0 is the intercept parameter, Λ is the slope of

the distribution, D is the particle diameter, and D_{max} is the maximum particle diameter

in the distribution. Figure 2.2 shows an example of the exponential distribution on a

semi-log plot. The exponential line is where $\mu = 0$. It can be seen where a large number

of small particles exist in the distribution, but as the particles become larger, the number

of hydrometeors decreases exponentially to where there are only a small number of

particles at the large diameter end of the distribution. Ulbrich (1983) mathematically

defines the gamma distribution:

11

$$N(D) = N_0 D^{\mu} e^{-\Lambda D} \quad (0 \le D \le D_{max}), \tag{2.2}$$

where μ is the shape parameter of the distribution and can be positive or negative, $N(D)$ is the particle size distribution, N_0 is the intercept parameter, Λ is the slope of the distribution, D is the particle diameter, and D_{max} is the maximum particle diameter in the distribution. Figure 2.2 illustrates an example of gamma distribution with both a positive and negative μ. The positive μ shows a relative emphasis on sizes within the middle of the distribution with a smaller number of particles on the tails of the distribution. The negative μ shows the opposite with a smaller number of particles in the middle of the distribution with more of a relative emphasis of particles on the tails of the distribution. Overall, there are a number of potential distributions that hydrometeors might fit.

This study focuses on one particular hydrometeor type, hail, so it is important to understand the potential size distributions of hailstones. Auer and Marwitz (1972) took hailstone size distribution samples from an airplane and ground teams near the updraft of hail producing storms. The study noticed that each storm had a narrow range of sizes and suggested that the size distributions in this study were almost monodisperse. Cheng and English (1983) took hailstone size distribution samples from the ground with a van equipped with a hail net from 41 samples. The study found that the distribution was best fit to the exponential size distribution. Ziegler et al. (1983) examined three hail samples from the NCAR hail intercepting vehicle. The study found that for each of these samples, the positive μ (5-9) gamma distribution was a much better fit compared to the exponential distribution. Hubbert et al. (1998) also concluded that a gamma distribution is a better fit for hailstone size distributions over Colorado. From exploring the literature,
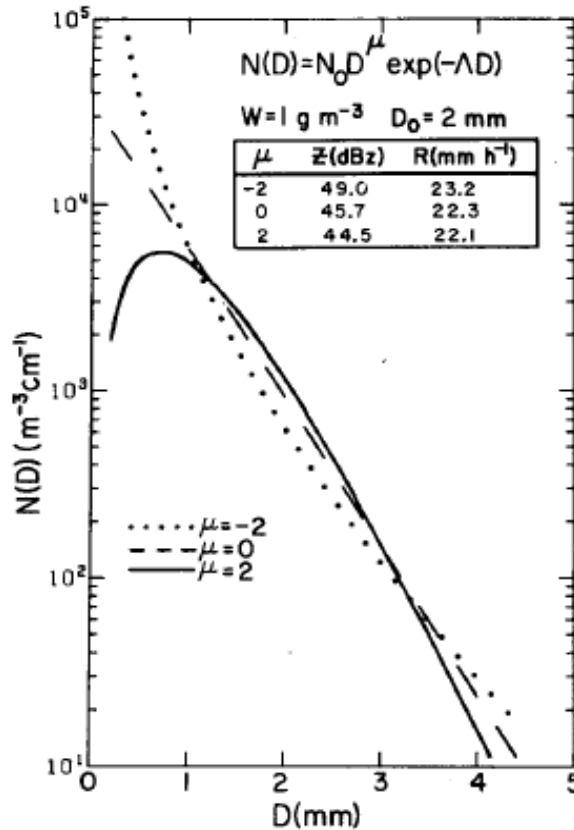
Figure 2.2: Adapted from Ulbrich 1983. Examples of exponential ($\mu = 0$), positive gamma ($\mu = 2$) and negative gamma ($\mu = -2$) with a liquid water content $W = 1 \text{gm}^{-3}$ and a diameter $D = 2$ mm. The table shows the corresponding radar reflectivity and rain rate.

it is clear that the optimal parametric fit to hailstone size distributions remains an open

and challenging question.

2.2   Polarimetric Radar Data

Studies have found that radar is one of the better meteorological instruments for

hail detection and Nowcasting (e.g., Donaldson 1961, Mather et al. 1976, Aydin et al.

1986, Bringi et al. 1986, Hubbert et al. 1998). In order to use radar for hail detection, the

variables that are calculated and estimated by the radar must be understood.   The

following section will discuss these variables and their expected values in rain. The

expected values expected in hail will be discussed in Section 2.3.

2.2.1   Radar Reflectivity Factor

Radar reflectivity factor (also known as reflectivity) is one of the more widely

used variables and is used in both traditional horizontally polarized radars and dual

polarimetric radars. Reflectivity is easily derived from the radar range equation and can

be expressed:

$$z = \frac{c p_r r^2}{|K|^2},$$
(2.3)

where z is the radar reflectivity factor, c is the radar constant which includes details about

the specifications of the radar, p_r is the power returned to the radar, r is the range from

the radar, and $|K|^2$ is the dielectric function of the particles that the radar is detecting. It

can be seen from the equation that the power received from the radar is proportional to

the radar reflectivity factor. Therefore, the stronger the power returned from the radar

signal, the higher the radar reflectivity. Radar reflectivity factor, z, is expressed in units

of $mm^6\ mm^{-3}$ and can possess a wide range of values from $0.001 - 36{,}000{,}000\ mm^6\ mm^{-3}$

(Rinehart 2004 p.97). Because of this wide range of values, radar reflectivity can be best

expressed by a logarithmic scale:

$$Z = 10\log_{10}\left(\frac{z}{1mm^6/mm^3}\right),$$
(2.4)

where Z is the logarithmic radar reflectivity factor in units of decibels and z is the linear

radar reflectivity factor is linear units of $mm^6\ mm^{-3}$. The linear units of radar reflectivity

factor above would become –30 dBZ and 76.5 dBZ (Rinehart 2004 p.97), which is a much more reasonable range of values to interpret radar data.

The fundamental definition of the radar reflectivity factor can be derived from the particle size distribution for Rayleigh conditions. Radar reflectivity factor can be expressed as a function of the sixth moment of the particle size distribution:

$$z = \int_0^\infty N(D)D^6 dD, \qquad\qquad (2.5)$$

where z is the radar reflectivity factor is linear units, $N(D)$ number of particles in a given volume, and D is the diameter of those particles. The linear units can be converted similarly to logarithmic units using the same conversion equation. From the particle size distribution equation, it can be seen that radar reflectivity factor is sensitive to the number of hydrometeors and the diameter of the hydrometeors in a given radar volume. Since z for Rayleigh scattering is the 6th moment of the particle size distribution, it can be seen that any subtle change in particle diameter can lead to a dramatic change in radar reflectivity factor. Reflectivity values for rain can range from 20 to 60 dBZ (Straka et al. 2000). The reflectivity values are highly dependent upon the diameter of the particles being observed with large raindrops producing higher reflectivity than smaller drops.

2.2.2 Differential Reflectivity (Z_{dr})

In a landmark paper, Seliga and Bringi (1976) proposed a new radar variable that would be useful in determining factors about the raindrop size distribution and has also been found useful for hail detection (e.g., Aydin et al. 1986, Bringi et al. 1986, Hubbert et al. 1998). The new variable, differential reflectivity (Z_{dr}), takes reflectivity measurements from both the horizontal and vertical and is the logarithmic difference

between horizontal and vertical reflectivity. Differential reflectivity (Z_{dr}) can be expressed mathematically:

$$Z_{dr} = 10 \log_{10} \left(\frac{z_h}{z_v} \right),$$
(2.6)

where z_h is the radar reflectivity factor in horizontal polarization and z_v is the radar reflectivity factor in vertical polarization. Jameson (1983) demonstrates that Z_{dr} is the measure of the reflectivity weighted oblateness. Beard and Chuang (1987) show that as drop size increases from 1 mm to 6 mm, drop sizes change from nearly spherical to highly oblate. Since raindrops become increasingly oblate with increasing size, Z_{dr} can be a useful parameter to derive the mean diameter of the particles being observed (Seliga and Bringi 1976). In addition, Z_{dr} is not sensitive to the number of concentration of homogenous particles in a volume. Since Z_{dr} is reflectivity weighted, Z_{dr} will be more sensitive to the largest drops because of the D^6 effect on reflectivity. Reflectivity dependence also implies that Z_{dr} is susceptible to differential attenuation (which will be addressed in Chapter 3). Seliga and Bringi (1976) presented Z_{dr} as a way to make more accurate rainfall estimations, and it has been found useful in many different studies (e.g., Seliga et al. 1986, Gorgucci et al. 1994). Bringi et al. (1991) and Carey et al. (2000) show through simulations that Z_{dr} ranges from 0 to 5.5 dB at C-band. Larger raindrops should produce larger Z_{dr} because of their increasing oblateness. With the advent of dual-polarimetric radar, other new radar variables have been found useful as well.

2.2.3 Specific Differential Phase (K_{dp})

In order to understand specific differential phase (K_{dp}), there must be a review on phase shift of the radar electromagnetic wave along with a review of the differential

propagation phase (Φ_{dp}). As a radar wave travels through the atmosphere and interacts with non-spherical hydrometeors, a phase shift of the wave occurs. With dual-polarimetric radar, this phase shift can occur in the horizontal and vertical polarization. Another variable, the differential propagation phase (Φ_{dp}), is a measure of the difference in phase shift between horizontal and vertical polarizations and can be expressed mathematically as

$$\Phi_{dp} = \Phi_{hh} - \Phi_{vv}, \tag{2.7}$$

where Φ_{hh} is the phase shift in the horizontal polarization and Φ_{vv} is the phase shift in the vertical polarization. Since raindrops are oblate with their major axis horizontal, this means that the horizontal wave is slowed more than the vertical ($\Phi_{hh} > \Phi_{vv}$) resulting in positive Φ_{dp}. The differential propagation phase (Φ_{dp}) can be estimated from the following (Jameson and Mueller 1985):

$$\Psi_{dp} = \delta + \Phi_{dp} + \Phi_0 + \Phi_{noise}, \tag{2.8}$$

where Ψ_{dp} is the measured total differential phase from the radar, δ is the backscatter differential phase, Φ_{dp} is the differential propagation phase, Φ_0 is the system offset phase, and Φ_{noise} is the system noise. The system offset phase is a known engineering quantity and can be subtracted out. However, the backscatter differential phase associated with resonance in Mie scattering can be significant at the C-band (e.g., Bringi et al. 1990, Hubbert et al. 1993). A filtering technique is used to remove δ from Ψ_{dp} (Hubbert and Bringi 1995). After all of the other variables are subtracted out of Ψ_{dp}, Φ_{dp} can be isolated and estimated. Now that Φ_{dp} has been calculated, the next step is to calculate K_{dp}.

The specific differential phase (K_{dp}) is defined as the two way range derivative of the differential phase. The specific differential phase (K_{dp}) can be expressed mathematically as

$$K_{dp} = \frac{\partial \Phi_{dp}}{2 \partial r},$$ (2.9)

where Φ_{dp} is the differential propagation phase and r is the range (Rinehart 2004 p.225). Specific differential phase is dependent upon number concentration, shape, dielectric, and wavelength of radar. The specific differential phase is not affected by receiver calibration errors, attenuation, and partial beam blockage because it is a function of the phase of the received signal and not its strength. When particles are isotropic (spheres), K_{dp} will be near 0, and when particles are oblate with their major axis horizontal, K_{dp} will be positive (Balakrishnan and Zrnic 1990a). Therefore, K_{dp} values in rain are expected to be positive due to the oblateness of raindrops (e.g., Beard and Chuang 1987). Values of K_{dp} in rain have been modeled from 0 to 10 $°km^{-1}$ at the C-band (Bringi et al. 1991, Carey et al. 2000) and from 0 to 5 $°km^{-1}$ at the S-band. Ryzhkov and Zrnic (1995) found that K_{dp} estimations of rainfall outperformed traditional rainfall measurements (Z-R relationships) by comparing results with a rain gauge network, and other studies have found similar results (e.g., Petersen et al. 1999). However, K_{dp} is the derivative of an already noisy field (differential propagation phase) and can be rather noisy in some instances (e.g., Gorgucci et al. 2000). The noisiness of this field and its potential impact on hail identification will be discussed in Chapter 4.

2.2.4 Correlation Coefficient (ρ_{hv})

The correlation coefficient (ρ_{hv}) is the correlation of the pulse to pulse returns between the horizontal and vertical polarizations in a given radar volume. The correlation coefficient can be expressed mathematically as

$$\rho_{hv} = \frac{\left\langle |s_{vv}s_{hh}^{*}| \right\rangle}{\left[\left\langle |s_{hh}|^{2} \right\rangle \left\langle |s_{vv}|^{2} \right\rangle^{\frac{1}{2}} \right]},$$
(2.10)

where s is the signal strength, $s*$ is the complex conjugate of signal strength, and subscripts h and v represent the horizontal and vertical polarization signals (Rinehart 2004 p. 226). In a radar volume that contains rain, the correlation coefficient is expected to be high, greater than 0.98 for the S-band and greater than 0.95 for the C-band (e.g., Bringi et al 1991, Carey et al. 2000, Keenan et al. 2000). Values for hail at the S-band have been found below 0.95 (Balakrishnan and Zrnic 1990b). Balakrishnana and Zrnic (1990b) explain that possible reasons for low (< 0.95) ρ_{hv} can be explained by non-Rayleigh (Mie or resonant) scattering, irregular shaped hydrometeors, mixture of hydrometeors (e.g., rain and hail), and a variety of hydrometeor shapes. Ryzhkov and Zrnic (1998) observed values of ρ_{hv} less than 0.9 in the melting zone or bright band associated with snow melting to rain. In addition, clutter can be removed using ρ_{hv} because clutter has a low correlation coefficient (< 0.7) (Ryzhkov et al. 2005). Therefore, any data below this threshold can be removed. Polarimetric radar offers a wide variety of new variables to analyze rainfall, hydrometeor type, and filter clutter.

2.3 Hail Detection

One of the main instruments used in hail detection has been radar (e.g., Donaldson 1961, Atlas and Ludlam 1961, Mather et al. 1976). Over the years there have been many different radar techniques for hail detection from using the 45 dBZ isosurface (Donaldson 1961), using the dual wavelength approach by using two different wavelength radars for hail detection (Atlas and Ludlam 1961), and using the Vertically Integrated Liquid (VIL) as an indication of hail (Greene and Clark 1972). As addressed in Chapter 1, all of these methods have their strengths and weaknesses in detecting hail. The current technique used by the National Weather Service is from Donavon and Jungbluth (2007). This technique uses the height of the 50 dBZ isosurface above the 0 °C level to determine the likelihood of hail being produced at the surface. For a limited sample over the Central and Northern Plains, the study showed a probability of detection of 90 % with the method and a false alarm ratio of 22 %. In preliminary tests, the Donavon and Jungbluth method appears to be a useful method for hail detection, but the new technology of dual polarimetric radar has been well tested by the research community and should prove to be useful for operational hail detection as well

2.3.1 S-band Polarimetric Techniques

There are numerous literature examples demonstrating the effectiveness of hail identification with S-band polarimetric radar. Even though hailstones have been found to be oblate (e.g., Knight 1986), they can appear to the radar as effective spheres because ot their tumbling motions and near random orientations. In this case, the value of Z_{dr} for hail would be expected to be near 0 dB associated with large reflectivity (Z_h). Several

studies have found that hail can be identified by low Z_{dr} (near 0 dB) and high Z_h (> 50 dBZ) at the S-Band (e.g., Aydin et al. 1986, Bringi et al. 1986, Aydin et al. 1990, Herzegh and Jameson 1992, Hubbert et al. 1998, Kennedy et al. 2001). The signature has been termed the "Z_{dr} hole" (Wakimoto and Bringi 1988) or "hail hole" because of the low Z_{dr} (hail) surrounded by higher Z_{dr} (rain). The "hail hole" concept is highly dependent upon the assumptions that hail tumbles (Knight and Knight 1970) and appears to the radar as an effective sphere. Figure 2.3 shows an example of the "hail hole" observed by Bringi et al. (1986). Aydin et al. (1986) developed a quantitative hail signal:

$$f(Z_{dr}) = \begin{cases} 27, & Z_{dr} \leq 0 \ dB \\ 19Z_{dr} + 27, & 0 \leq Z_{dr} \leq 1.74 \ dB \\ 60, & Z_{dr} > 1.74 \ dB \end{cases}$$ (2.11)

$$H_{dr} = Z_h - f(Z_{dr}),$$

where Z_{dr} is the differential reflectivity, Z_h is the horizontal reflectivity, and H_{dr} is the hail signal. The study finds that positive values are associated with hail, and the larger the value of H_{dr}, the higher the confidence exist that hail is being detected. The study finds that if H_{dr} is negative, then raindrops are being detected. The Aydin et al. (1986) study confirmed the accuracy of the hail signal by comparing the values with actual hail reports from two storms. Recently, Depue et al. (2007) found that H_{dr} is a useful variable in determining hail size in the front range of Colorado. With S-band polarimetric radar, Z_{dr} has been one of the more widely used variables for hail identification, but other variables have been found useful.

Other polarimetric variables have been found useful in identifying areas of hail. Specific differential phase (K_{dp}) can be useful in hail identification because it is not affected by isotropic (e.g., spherical) hydrometeors such as hail (Balakrishnan and Zrnic

21

ORIGIN = (0.00, 0.00)KM   X-AXIS = 90.0 DEG

ORIGIN = (0.00, 0.00)KM   X-AXIS = 90.0 DEG
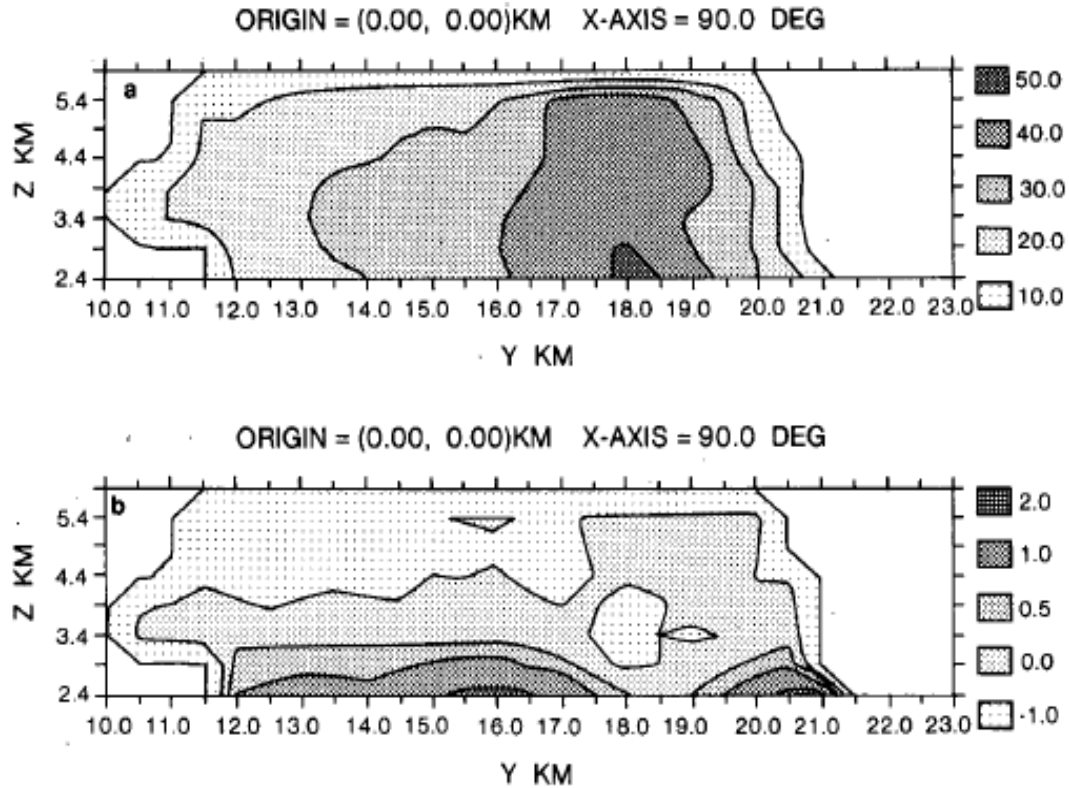
Figure 2.3: Adapted from Bringi et al. 1986. (a) Range Height Indicator (RHI) of reflectivity and (b) Z_{dr} in contours through a convective cell. "Hail hole" signature observed between 18 and 19 km.

1990a). Straka et al. (2000) notes that hail should have values of approximately zero for K_{dp}. In addition, ρ_{hv} can be used to identify regions of hail. Balakrishnan and Zrnic (1990b) show that decreases in ρ_{hv} are associated with hail size increases into the resonant regime. In addition, mixtures of hydrometeors (e.g., rain and hail mixtures) can cause a lowering in ρ_{hv} due to the variety of shapes, sizes, fall modes, and dielectrics associated with the mixture (Balakrishanan and Zrnic 1990b). Irregular shape hydrometeors (e.g., lumps and lobes) can also cause a decrease in ρ_{hv} (Balakrishanan and Zrnic 1990b). Observational studies at the S-band have shown that areas associated with hail produce ρ_{hv} values lower than rain (< 0.95) (e.g., Balakrishnan and Zrnic 1990b, Hubbert et al.

22

1998). Therefore, polarimetric variables have been found useful for hail identification in numerous studies performed at the S-band.

2.3.2   C-band Polarimetric Techniques

At the C-band other factors must be considered before being able to correctly identify hail. Special consideration must be made when interpreting C-band data due to the enhanced effects of attenuation and resonant (Mie or non-Rayleigh) scattering at the shorter wavelength (e.g., Zrnic et al. 2000). Zrnic et al. (2000) show that the peak of resonance at the C-band is around 6 mm and can greatly effect polarimetric variables. The study shows the resonance leads to a pronounced peak of Z_{dr} near 6 mm using the T-matrix backscattering method. Ryzhkov et al. (2007) noted that Z_{dr} for the same drop size distribution of rain can be 3 dB higher for the C-band compared to the S-band. The study also shows that ρ_{hv} can be much lower in pure rain near 0.94 for the C-band and near 0.98 for S-band due to the resonant sized drops at C-band and not the S-band. Vivekanandan et al. (1990) and Meischner et al. (1991) similarly modeled melting hail using the Rasmussen and Heymsfield (1987a) melt model and the T-matrix. The melt model was used to arrive at the size and shape while the T-matrix was used to calculate the polarimetric variables of the melting hailstones. The maximum initial hailstone size before melting in both studies is only 9 mm. The severe hailstone size criterion was (prior to January 5, 2010) 1.9 cm and is currently 2.5 cm. Both of these values are well above the 9 mm maximum hail size used in Vivekanandan et al. (1990) and Meischner et al. (1991). Vivekanandan et al. (1990) demonstrates that a peak in Z_{dr} occurs around 8 dB for these small melting hailstones below the 0 °C level. The study, however, states

23

that if the initial hailstone sizes exceed 12-15 mm, then the additional melt water would be shed off and the hailstone will tumble and would produce the traditional "hail hole" signature based on the wind tunnel experiments by Rasmussen et al. (1984). Meischner et al. (1991) indicates that a similar peak in Z_{dr} occurs around 9 dB for these small melting hailstones below the 0 °C level. Meischner et al. (1991) also states that large sized hail would shed their melt water and produce near 0 dB Z_{dr}. Ryzhkov et al. (2009) similarly modeled melting hailstones using the T-matrix and showed a Z_{dr} peak near 6 mm of 8 dB for the C-band and a less amplified resonance peak near 9 mm of 4.5 dB for the S-band. However, the study concludes that large hail (> 25 – 30 mm) at the C-band will not contribute significantly to Z_{dr} and produce a similar hail signature to those observed at the S-band. All of these modeling studies agree that small melting hail can produce high Z_{dr} (> 5 dB) and large melting hailstone shed their melt water and randomly tumble leading to near 0 dB.

In addition to the modeling studies at the C-band observational studies have been performed as well. Meischner et al. (1991) and Ryzhkov et al. (2007) have shown that near 0 dB is not necessarily what can always be expected in areas of hail at the C-Band. Meischner et al. (1991) shows that high Z_{dr} is observed for areas of hail (Figure 2.4). However, the study did not carefully document the hail based on location and size. The study attributes the anomalously high Z_{dr} (> 5 dB) to smaller melting hail. Smaller melting hail stones can appear to the radar as large wet raindrops and exhibit high Z_{dr} and melt water can act to stabilize the hailstones (Aydin and Zhao 1990). If the melting hail stone falls rather stably, then it would appear to the radar as a large raindrop and exhibit high Z_{dr} (> 5 dB). Meischner et al. (1991) also concludes that pronounced resonant

24
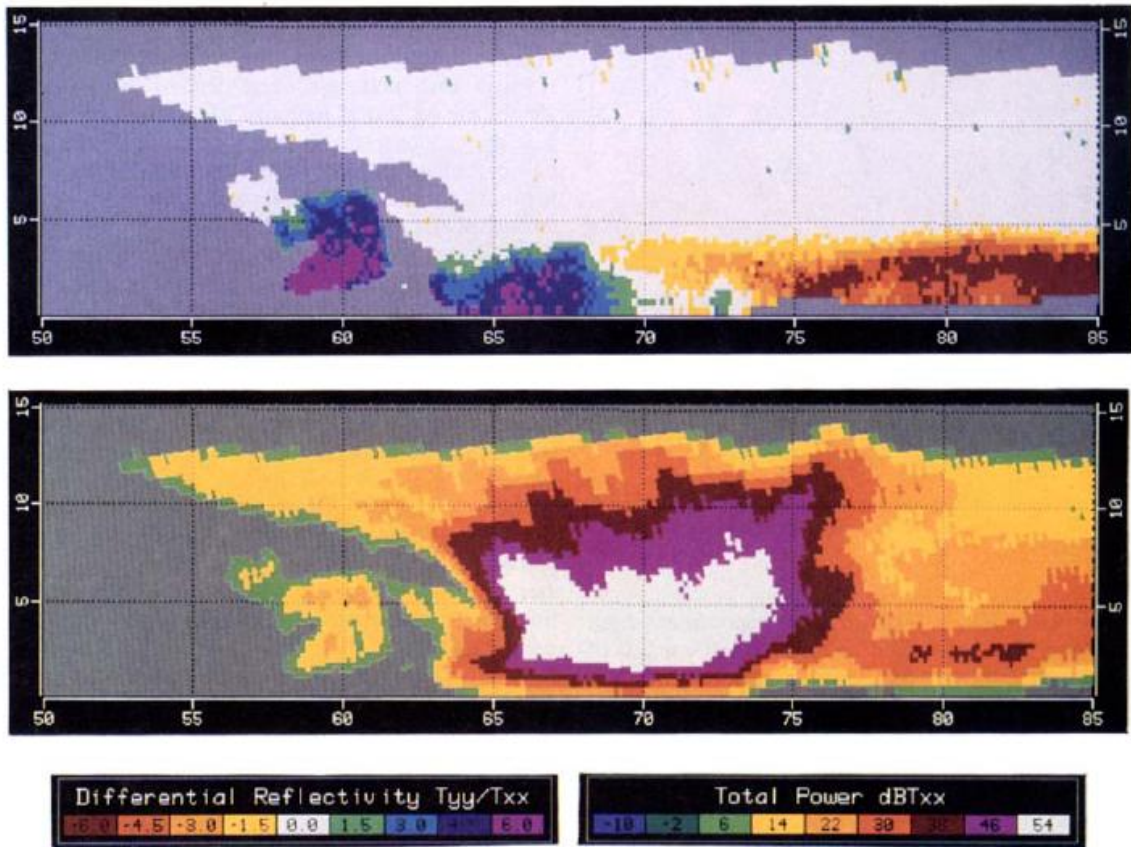
Figure 2.4: Adapted from Meischner et al. 1991. Vertical cross section (RHI) of Z_{dr} (top panel) and Z_h (bottom panel). High Z_{dr} (> 5 dB) associated with high Z_h (> 45 dBZ) can be seen between 65 and 70 km.

effects could be taking place due to the smaller wavelength. These peaks in resonant sized particles cause anomalously high Z_{dr} (> 5 dB) (Zrnic et al. 2000). Ryzhkov et al. (2007) and Kumjian and Ryzhkov (2008) observed 11 summer time hail producing storms in Alabama and Canada with a C-band radar and observed no noticeable drop in Z_{dr} near high Z_h where hail was observed. These studies knew there was hail in the storms based on hail reports. However, the specific locations, times, and sizes were not carefully documented to analyze the polarimetric signature near the hail reports. The studies suggest that the anomalously high Z_{dr} can be explained by large raindrops and

small melting hail that dominate Z_h and Z_{dr} in melting hail shafts. From these studies, it is easy to see that hail signatures between the C-band and S-band are at least sometimes obviously different. However, Bringi and Chandrasekar (2001) (p.451-452) and Ryzhkov et al. (2009) suggest that the hail hole (large Z_h > 50 dBZ and $|Z_{dr}|$ < 1.0 dB) should be observed at the C-band when hailstones are large (> 1.5 cm) and numerous enough to dominate the reflectivity and appear as effective spheres. This study will explore this concept by carefully documenting the C-band polarimetric signatures of hail based on hail reports from a variety of networks. The study will compare the signature of large (> 4.44 cm in this study) and small (< 4.44 cm in this study) hailstones because other studies suggest large (> 1.5 cm) hailstones should produce near 0 dB Z_{dr} at the C-band (e.g., Vivekanandan et al. 1990, Meischner et al. 1991, Bringi and Chandrasekar 2001 p.451-452, Ryzhkov et al. 2009). This study has an ample number of hail reports to test this idea. The observations from the hail reports will be addressed in Chapter 4.

2.4   Hydrometeor Identification

2.4.1 Boolean Logic

One of the key advantages of polarimetric radar data is its ability to make a best possible qualitative estimate of hydrometeor type. This has been demonstrated in studies at the S-band to determine areas of hail and rain (e.g., Aydin et al. 1986, Bringi et al. 1986, Aydin et al. 1990, Hubbert et al. 1998). Straka and Zrnic (1993) used previous studies to compile known results into convenient tables and then suggest a method to integrate all variables together into a joint approach using Boolean (i.e., yes or no) logic. The study used a decision tree (Boolean logic) approach to classify hydrometeors based

on two-dimensional space (Figure 2.5) using radar variables (e.g., Z_h versus Z_{dr}, LDR, K_{dp}, and ρ_{hv} space). The study was later formally completed in Straka et al. (2000). Straka et al. (2000) also developed a set of tables to determine different hydrometeor types designed from previous studies. One of the obvious problems with Boolean logic is the overlap that can occur in the 2-D space (Figure 2.5). No one hydrometeor type is exclusive from others in the space. One location in the space may be true for multiple hydrometeor types, and there is no method to determine which hydrometeor type is the most likely to occur (Straka et al. 2000). Therefore, it is important to come up with an alternative method for hydrometeor identification because of this setback.

2.4.2   Fuzzy Logic

The approach considers this uncertainty explicitly when determining the hydrometeor type from polarimetric variables is fuzzy logic (Vivekanandan et al. 1999, Liu and Chandrasekar 2000). Fuzzy logic is similar to Boolean logic except there are no hard boundaries. The boundaries are "fuzzy" or uncertain. The fuzzy logic approach is an improvement to the Boolean logic approach because the boundaries of hydrometeor types are not highly defined. There exists some uncertainty about what kind of signatures certain hydrometeors produced. There are several steps in fuzzy logic; one of them is "fuzzification." The "fuzzification" step is used to convert crisp inputs (e.g., polarimetric observations, temperature) to a fuzzy set with corresponding membership degree (Liu and Chandrasekar 2000). This step assigns a probability that a given radar variable or set of radar variables belongs to a given particle set. The membership function determines to what degree each crisp input indicates a specific output (e.g., particle type). Figure 2.6

27
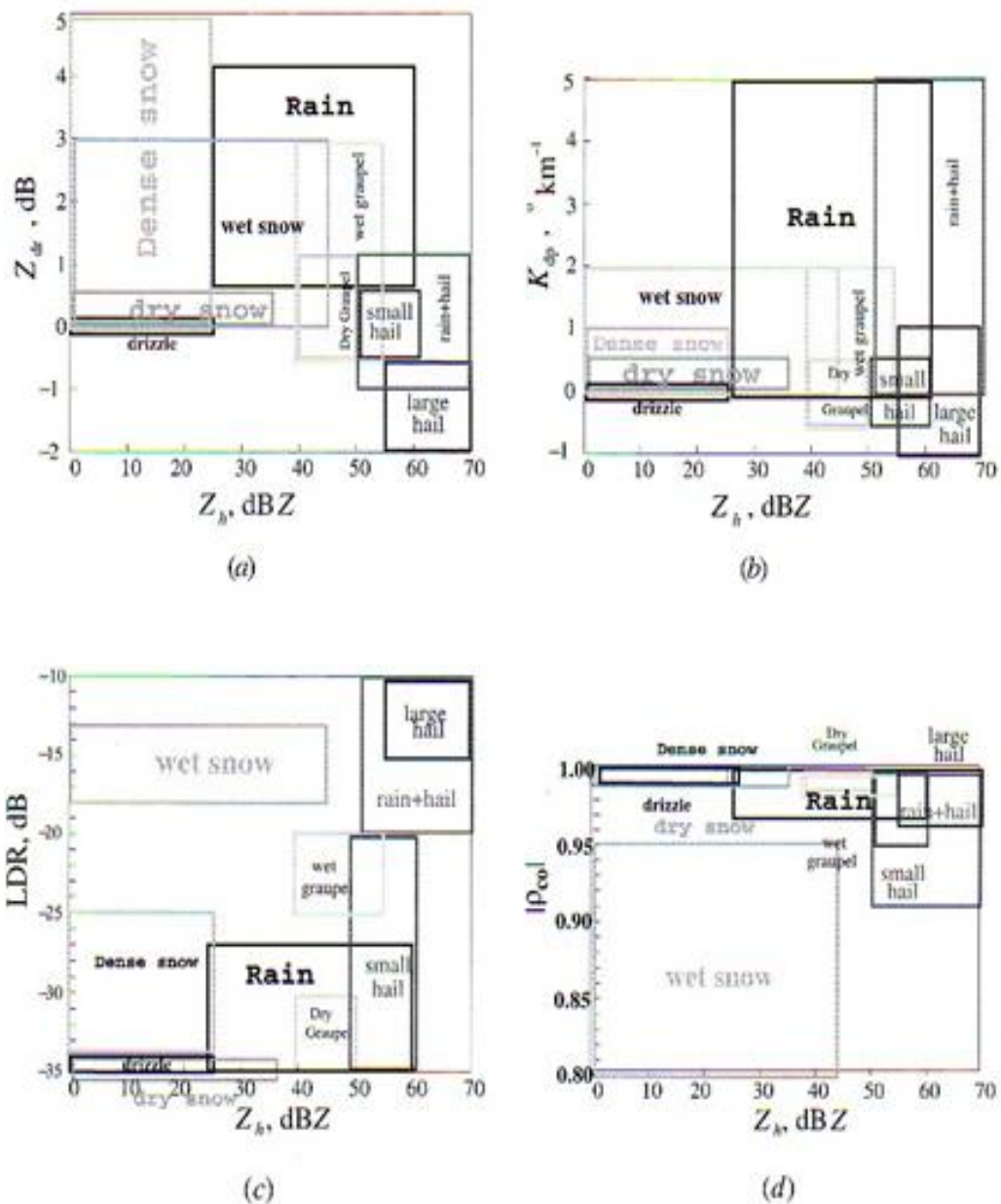
Figure 2.5: From Bringi and Chandrasekar 2001 adapted from Straka and Zrnic 1993. Hydrometeor classification using Boolean logic in Z_h versus (a) Z_{dr}, (b) LDR, (c) K_{dp}, and (d) ρ_{hv} space. The boundaries are valid for use at S-band.

shows the two-dimensional membership functions for rain from Liu and Chandrasekar (2000). In addition to the membership function, weighting functions are used for each input (Vivekanandan et al. 1999). Weighting functions are determined based on how well the variable indicates different particle types (Vivekanandan et al. 1999). After the "fuzzification" step is complete, the results are multiplied by the weight of each variable (Vivekanandan et al. 1999). The results from all of the inputs are then summed to produce a single aggregated value for each particle type in the algorithm (Vivekanandan et al. 1999). Then the particle type with the maximum aggregated value is identified as the most likely particle type for the crisp input (Vivekanandan et al. 1999). The fuzzy logic approach has been tested at the S-band by other studies and works well (e.g., Liu and Chandrasekar 2000).

2.5   Modeling Melting Hailstones

One of the possible explanations presented by Vivekanandan et al. (1990), Meischner et al. (1991), and Ryzhkov et al. (2007) for the high Z_{dr} associated with areas of hail is due to melting of small hail in the radar volume. Rasmussen and Heymsfield (1987a) developed a one-dimensional microphysical hail melting model to understand the process of melting hail. The study used equations about the heat transfer between the hailstone and the environment, the terminal velocity of the melting hailstone, and the shedding of liquid water of the melting hailstone. Rasmussen and Heymsfield (1987b) sensitivity tests concluded that the melt model was sensitive to the initial hail density (lower ice density melted quicker), initial size (smaller sizes melted completely), temperature profile (warmer temperature profile more melting), and relative humidity
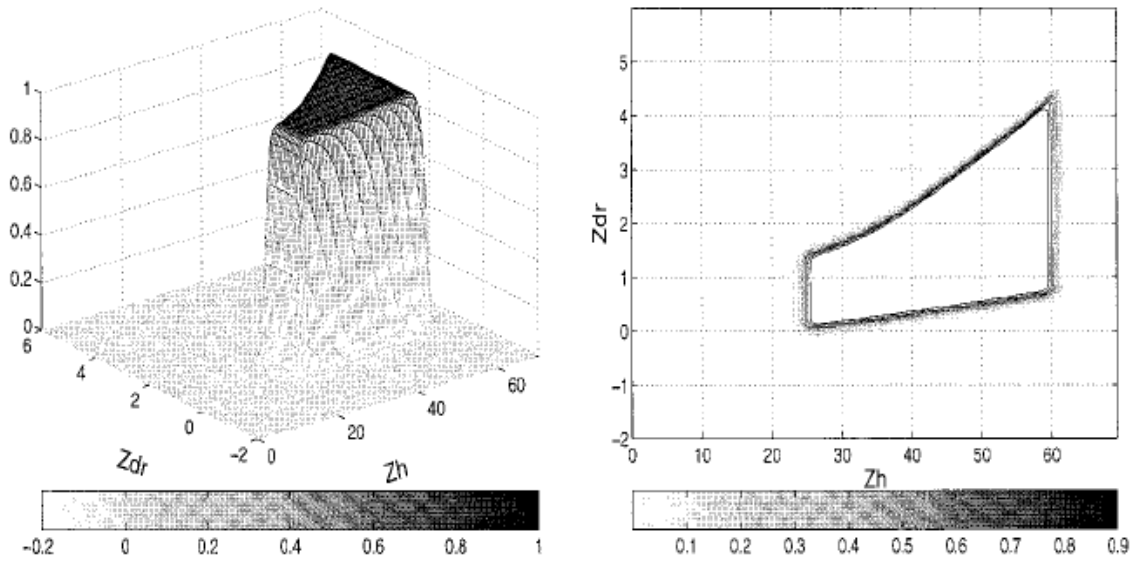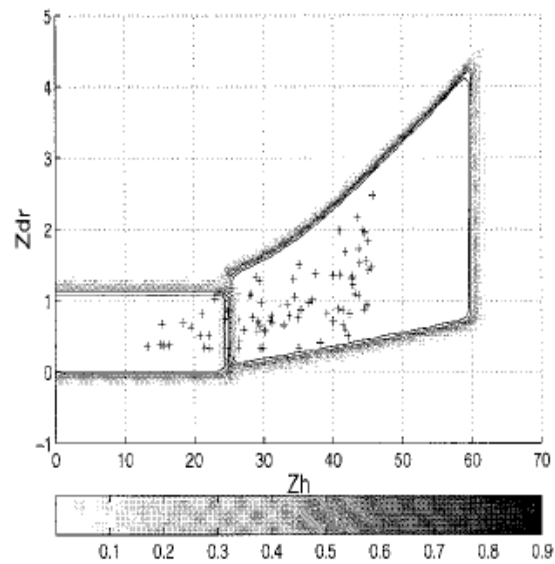
Figure 2.6: Adapted from Liu and Chandrasekar 2000. (a) 2D membership function of Z_h and Z_{dr} for rain, (b) contour of the 2d membership function, (c) scatterplot of Z_h and Z_{dr} for rain with the contour of the membership function.

(higher relative humidity quicker melting). Meischner et al. (1991) derived a figure of the melting process of a 7.3 mm melting hailstone. The figure shows how the hailstone becomes oblate as it melts and can appear as a giant raindrop. Ryzhkov et al. (2009) used the Rasmussen and Heymsfield (1987a,b) melt model to investigate possible effects of melting hailstones on C-band radar. From the assumptions in the study, Ryzhkov et al. (2009) find that all hailstones smaller than 1.4 cm melt completely before they reach the ground while larger hailstones reach the ground with only minor changes. The study concludes that the high concentration of large rain drops (from melting hail and shed drops) contribute significantly to Z_{dr} and thus produce large values greater than 5 dB, while larger melting hailstones contribute little and should produce lower Z_{dr} (< 2 dB). In this instance the number of concentration would outweigh the effects of diameter in equation 2.5. In equation 2.5, diameter is to the sixth power and should be most sensitive to the largest particles in the radar volume (e.g., large hail).

In this study, the empirical approach was emphasized to unambiguously determine the polarimetric signatures of hail at the C-band. As a result, the complex melt model was beyond the scope of this study. The model would have been helpful to determine the behavior of a melting hailstone. However, the T-matrix was used to calculate the polarimetric variables of melting hailstones. The T-matrix Mueller matrix modeling approach is similar to the approach used in other studies (e.g., Kennedy et al. 2001, Dupue et al. 2007). Assumptions about melting hailstones were used in the T-matrix from previous studies discussed in this section. A number of simulations were run using the T-matrix to try and determine what polarimetric signatures for hail and rain hail mixtures can be expected at the C-band.

CHAPTER 3

DATA AND METHODOLOGY

In order to achieve the objective of better characterizing the C-band polarimetric signatures of hail, a dual approach utilizing both radar observations and modeling will be implemented. Because of the limitations of the radar model, the emphasis of this study will be on the observations. However, some knowledge can be gained by using the radar model if careful assumptions are made and their sensitivity tested.

3.1 Case Selection

The geographical domain for this study is defined by the useful range of the ARMOR C-band polarimetric radar, which is situated in the Tennessee Valley area of Northern Alabama and South Central Tennessee (Figure 3.1). The period used in this study ranges from 2005 to 2010. Events ranged in season from warm to cool. There were a total of 9 events investigated in this study involving 46 different cells and 172 reports of hail. The overview of the events can be seen in Table 3.1. Figure 3.2 is a histogram that shows the distribution of reports relative to the radar. Figure 3.2 reveals a minimum, mean, and maximum distance from the radar as 4, 34, 99 km with a median of
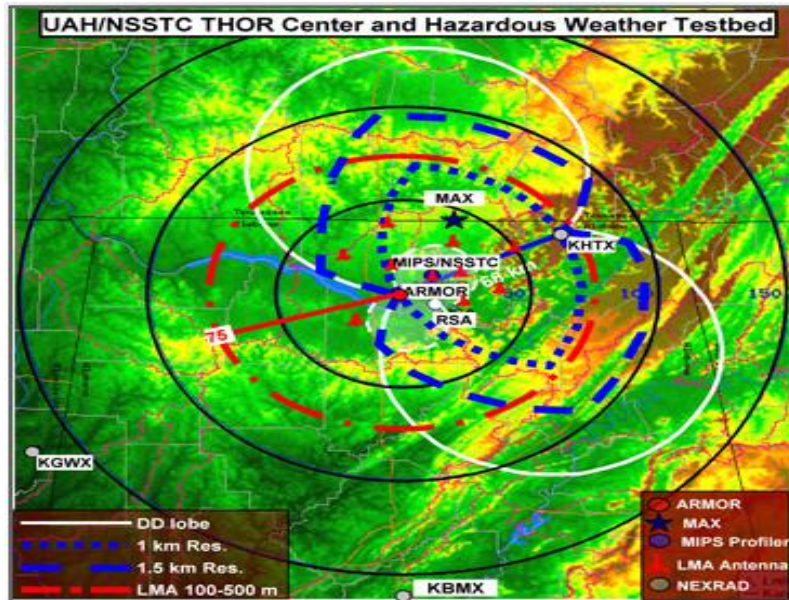
Figure 3.1: Location of the ARMOR radar relative to the Hytop NEXRAD radar, and Redstone Arsenal (RSA).

Table 3.1: Overview of Events

Date	Number of Cells	Number of Hail Reports
February 21, 2005	9	25
April 3, 2007	2	9
March 15, 2008	4	7
August 2, 2008	4	19
March 28, 2009	4	4
April 10, 2009	5	77
April 13, 2009	3	4
January 21, 2010	2	6
March 12, 2010	10	21
Total:	46	172
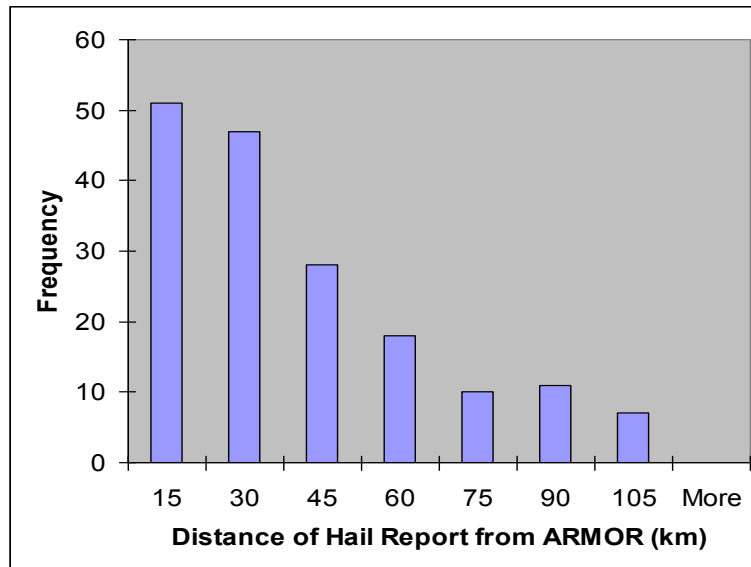
Figure 3.2: Histogram of locations of reports relative to ARMOR. The x-axis is the distance of the report to the radar in kilometers and the y-axis is the frequency of distance in the given bin. The number on the x-axis is the highest size in the bin. Therefore, 30 km contains all reports between the sizes of 15 – 30 km.

23 km. In addition to these events, storm reports on April 7, 2005 were tested but did not meet the quality control criteria outlined in Section 3.2.1.

The event dates were arrived at by looking at archived data from different resources. The National Oceanic and Atmospheric Administration's (NOAA's) National Climate Data Center's (NCDC's) *Storm Data* was used to identify numerous events as well as the Storm Prediction Center's (SPC) event archive webpage that documents Local Storm Report's (LSR's) of severe weather. In some instances, reports of hail were used from the National Weather Service (NWS) Chat. The NWS Chat documents all LSR's of severe and non-severe hail reported to the National Weather Service. The SPC event archive report was used for the March 15, 2008 reports and the NWS Chat was used for

two reports that were below severe criteria. An additional survey was used for the April 10, 2009 widespread hail event as discussed in the next section. All other reports were taken from the NCDC's *Storm Data*.

3.2   Data Collection and Analysis

The locations, magnitudes, and timing of observed severe hail reports were obtained from the National Oceanic and Atmospheric Administration's (NOAA) National Climate Data Center (NCDC) *Storm Data*. Unfortunately, there are several documented cases of error in reporting time and magnitude (e.g., Witt et al. 1998, Trapp et al. 2005). However, this data set is the most accurate for severe storm reports. Temporal and spatial errors can be important when trying to determine the location of hail at the ground. Despite the errors associated these storm reports, the dataset provided by NCDC is still the most accurate in determining what is happening involving severe storm events. Additional care was taken to manually go through each report to determine if the report was reliable.

Each report was evaluated carefully for accuracy in both time and location of the report. Each report was evaluated by comparing archived radar data to the time and locations of the report. If the report did not correspond to a 50 dBZ echo occurrence within plus or minus 15 minutes and 1 km of the report, then the report was thrown out and not used in the study. Archived radar data was loaded into Gibson Ridge Level 2 (GRLevel2) along with place files of storm reports to help determine if criteria for each storm report was met. The 1 km criterion is used to capture all potential hail data points and to account for any inaccuracy in the location of reports. In addition, sensitivity tests

of changing the radius to different lengths are addressed in the Appendix. Also, observational studies have shown the "hail hole" signature to be on the order of 1 km (e.g., Bringi et al. 1986). In addition to this method, Universal Format (UF) read and write routines were used to convert ARMOR files into ASCII files that contained data within 1 km of each hail report. If the ASCII file did not have a reflectivity value greater than 50 dBZ, then the report was not used. In addition, the report had to be within 100 km of the ARMOR C-band radar located at the Huntsville International Airport. The location was important because reports within close proximity of the ARMOR C-band radar have higher resolution data and do not suffer as much from data quality issues such as beam broadening (Ryzhkov 2007). If the report was outside of 100 km range, it was not used in this study. Due to the close proximity of some of the reports to each other, there is the potential that certain radar range gates may be used multiple times. However, a filter was used to identify any radar range gates that are non-unique and remove all duplicate data.

Although most of the reports in the study were obtained using NCDC's *Storm Data*, there were additional methods used to obtain storm reports. In some cases, hail reports were used from the NWS Chat. In the NWS Chat, any hail report that is relayed to the NWS whether it is severe or non-severe hail is reported across the chat as a LSR. This method of receiving storm reports is mostly used for hail that is below severe criteria because hail that meets severe criteria can later be found in *Storm Data*. Another way that hail reports were gathered was using an internet survey. This method was used with the prolific hail producing event of April 10, 2009. The survey was sent out to email addresses from the National Aeronautics and Space Administration's (NASA's) Marshall

Space Flight Center and National Science Space and Technology Center's (NSSTC's) lists. Questions in the survey asked about the size, shape, hail characteristics, location, time, confidence of report, and how the measurements were made. The internet survey generated 55 hail reports of which 41 reports met the quality control specifications and were used in this study. All of the responses in the survey were received from two different storms in the early afternoon due to their close proximity to population centers. The participants in the survey reported hail sizes from 0.5 – 5.7 cm. Surveyors mentioned that the hail contained lumps, lobes, and noticeable growth rings. The shapes ranged from spherical, disc, and oblate with smaller hail being mostly spherical and the large hail mostly oblate. The survey helped to provide a dense network of reports for the April 10, 2009 case.

During this study, the NWS definition of severe hail changed. The definition of severe hail up until January 5, 2010 was defined as hail with a diameter of 0.75 inch or 1.95 cm. After this date, the criterion for severe hail is defined as hail that has a diameter of 1.00 inch or 2.54 cm. However, NCDC *Storm Data* still contains data for reports that are 0.75 inches and above. The only sources of data for hailstones below this size were limited to reports from the NWS Chat and the internet survey conducted for the April 10, 2009 event. Figure 3.3 shows the histogram of the hailstone diameter observed from each report in this study. The histogram reveals that the average hailstone diameter observed is 1.3 inches (3.3 cm), a minimum of 0.25 inches (0.64 cm), and a maximum of 4.25 inches (10.8 cm). The number of reports used below severe hail criteria was small (61) in this study compared to the severe reports used (111) according to the new 1.0 inch (2.54 cm) definition of severe hail (see also Figure 3.1).
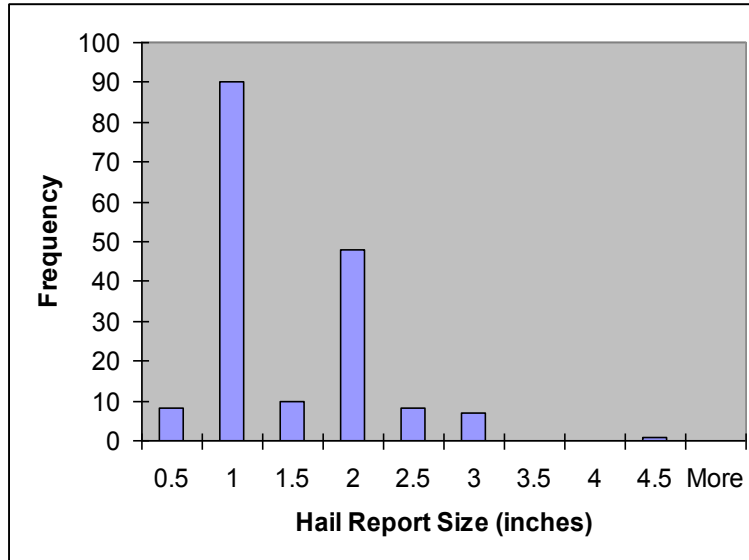
Figure 3.3: Histogram of hail report sizes (inches). The x-axis is the maximum size in the bin in inches and the y-axis is the frequency of reports in the given bin. The number on the x-axis is the highest size in the bin. Therefore, 1.5 contains all reports between the sizes of 1.01-1.50 inches

The data from the hail reports are then evaluated using UF read and write routines. The routine takes the UF and puts the data into an ASCII file. The ASCII file contains data from radar range bins that are located within 1 km of the hail report. The data in the ASCII file includes time, height, elevation angle, latitude, longitude, reflectivity, differential reflectivity, correlation coefficient, specific differential phase, and range. The data are then stored for each hail report and evaluated using Interactive Data Language (IDL). In IDL, the data are put into different bins so that joint frequency histogram plots and other statistical figures can be made to evaluate the polarimetric signatures of hail. The joint frequency histogram plots were made from comparisons of Z_h and polarimetric variables that focus on the lowest 1 km near the surface and height and polarimetric variables in order to evaluate the vertical structure of C-band polarimetric hail signatures. The following bin sizes were consistently used unless

otherwise noted in the histogram plots: 2 dBZ for Z_h, 250 m for height, 0.5 dB for Z_{dr}, 0.01 for ρ_{hv}, 0.5 °km^{-1} for K_{dp}. These joint frequency histograms use absolute frequency to evaluate the C-band polarimetric signatures of hail. In addition, the composite plots are evaluated using joint relative frequency distribution figures where the absolute count in each bin is divided by the total bin count and are expressed in percent. These figures are made for comparisons of Z_h versus Z_{dr}, Z_h versus ρ_{hv}, and Z_h versus K_{dp}. For comparisons of polarimetric variables with height, contoured frequency by altitude diagrams (Yuter et al. 1995) were made. These diagrams are also made by dividing the absolute count in each bin by the total bin count and are expressed in percent. Unlike Yuter et al. (1995), the CFAD values herein were not normalized by bin size. These figures are made for comparisons of Z_{dr} versus height, ρ_{hv} versus height, and K_{dp} versus height. These figures will be evaluated in Chapter 4.

3.3 Polarimetric Radar Data Processing

The instrumentation used in this study is vital to the results that are produced in Chapter 4. In addition, there are many different corrections and continuous testing that are performed on the data to make sure the data quality remains superb. The following section will address the ARMOR C-band radar and corrections that are applied to the data.

3.3.1 Instrumentation

For the observational part of this study, the main instrumentation used is the ARMOR C-band polarimetric radar located at the Huntsville International Airport

(Petersen et al. 2007). Polarimetric implies that ARMOR sends and receives electromagnetic pulses in the horizontal and vertical polarization. The current simultaneous transmit and receive technology that ARMOR sends the electromagnetic pulse is at a 45 ° angle and the computer processing separates the signal into horizontal and vertical components. ARMOR is a C-band radar and has a wavelength of 5.3 cm. The dish diameter on ARMOR is 3.7 m making the beam width 1.0°. The following variables are available for use from ARMOR: Z_h (horizontal reflectivity or just reflectivity hereafter), Z_{dr} (differential reflectivity), Velocity, ρ_{hv} (correlation coefficient), Φ_{dp} (specific differential phase), and K_{dp} (specific differential phase). The K_{dp} used from ARMOR is calculated from a filtering algorithm using Hubbert and Bringi (1995) recommendations. The radar in this study is operated in two modes volume and rain1 scanning modes. The sector volume scan mode involves numerous elevation angles at operator selected azimuth angles that are used to sample the storms well in the vertical. The volume scan mode is the preferred approach used to evaluate supercells that produce hail at the surface. With this method, the vertical structure of the radar variable can be evaluated. The rain1 surveillance scan is the scan the ARMOR runs in routinely. This scan only provides the lowest three elevation angles for all azimuths at five minute intervals. Therefore, this method is not the preferred scanning method because it only captures what is happening near the surface and not what is occurring aloft in the storm. However, this scanning technique is used when the volume scan data is not available. The only two event days that do not contain volume scan data are May 20, 2008 and August 2, 2008. All other dates contain volume scan data that match the time and location of hail reports used in this study.

3.3.2 Attenuation Correction

Attenuation is the reduction of power of the electromagnetic wave that is sent from the radar. The total attenuation at meteorological radar wavelengths is due to both scattering and absorption of energy due to intervening particles. Before using quantitatively, Z_h must be corrected for attenuation. Since Z_{dr} is the ratio of two powers, it is affected by differential attenuation between the vertical and horizontal polarizations. Since large raindrops are oblate spheroids, attenuation can be greater in the horizontal than vertical polarization. For wavelengths larger than 3 cm, the majority of attenuation is due to hydrometeors, with only minor effects from other sources (Hitschfeld and Bordan 1954). Therefore, the main goal of attenuation correction algorithms is to correct for attenuation due to rain. It is evident that attenuation is always a concern when using radar data, but attenuation corrections are available and can be applied.

There have been many different approaches to C-band attenuation correction. One of the first approaches was to calculate specific attenuation from reflectivity and rainfall estimations (Hitschfeld and Bordan 1954). There are large errors associated with this method because it depends on the accurate calibration of the radar and was later determined an impractical approach (Hildebrand 1978). With the advent of dual-polarimetric radar new approaches to attenuation, corrections are possible to correct Z_h and Z_{dr} (Aydin et al. 1989, Bringi et al. 1990, Gorgucci et al. 1996, Carey et al. 2000, Bringi et al. 2001, Tabary et al. 2009). Bringi et al. (1990) proposed using the differential propagation phase (Φ_{dp}) for attenuation correction. The differential propagation phase is the difference between horizontally and vertically polarized waves as they travel through rain (Oguchi 1983). Carey et al. (2000) notes that there are three

advantages to this approach: 1) the differential propagation phase is unaffected by attenuation, 2) independent of radar calibration errors (Zrnic and Ryzhkov 1996), and 3) the specific differential phase is approximately linear proportional to both the specific horizontal and differential attenuation (Bringi et al. 1990). The approach in Ryzhkov and Zrnic (1995) and Carey et al. (2000) uses estimated correction coefficients on an entire radar volume. Carey et al. (2000) also noticed that in areas of large drops where Φ_{dp} is large, the attenuation correction method did not work well and new correction coefficients must be used in these drop resonance (non-Rayleigh or Mie) regions. The resonant scattering region begins to take place at C-band for particles greater than 5 mm (e.g., Zrnic et al. 2000).

The method used operationally on the ARMOR C-band radar is the methodology presented in Bringi et al. (2001). This method builds upon earlier methods (e.g., Bringi et al. 1990, Ryzhkov and Zrnic 1995, Carey et al. 2000, Testud et al. 2000). The Bringi et al. (2001) method uses a Φ_{dp} at range locations beyond the attenuation cell as a constraint. This more sophisticated method uses different values of α and β for each radar ray (Bringi et al. 2001). The total specific attenuation in each ray is integrated and a correction is implemented to the Z_h and Z_{dr} data (Bringi et al. 2001). Recently, attempts have been made to use different α and β within these "large drop," "hot spots," or drop resonant regions in order to make better corrections in these zones (Tabary et al. 2009). Currently, the Bringi et al. (2001) is the only method used in operational attenuation correction for the ARMOR C-band radar.

Overall, ARMOR data has been useful and helpful in a number of studies (e.g., Deierling et al. 2005, Gatlin et al. 2009). In Deierling et al. (2005) ARMOR data was

used to arrive at solutions for the National Center for Atmospheric Research's (NCAR's) Particle Identification (PID). The results from using the NCAR PID require that accurate attenuation corrections have been made to Z_h and Z_{dr} to arrive at reasonable results (Bringi et al. 2001). In addition, Gatlin et al. (2009) has demonstrated that ARMOR data using the Bringi et al. (2001) algorithm are useful in making accurate rainfall estimations across the Tennessee Valley. This study helps the Tennessee Valley Authority (TVA) make decisions about their water resources management. In order to make accurate rainfall estimations, attenuation must be accurately corrected (Bringi et al. 2001). Attenuation corrected ARMOR data in this study appears reasonably accurate as well from the joint frequency histograms and Plan Position Indicators (PPIs) that will be examined later. There are also a few instances where Bringi et al. (2001) methodology may lead to an under-correction of Z_h and Z_{dr} and these cases will be discussed in later sections. Borowska et al. (2009) mentions that in the case of strong hail bearing storms, the Bringi et al. (2001) approach can under estimate the attenuation and differential attenuation. If this is the case, then even higher Z_h and Z_{dr} would be expected in hail producing cells.

3.3.3 Z_{dr} Calibration

The ARMOR C-band radar routinely does Z_{dr} calibrations based on the "bird bath scanning" technique (Gorgucci et al. 1999). The method involves pointing the radar vertically at known targets such as light rain and drizzle. At this angle, all hydrometeors should appear to the radar as near spherical with Z_{dr} of near 0 dB. Gorgucci et al. (1999) states that any non-zero value can be attributed to radar system bias between the

two polarization channels. After the vertical scan, the data is assessed and a correction is implemented if the Z_{dr} is off by more than 0.2 dB. The "bird bath" technique is used on the ARMOR C-band radar whenever the right meteorological conditions present themselves. In this study, there is only one instance where the correction is off by more than 0.2 dB. On April 4, 2007 the "bird bath" scan was used and found a -0.38 dB bias in the Z_{dr} data. This correction was then added into the Z_{dr} used from the event on April 3, 2007. Additionally, the joint frequency histograms in this study show Z_{dr} consistently near 0 dB above the 0 °C level which is what would be expected when ice particles, which are spheres or "effective spheres," are present. This further illustrates the accuracy of the data utilized in the study. Correctly assessing biases associated with Z_{dr} is important so that correct analysis of polarimetric variables can be made in this study.

3.3.4 Z_h Self Consistency Calibration

The Z_h calibration method used with ARMOR is the self consistency approach presented by Ryzhkov et al. (2005). The difference between the measured and actual Z_h is what is known as the Z_h bias. The bias can be both negative and positive. If the bias is negative (positive), then the bias is added (subtracted). Ryzhkov et al. (2005) suggests that the calibration of Z_h should be within 1 dB. The self consistency method of Z_h calibrations uses both Z_{dr} and K_{dp}. The physical basis of the method relies on the fact that $Z_{h,}$, Z_{dr}, and K_{dp} are not independent in rain (Ryzhkov et al. 2005). Therefore, an estimation of Z_h can be made from the measured Z_{dr} and K_{dp}. Of course, there are a few assumptions with this method. The method assumes that Z_{dr} is well calibrated (0.2 dB accuracy) because if Z_{dr} is not calibrated well, then the method will arrive at an incorrect

estimation of Z_h. Attenuation and differential attenuation must be corrected to arrive at correct values for Z_h and Z_{dr} in order for the method to work. Another assumption is that the method only works on rain because of the idea that Z_h, Z_{dr}, and K_{dp} are not independent in the rain medium. This means that there can be no ice involved in the calibration, so it must be used well below the 0 °C level where no ice is found. In addition, using a ρ_{hv} threshold can be helpful by eliminating most non-rain particles. The method must be limited to Z_h values that would be expected to be found with rain (30 – 45 dBZ). The method must also be sure that ground clutter is not being used in the

Table 3.2: Z_h and Z_{dr} bias

Date	Z_h Bias	Z_{dr} Bias
February 21, 2005	- 0.70 dB	N/A
April 3, 2007	- 1.72 dB	- 0.38 dB
March 15, 2008	- 1.43 dB	- 0.15 dB
August 2, 2008	- 1.45 dB	+ 0.15 dB
March 28, 2009	+ 0.70 dB	- 0.08 dB
April 10, 2009	- 2.21 dB	N/A
April 13, 2009	- 2.16 dB	N/A
January 21, 2010	+ 0.82 dB	N/A
March 12, 2010	- 0.08 dB	N/A

sample as well. After all these issues are resolved, the calculation can be made and the calculated Z_h can be compared to the actual Z_h and the bias can be assessed.

The self consistency method was used on the nine hail cases examined in this study. The intent of the study is to have no more than a 2 dB bias in the Z_h data because of the 2 dB bin size of the histograms presented in Chapter 4. If the bias is greater than 2 dB, the bias is added or subtracted. The study used Z_{dr} bias data obtained from the routine "bird bath" calibration method found in the previous subsection. The Z_h values were limited to $37 - 45$ dBZ so that only rain was used in the calibration. The 0 °C level was determined by looking at forecast soundings from the Rapid Update Cycle (RUC) model. The sample was limited to radar range gates that were 1 km below the 0 °C level to assure that there would be no ice in the sample. Additionally, there was a ρ_{hv} threshold of ≥ 0.95, where only rain is expected (Carey et al. 2000). The results can be seen in Table 3.2. The results for the self consistency calibration method reveal that only three of the dates used in the study have a bias of 2 dB. Those dates are April 3, 2007, April 10, 2009, and April 13, 2009. The negative bias in all three cases was subtracted from the data. The results from January 21, 2010 indicate a Z_h bias of $+ 3.07$ dB using the self consistency method (Ryzhkov et al. 2005). This bias was calculated on a day with an isolated cell that contained resonant sized particles that caused insufficient filtering of δ (backscatter differential phase) that led to incorrect values of K_{dp} and large errors in the self-consistency method. Therefore, for this case, the reflectivity from ARMOR was compared to the reflectivity from the Hytop NEXRAD WSR-88D radar. Because of the relatively close proximity of these two radars, there are sufficient radar range gates in which radar reflectivity should be approximately the same under good sample and

Rayleigh scattering conditions. This analysis compared 3 different times for this date that revealed the bias was + 0.82 dB. All other dates remained unchanged because the biases did not exceed the threshold for this study of 2 dB.

3.4   Radar Modeling

3.4.1   T-matrix

In addition to looking at signatures of hail using C-band polarimetric radar, a model was used as well. One of the two models is the transition (T) matrix developed by Waterman (1971). The T-matrix provides the backscattering and forward scattering properties of the modeled hydrometeors. There are many assumptions that the T-matrix makes. One of the key limitations for this study is that the model assumes that all hydrometeors are smooth oblate spheroids. Although the T-matrix is a highly sophisticated model, it is unable to simulate lumps and lobes such as those often observed on the surface of hailstones. Another limitation is that many assumptions have to be made about the hydrometeor. The user must be able to determine the size, shape, and dielectric of the hydrometeor. The dielectric is a property of the state of the hydrometeor and the temperature of the surface of the hydrometeor and is determined from Ray (1972). Ice density is assumed to be 0.917 gcm^{-3} if solid ice is used. Another limitation of the T-matrix is that it assumes refractive index of the ice is uniform even though the refractive index for ice may vary (Depue et al. 2009). The model is able to calculate a variety of sizes of a particular hydrometeor type. The one layer T-matrix is only useful for a hydrometeor with one dielectric.

However, the more advanced two-layer T-matrix is able to calculate the backscattering and forward scattering properties of hydrometeors with two dielectrics. In this case, the T-matrix is able to model more sophisticated hydrometeors such as melting hail with an inner layer of ice and an outer layer of water. The user can change the size of the inner and outer layer of the hydrometer producing a variety of different ice to water fractions. The two-layer T-matrix possesses all of the same strengths and limitations of the one layer T-matrix except for its ability to model hydrometeors with two different dielectric stengths.

3.4.2 Mueller Matrix

The other model used in this study is the Mueller matrix. The Mueller matrix uses the T-matrices of individual particles as input to give radar backscattering and forward scattering observable integrated over different size distributions (e.g., monodisperse, exponential, and gamma). In addition, the Mueller matrix is used to provide the backscattering and forward scattering for various orientations of the particles symmetry axis (canting angle) and for various radar elevation angles (Vivekanandan et al. 1991). In this study, the elevation angle for the simulations remained constant at 0°. For the scan strategies, heights, and ranges employed in this study, the elevation angle remained fairly small and rarely exceeded 15°. Hence, the modeled 0° elevation angle should be generally representative of the observations in this study. Two different orientation models can be used in the Mueller matrix simple harmonic and Gaussian. In this study, the Gaussian orientation model was used for all simulations (Vivekanandan et al. 1991). Additionally, a standard deviation of the canting angle for each particle must

be used where a high standard deviation indicates a particle that tumbles ($\sim$ 45°) and a low standard deviation ($\sim$ 5°) suggests that the particle falls rather stable. The Mueller matrix allows calculations of polarimetric variables Z_{dr} (differential reflectivity), K_{dp} (specific differential phase), and δ (backscatter differential phase) for different mixtures and types of hydrometeors. However, with the limitation of the T-matrix and Mueller matrix, the modeling results should only be regarded as approximations of the polarimetric signatures observed from hailstones that occur in nature.

3.4.3 Modeling Assumptions

As discussed in the previous sections, there are a number of assumptions that go into calculating the T-matrix and Mueller matrix. The model was used in this study to determine what the C-band polarimetric signatures of hail should be using reasonable assumptions that the model needs. Most of the assumptions needed are about the microphysics of the hydrometeors including size, shape, orientation, and fall mode. The range of sizes used for hail in this study range from 0.5 − 7.0 cm. The shapes of hailstones vary from axis ratios of 0.6 to 0.8 (Knight 1986). Fall modes of hailstones are debated in the literature. There are studies that suggest hailstones fall with their major axis horizontal (List et al. 1973) while other studies suggest that large hail falls with its major axis vertical (Zrnic et al. 1993). For this study, both orientations were tested to analyze results from different assumptions. In addition to the fall mode, assumptions have to be made about the standard deviation of the canting angle. Many studies suggest that hail tumbles at it falls (e.g., Knight and Knight 1970). The idea that hail tumbles as it falls is a fundamental premise behind the S-band "hail hole" concept. The theory is

that hail tumbles and therefore appears to the radar as an effective sphere. However, if there is a water film or torus on the hailstone, then there is the possibility hail does not tumble but falls stable with limited canting (Rasmussen and Heymsfield 1987). In this study, both tumbling and stable hailstones are considered. Herein, stable hailstones are limited to those with a water torus. The two layer T-matrix is used in this study to model melting hailstones. Water torus thickness remains constant across the modeled hailstones in this study at 0.5 mm (Depue et al. 2009) even though other studies involving wind tunnels suggest that the water torus thickness varies as a function of shape and size (Rasmussen and Heymsfield 1987). This assumption is one of the key limitations of accurately modeling melting hailstones in the study. Lastly, assumptions have to be made about the hailstone size distributions. In the literature, there is no clear consistency on what type of distribution best characterizes hail size, including monodisperse (Auer and Marwitz 1972), exponential (Cheng and English 1982), and gamma (Ziegler et al. 1983). Due to the uncertainty of hailstone size distribution, all three types are explored in this study. The model provides radar variables for the hydrometeors but is highly dependent upon the assumptions made by the model and by the user.

3.5   Hydrometeor Identification

Studies have shown that polarimetric radar can help determine what type of hydrometeor is being observed (e.g., Vivekanandan et al. 1999, Straka et al. 2000, Zeng et al. 2001). It is important to be able to classify different types of hydrometeors so that quick and effective warnings can be issued. There have been two different approaches to

hydrometeor identification, Boolean (decision tree) logic (e.g., Straka et al. 2000, Zeng et al. 2001) and fuzzy logic (e.g., Vivekanandan et al. 1999, Liu and Chandrasekar 2000).

The first approach Boolean logic is a decision tree or flow chart logic. The logic uses polarimetric radar variables to best determine what type of hydrometeor is observed. The hydrometeors are determined by the polarimetric radar variables and have hard boundaries. The value of the polarimetric radar variable either falls into the true or false category for the hydrometeor type. If the polarimetric radar data is outside of this true criterion, it cannot be that hydrometeor type. Using Boolean logic there can also be many hydrometeor types that overlap (Straka et al. 2000). This overlap can lead to uncertainty about what hydrometeor type is being observed. Boolean logic can also lead to radar range gates that do not correspond to any hydrometeor type due to the rigid boundaries. Straka et al. (2000) explains that confidence is not high with this method and uncertainty exists determining hydrometeor type and a new method is needed to account for this uncertainty and overlap in Boolean logic.

The fuzzy logic approach in this study is from the National Center for Atmospheric Research's (NCAR's) Particle Identification (PID) (Vivekanandan et al. 1999). There are eight polarimetric radar inputs used in the algorithm (Z_h, Z_{dr}, K_{dp}, ρ_{hv}) a temperature profile and three variables derived from radar data (the standard deviations of velocity, Z_{dr}, and Φ_{dp}). The three standard deviation variables are used in the algorithm to separate meteorological targets from clutter. The NCAR PID provide 17 different particles types including cloud, drizzle, light rain, moderate rain, heavy rain, hail, rain and hail mixture, graupel small hail, graupel rain, dry snow, wet snow, ice crystal, irregular ice crystals, supercooled liquid drops, flying insects, second trip, and

51

ground clutter. Fuzzy logic is useful for hydrometeor identification because it does not have hard boundaries and allows for overlap of different particle types, two of the setbacks to the Boolean logic approach. The PID uses 2-dimensional membership functions to determine the degree to which input indicates a specific output. For each particle type, the membership function has a value from 0 to 1 for an input from a radar range gate. The data from the radar range gates is given a value from each membership function and the particle type with the highest score is selected. In addition, thresholds are applied for different hydrometeor types. For example, wet snow cannot exist for temperatures above 3 °C or below -3 °C. The accuracy of the NCAR PID is highly dependent upon the radar providing accurate data to be used as input into the algorithm.

The version of this program used in this study was modified by Deierling et al. (2008) for use at the C-band. Some adjustments were made by Deierling et al. (2008) to the membership functions at the S-band to make them suitable for the C-band. The Z_h and Z_{dr} membership functions for moderate and heavy rain were shifted up slightly by 0 to 2 dB higher than the S-band for the C-band because of resonant effects at the C-band. In addition, the Z_h and K_{dp}, membership functions of moderate and heavy rain were shifted up slightly higher by 0.2 to 2 °km^{-1}. The membership functions of Z_h and ρ_{hv} for heavy rain are shifted down by 0.03 for the C-band compared to the S-band. The hail membership functions are only changed slightly for Z_h and Z_{dr} is only shifted up by 0.2 dB, for Z_h and K_{dp} is shifted up by 0 to 1 °km^{-1}, and for Z_h and ρ_{hv} is shifted down by 0.1 from the S-band membership functions. The modifications in the membership functions are due to the difference in wavelength between the C-band and S-band particles. The membership functions currently used in the NCAR PID modified by

Deierling et al. (2008) are evaluated in this study to see how well they detect hail in areas were hail is reported. The modified version is run on data located within 1 km of a hail report to determine what are the most common particle types detected in the region. Also, suggestions are made to modify membership functions to fit the joint frequency histograms from the observed radar data within 1 km of a hail report. The NCAR PID is then modified to the joint frequency histograms to evaluate the sensitivity of the algorithm. The NCAR PID produces sweep files that can be used in the radar editing software SOLOII, also developed by NCAR.

CHAPTER 4

OBSERVATIONS

The study focuses on hail producing thunderstorms in the Tennessee Valley from February 2005 to March 2010. No seasonal limits are placed on the thunderstorms examined because hail can be produced at any time of the year in the Tennessee Valley. An attempt is made in the study to examine the polarimetric signatures of several types of convection including supercells, pulse thunderstorms, tornadic thunderstorms, and line echo wave patterns. Polarimetric signatures of hail will be analyzed from 9 events, 46 different cells, and 172 hail reports. Section 4.1 will examine in detail the polarimetric signatures of three of these events that produced a large number of hail reports that met the criteria to be used in this study. A composite of all reports will also be analyzed to look at the overall signature of the events. In addition, another case that did not meet storm report criteria will be examined in the section for "hail hole" potential. The signatures will be examined to carefully document the C-band polarimetric signature of hail.

4.1   Empirical Results

The following section is organized as a complete polarimetric overview of the three most prolific hail producing events in this study: April 10, 2009, February 21, 2005, and August 2, 2008. These events will be analyzed to carefully document the C-band polarimetric signatures of hail. The other seven events will address the Z_{dr} signatures only. The Z_{dr} signature will be more thoroughly examined because other studies (e.g., Meischner et al. 1991, Ryzhkov et al. 2007, Kumjian and Ryzhkov 2008) have noted that there appear to be clear differences in Z_{dr} for hail at the S- and C-bands.

4.1.1   April 10, 2009

Severe thunderstorms affected the entire Southeast US as a storm system moved across the region. The Storm Prediction Center (SPC) issued a high risk for severe storms across north Alabama, southern middle Tennessee, and northeast Georgia. Supercells associated with significant wind shear and instability, developed ahead of the cold front early in the day across north Mississippi and western Tennessee. The storms then tracked across north Alabama and south Tennessee in the early afternoon. The most significant storm to impact the Southeast US produced an EF-4 tornado in Murfreesboro, TN. There was also an EF-3 tornado that affected north Alabama in Marshall, Jackson, and Dekalb counties. The event also produced 85 reports of severe hail with a range of sizes from 0.25 – 4.25 inches (0.64 – 10.80 cm) with a mean of 1.56 inches (3.96 cm) , by far the largest number of hail reports, across the Huntsville National Weather Services (NWS) County Warning Area (CWA).

The joint frequency histogram of Z_{dr} versus Z_h (Figure 4.1a) from the radar range gates located within 1 km of the hail reports are characterized by anomalously high Z_{dr} for areas of high Z_h. There is a Z_{dr} mode of 5 dB that occurs at 54 dBZ with over 400 gates falling into this location. Maximum Z_{dr} values are observed as high as 10 dB (Figure 4.1a). For the Z_h bin from 55-57 dBZ, the 25th, 50th, and 75th percentiles of Z_{dr} are 4.04, 5.61, and 7.02 dB with a mean of 5.42 dB. This indicates that 50 % of the Z_{dr} data within the 55 – 57 dBZ bin can be found between 4.04 and 7.02 dB. These results are similar to what was found in Meischner et al. (1991). However, the anomalously high Z_{dr} observed in Meischner et al. (1991) is theorized to be due to smaller melting hailstones that appear as large raindrops to the radar. When melting occurs, the water torus on the outside of the drop can become sufficient enough to stabilizing the drop (Rasmussen and Heymsfield 1987a). In this case, one would expect high Z_{dr}. Zrnic et al. (2000) notes that particles over 5 mm at the C-band are in the resonant scattering regime and can cause peaks in Z_{dr} for particles greater than 5 mm. All hailstones in this study are well over 5 mm; therefore, resonant scattering could be contributing to the anomalously high Z_{dr}. However, there is no certainty that only hail and melting hail is present in the data set and other factors, such as rain, could be contributing to the signatures.

In addition to analyzing the Z_{dr} and Z_h polarimetric signatures, the hail signal H_{dr} developed by Aydin et al. (1986) for use at the S-band was plotted (Figure 4.1a). Aydin and Giridhar (1992) suggest that this method can be transferred and applied to the C-band with little modification. The solid red line in Figure 4.1a is where H_{dr} is 0 dB. Areas to the right and bottom of the line are where H_{dr} is positive and is taken to signify the region of hail, while areas to the left and top of the line are where H_{dr} is negative and is assumed
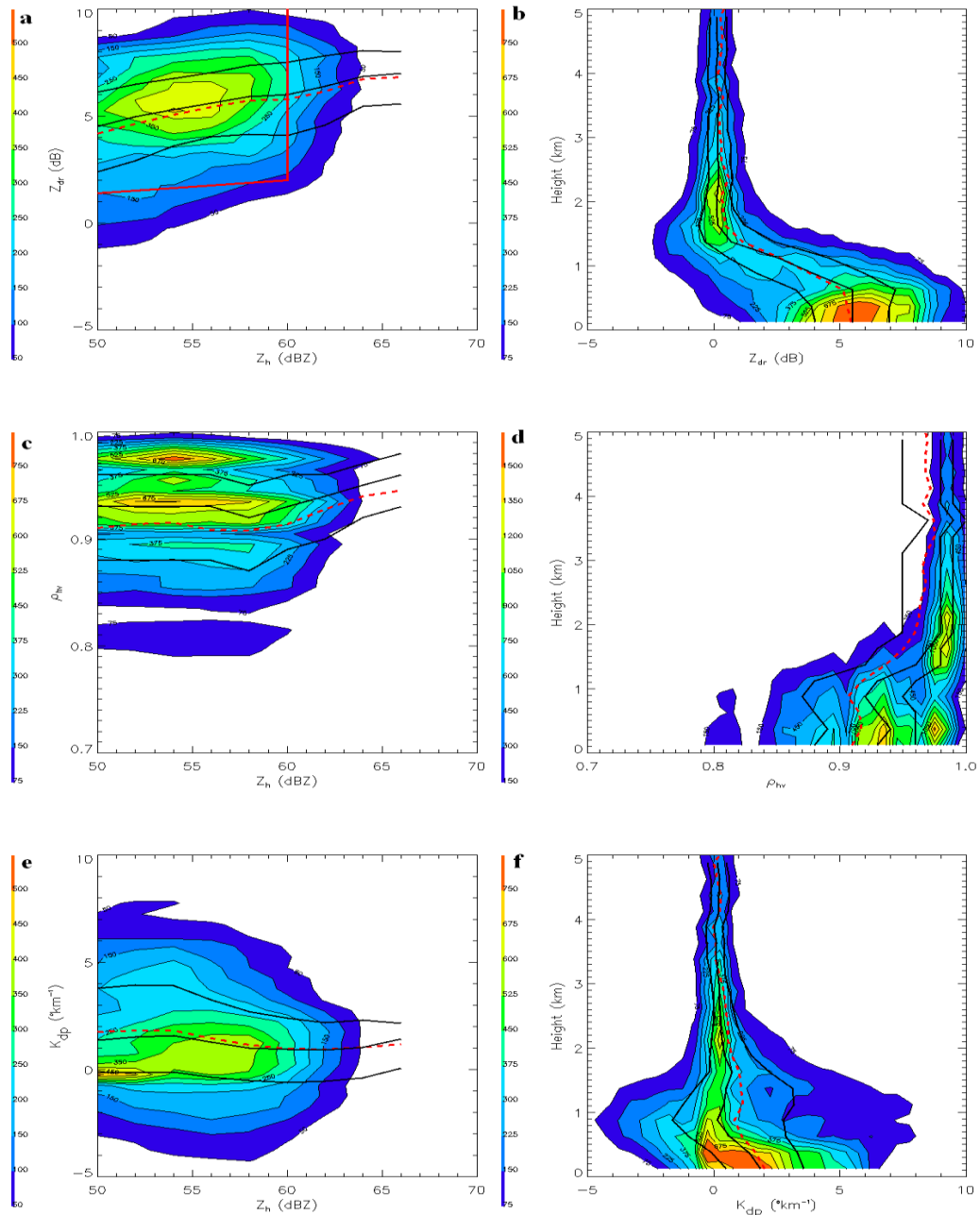
Figure 4.1: Joint frequency histograms of (a) Z_{dr} versus Z_h, (b) Z_{dr} versus height, (c) ρ_{hv} and Z_h, (d) ρ_{hv} versus height, (e) K_{dp} versus Z_h, and (f) K_{dp} versus height. All data is below 1 km for figures (a),(c), and (e) and within a 1 km radius of a hail report from April 10, 2009 data set for all figures. The Z_h data is in 2 dB bins, the Z_{dr} is in 0.5 dB bins, the K_{dp} data is in 0.5 °km^{-1} bins, the ρ_{hv} data is in 0.01 bins, and the height data is in 250 m bins. The 0 °C level for this case is at 3 km. The black lines from bottom to top are the 25th, 50th, and 75th percentile lines (a,c,e) and from left to right the 25th, 50th, and 75th percentiles (b,d,f) with the dashed red line is the mean (a-f). The solid red line in (a) is where H_{dr} = 0 dB.

57

to be regions of rain (Aydin et al. 1986). It can be seen that just the opposite occurs in the C-band ARMOR observations of April 10, 2009. Most of the hail observations fall on the negative side of the plot where rain is expected at the S-band except for the points greater than 60 dBZ where Aydin et al. (1986) assumes data above this value are associated with hail. These results indicate that the conventional behavior of the S-Band Z_h and Z_{dr} does not apply at C-Band for this hail event.

A striking result that goes against traditional S-Band knowledge can be found in the joint frequency histogram of Z_{dr} versus height Z_{dr} (Figure 4.1b). The 0 °C level indicated on the 17 UTC sounding from Redstone Arsenal, located 8 km to the east of the ARMOR C-band polarimetric radar, is around 3 km. Z_{dr} in this example is around 0 dB above the 0 °C level, which is what has also been observed at the S-Band. As the hail continues below the 0 °C level, Z_{dr} begins to increase toward high positive values with a mode near the surface of 5.5 dB and a maximum of near 10 dB, which is unlike past S-Band studies. For the height bin from 0 to 250 m, the 25th, 50th, and 75th percentiles of Z_{dr} are 4.03, 5.47, 6.93 dB with mean of 5.45 dB while well above the 0 °C level at the 4 to 4.25 km bin the 25th, 50th, and 75th percentiles of Z_{dr} are -0.22, 0.10, and 0.46 with a mean of 0.23 dB. This indicates that near the surface (0 – 250 m) 50 % of the Z_{dr} data occurs between 4.03 and 6.93 dB while aloft the distribution of data is more narrow with the 50 % of data occurring between -0.22 and 0.46 dB. Therefore, near the surface, resonant sized (> 5 mm at the C-band), stably oriented and melting hailstones are likely influencing the Z_{dr} results. The increase in Z_{dr} takes place below 2 km where the hailstones have likely had enough time to begin to melt and likely develop a sufficient water torus.

When comparing the joint frequency histogram of ρ_{hv} versus Z_h histogram (Figure 4.1c), the signatures are similar to what has been observed at the S-Band for situations involving hail (e.g., Balakrishnan and Zrnic 1990b). There is a ρ_{hv} mode of 0.975 with Z_h between 53-55 dBZ with a secondary mode of ρ_{hv} of 0.935 with a Z_h of 53 dBZ. For the Z_h bin from 55-57 dBZ, the 25th, 50th, and 75th percentiles of ρ_{hv} are 0.88, 0.93, and 0.96 with a mean of 0.91. These percentiles are most likely lower than the mode because ρ_{hv} ranges from 0.60 – 1.00 and outliers in the range of 0.60 – 0.80 are most likely lowering the percentiles. Previous studies have observed that ρ_{hv} in pure rain can drop as low as 0.94-0.95 at the C-Band because of resonant effects at shorter wavelengths (Zrnic et al. 2000, Keenan et al. 2000, Carey et al. 2000). Therefore, the secondary mode and minimum near 0.80 suggests that the radar volumes in this study likely contained a mixture of rain and melting hail in the resonant region (Tabary et al. 2009). Balakrishnan and Zrnic (1990b) explained possible reasons for drops in ρ_{hv}, such as Mie scattering, irregular shaped hydrometeors, a mixture of hydrometeors, and a variety of hydrometeor shapes. Therefore, it is possible that there was a mixture of hydrometeors including rain and hail. It also suggests that the lobes and lumps from the hail observed by the participants in the study could have contributed to the lowering in ρ_{hv} along with hydrometeors in the resonant sized region (> 5 mm at the C-band).

Clear distinctions can be made for ρ_{hv} above and below the 0 °C level. Above the 0 °C level, ρ_{hv} is near unity indicating a uniform hydrometeor type such as hail (Figure 4.1d). Below the 0 °C level, a decrease in ρ_{hv} occurs with a secondary mode near 0.935, which is indicative of hailstones with irregular shapes and that there is likely a variety of hydrometeors below the 0 °C level along with resonant sized hydrometeors

(Balakrishnan and Zrnic 1990b).   For the $0 - 250$ m bin, the 25th, 50th, and

75th percentiles of ρ_{hv} are 0.88, 0.93, and 0.96 with a mean of 0.91 while well above the

$0 \,°C$ level in the 4-4.25 km bin the 25th, 50th, and 75th percentiles of ρ_{hv} are 0.95, 0.98,

0.99 with a mean of 0.97. Therefore, the lowering of ρ_{hv} can be attributed to a variety of

possibilities such as resonance (large rain drops and/or wet hail), irregular shaped

hydrometeors (hail with lumps and lobes), and a mixture of hydrometeors (rain and hail).

All of these interpretations are generally consistent with the hail reports.

        The distribution of the joint frequency histogram of K_{dp} versus Z_h (Figure 4.1e) is

consistent with prior S-Band studies. One of the nuances of K_{dp} is that it is proportional

to frequency. Therefore, for the same particle conditions K_{dp} should roughly two times

higher at the C-band than at the S-band. The mode for the figure occurs at $0 \,°km^{-1}$ for K_{dp}

at the lower end of Z_h (< 53 dBZ); as Z_h increases to 53 dBZ, the K_{dp} mode become

slightly positive ($0 - 2 \,°km^{-1}$). For the Z_h bin from 55-57 dBZ, the 25th, 50th, and

75th percentiles of K_{dp} are -0.36, 1.28, and $3.25 \,°km^{-1}$ with a mean of $1.46 \,°km^{-1}$. This

indicates that 50% of the K_{dp} data in the Z_h bin of 55-57 dBZ are between -0.36 and

$3.25 \,°km^{-1}$. Specific differential phase (K_{dp}) depends only on the hydrometeor size,

shape, orientation, and number concentration. When K_{dp} is near zero, this indicates that

the targets are isotropic (Balakrishnan and Zrnic 1990a). Therefore, it has been observed

that near $0 \,°km^{-1}$ K_{dp} is associated with hail in the case of high Z_h (Balakrishnan and Zrnic

1990a). There is a secondary maximum that occurs near $4.5 \,°km^{-1}$ and 53 dBZ. It is

theorized that this maximum may occur in an area where heavier rain is mixed with the

hail. Assuming that the hail is isotropic and doesn't contribute to K_{dp}, the rain rate is

calculated at 58 mm/hr in this area using K_{dp}-based calculations at the C-Band (Aydin

and Giridhar 1992). The secondary maximum was caused specifically within one cell that might have produced more of a mixture of rain and hail. The values of K_{dp} near 4.5 $^{\circ}$km^{-1} in this secondary maximum are more associated with values found in rain from the C-Band at the specified Z_h values (Bringi et al. 1991).

It can been seen in the joint frequency histogram of K_{dp} versus height that K_{dp} is consistently near 0 $^{\circ}$km^{-1} above the 0 $^{\circ}$C level but becomes rather noisy below (Figure 4.1f). The near 0 $^{\circ}$km^{-1} mode above the 0 $^{\circ}$C level suggests hydrometeors above the 0 $^{\circ}$C level are probably tumbling and canting and appear to the radar as effective spheres (e.g., isotropic), but below the 0 $^{\circ}$C level, K_{dp} values range from -5 to 7 $^{\circ}$km^{-1}. The mode, however, stays near 0 $^{\circ}$km^{-1}. For the 0 – 250 m bin, the 25th, 50th, and 75th percentiles of K_{dp} are 0.50, 1.85, and 3.56 $^{\circ}$km^{-1} with a mean of 2.03 $^{\circ}$km^{-1} while well above the 0 $^{\circ}$C level in the 4.0-4.25 km bin, the 25th, 50th, and 75th percentiles of K_{dp} are -0.22, 0.10, and 0.46 $^{\circ}$km^{-1} with a mean of 0.24 $^{\circ}$km^{-1}. Ryzhkov et al. (2007) suggested that K_{dp} may be useful for identifying regions of hail at the C-Band. However, the overall noisiness of the K_{dp} observations suggests that it may have limitations in reliably distinguishing between areas of rain, hail, and their mixtures because significant overlap may occur for different hydrometeor types using K_{dp}. Since it is one-half the range derivative of the already, the noisy differential propagation phase, K_{dp}, can be a particularly noisy field (e.g., Bringi and Chandrasekar 2001, p. 548-550). The combination of random and systematic errors in K_{dp} and intrinsic variability of K_{dp} in a rain and hail mixture could make it difficult to use reliably to locate hail at the C-Band. Smyth et al. (1999) suggest that oblate hail can cause non-zero values of K_{dp} in hail due to both the intrinsic positive propagation phase and the improperly removed backscatter

phase during resonance, further complicating the matter at the C-Band. The joint

frequency histogram provides important insight into the polarimetric signatures that are

occurring around hail.

In addition, the Plan Position Indicator (PPI) can provide additional information

about the signatures of hail producing storms. The PPI shows a storm in close proximity

to the radar (10-15 km) crossing over highly populated areas where a large number of

reports were received (Figure 4.2-4.7). The PPI is taken from the lowest elevation scan

of 0.7° and should show a good representation of the polarimetric variable closest to the

surface. The circles in Figures 4.2-4.7 are the 1 km radius circles around each hail report.

There is some overlap in some of the circles, but as discussed in Chapter 3, a filter was

put in place to eliminate any duplicate data. The corrected Z_h shows areas in the cell of

high values (> 55 dBZ) associated with particles of large diameters, possibly large

raindrops, hail, and melting hail that falls into the resonance size region (Figure 4.2). The

corrected Z_{dr} indicates values similar to those seen in the joint frequency histograms,

where high Z_h (> 50 dBZ) is associated with high corrected Z_{dr} (3-8 dB) (Figure 4.3).

Figure 4.2 shows in some cases that the corrected Z_{dr} is as high as 10 dB. It can be seen

in Figure 4.3 that there is no evidence of the "hail hole" that is found at the S-band. Even

the uncorrected Z_{dr} (Figure 4.4) indicates high Z_{dr} (> 3 dB) for locations in and near the

hail reports associated with this storm. Specific differential phase (K_{dp}) is rather noisy

within the supercell and ranges from positive and negative values (Figure 4.5) due to the

fluctuations in the differential propagation phase (Φ_{dp}) (Figure 4.6). The noisy K_{dp} is

likely due to insufficient removal of the backscatter differential phase (δ). Therefore, in

this case the K_{dp} data is difficult to use for hail detection as suggested by Ryzhkov et al.
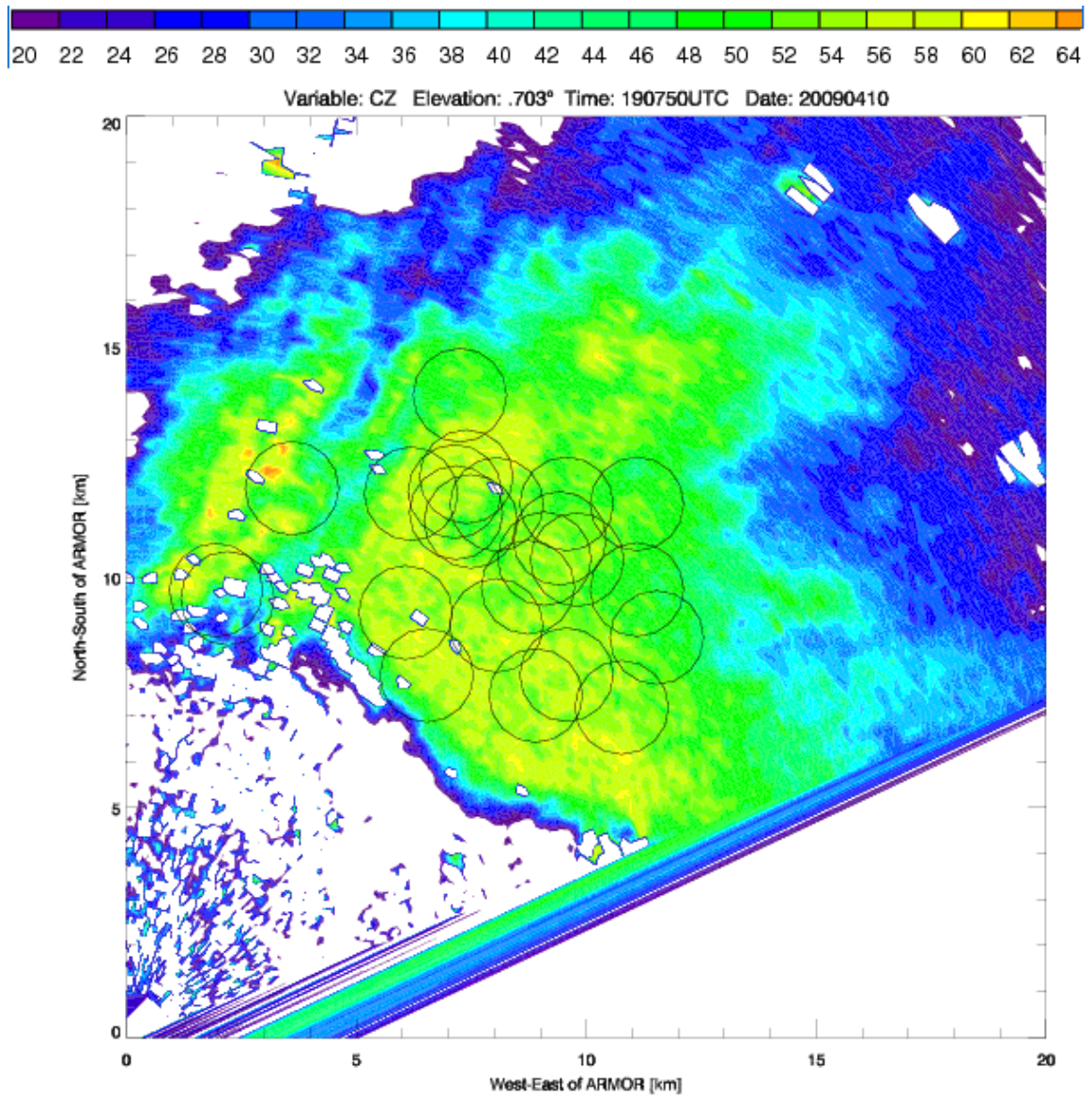
Figure 4.2: Plan Position Indicator (PPI) view of contoured corrected Z_h (dBZ) on April 10, 2009 at 1907 UTC at 0.7° elevation angle. The circles are reports +/- 3 minutes from the time of the scan. The circles represent the 1 km radius from each hail report. Horizontal east-west distance from ARMOR (km) versus north-south distance from ARMOR is shown.
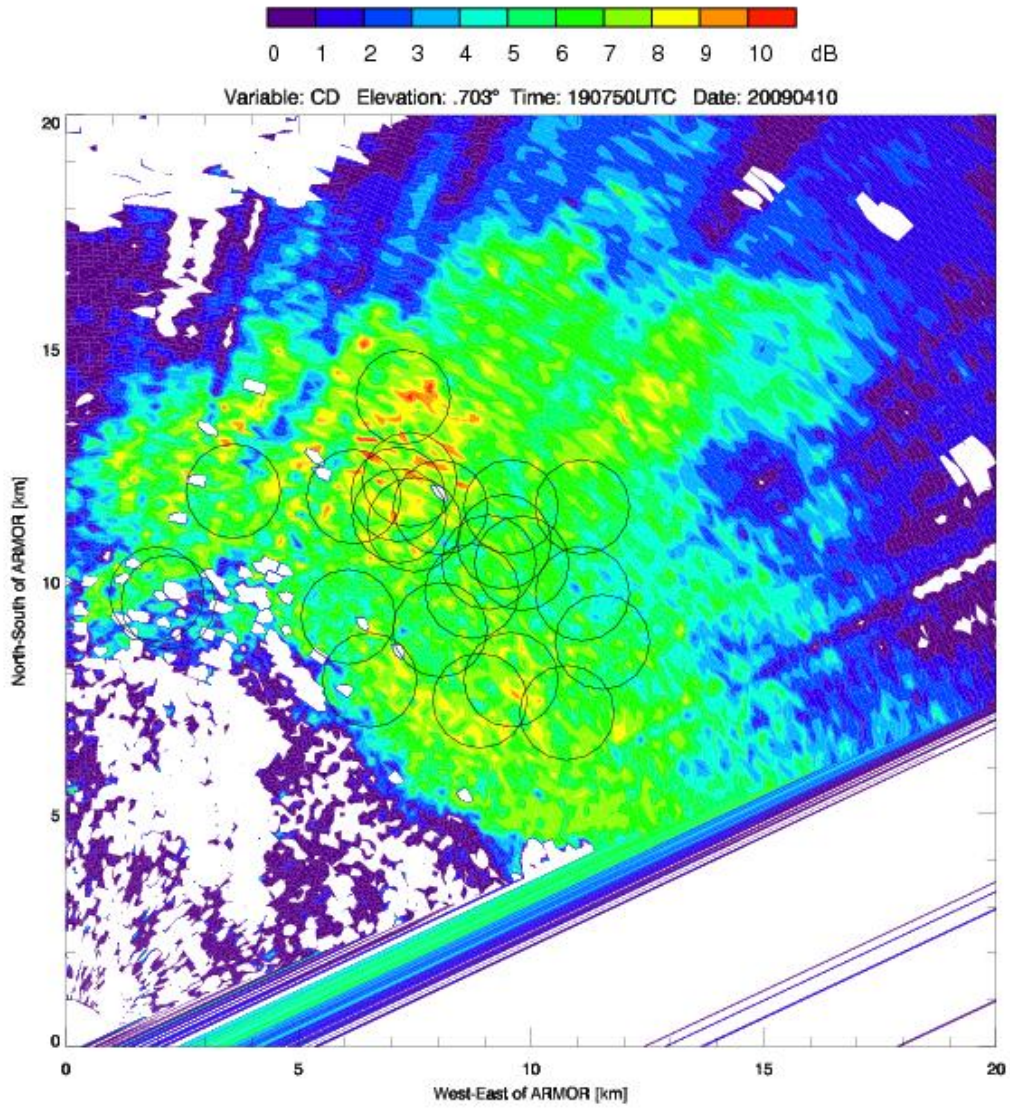
Figure 4.3: Same as Figure 4.2 except contoured corrected Z_{dr} (dB).
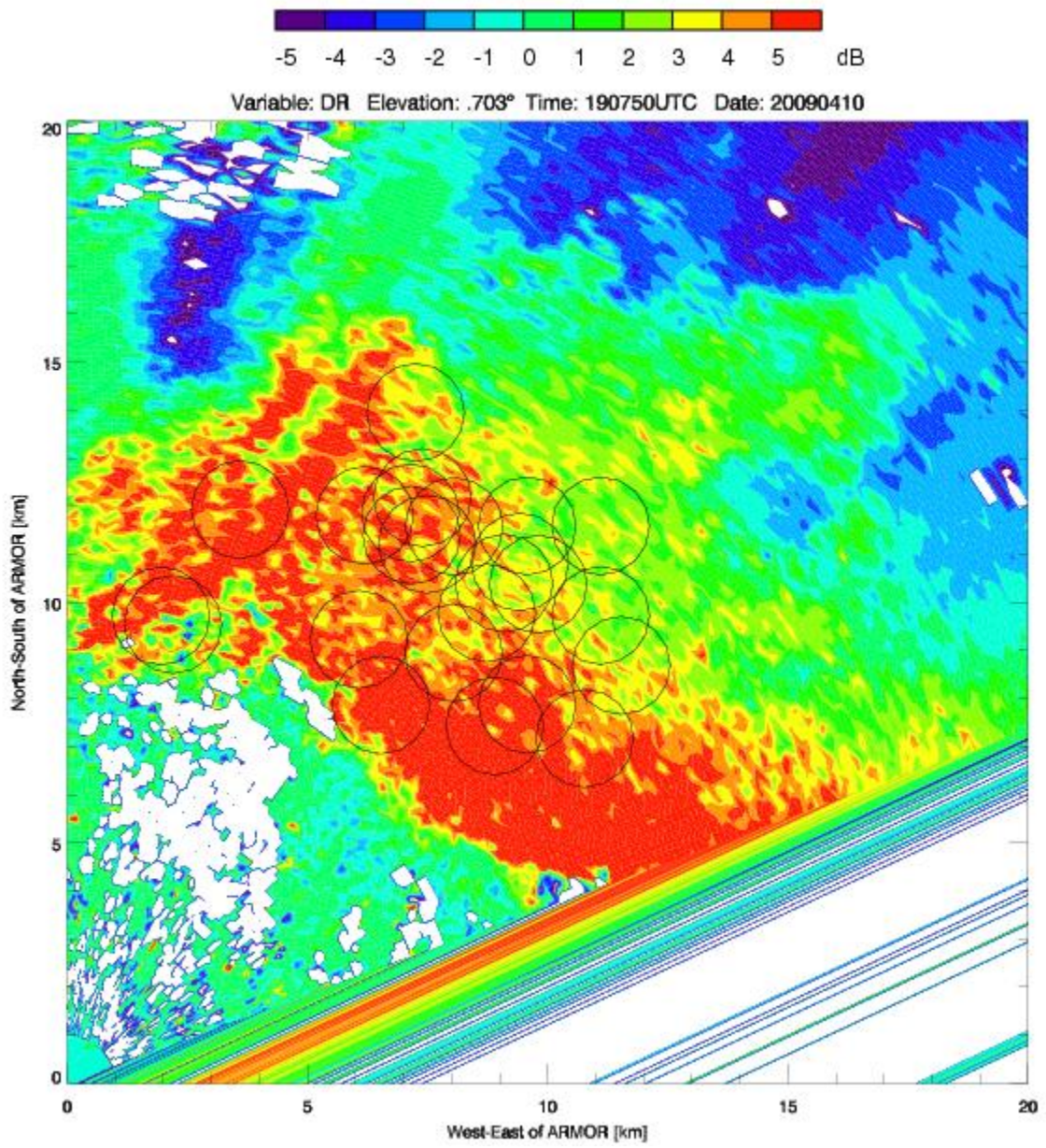
Figure 4.4: Same as Figure 4.2 except contoured uncorrected Z_{dr} (dB).
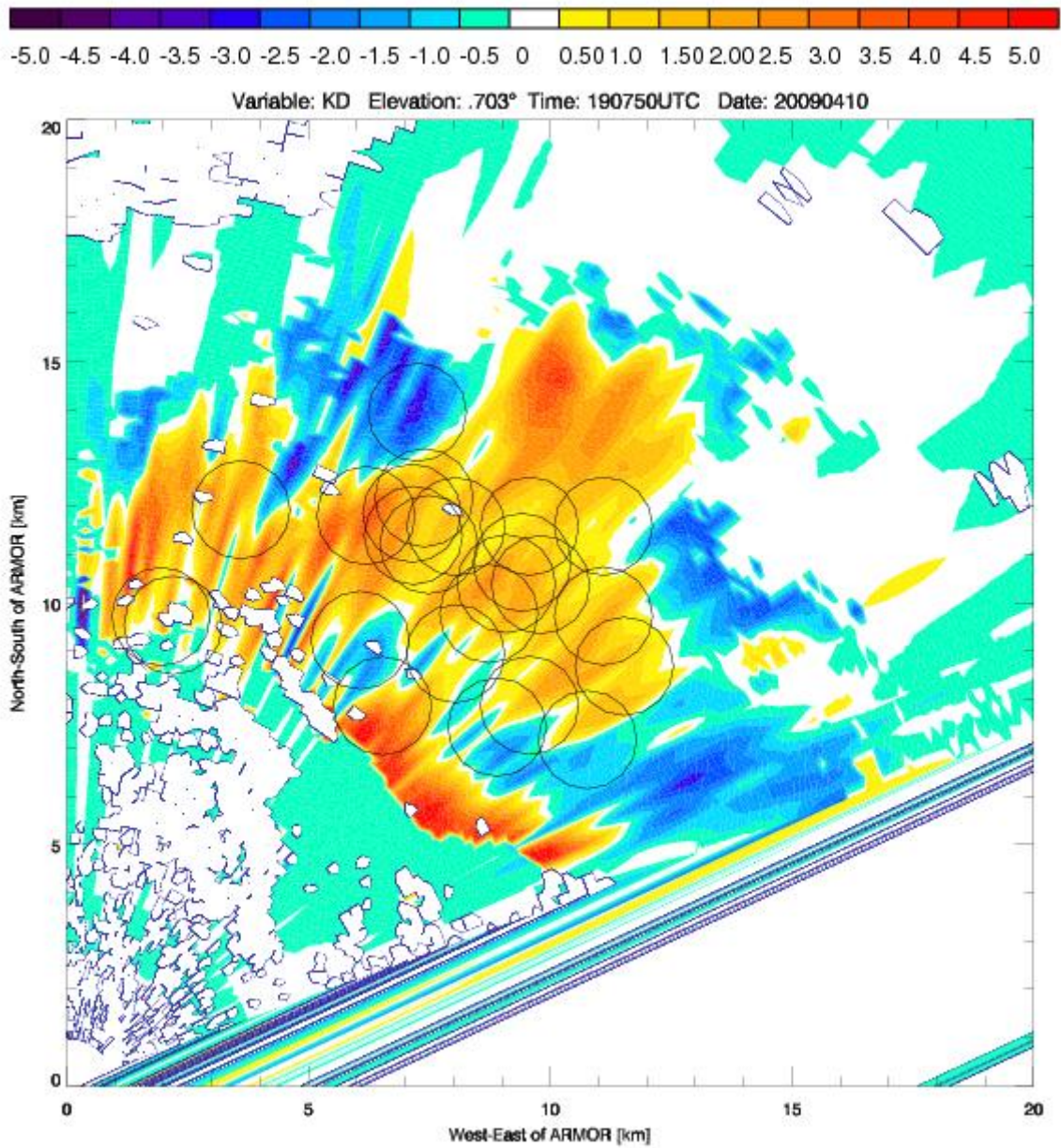
Figure 4.5: Same as Figure 4.2 except for contoured K_{dp} (°km^{-1}).
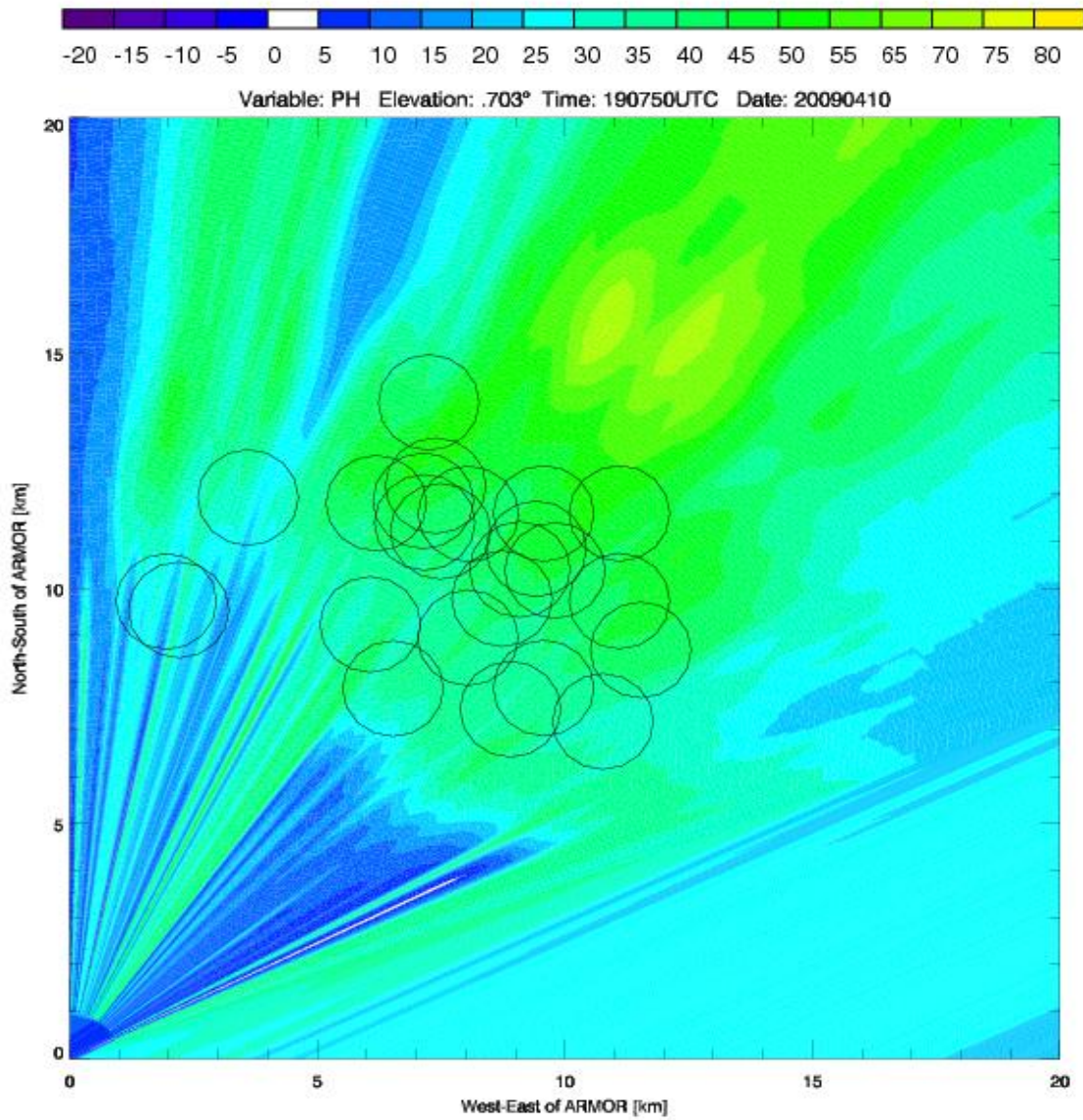
Figure 4.6: Same as Figure 4.2 except contoured Φ_{dp} (°).
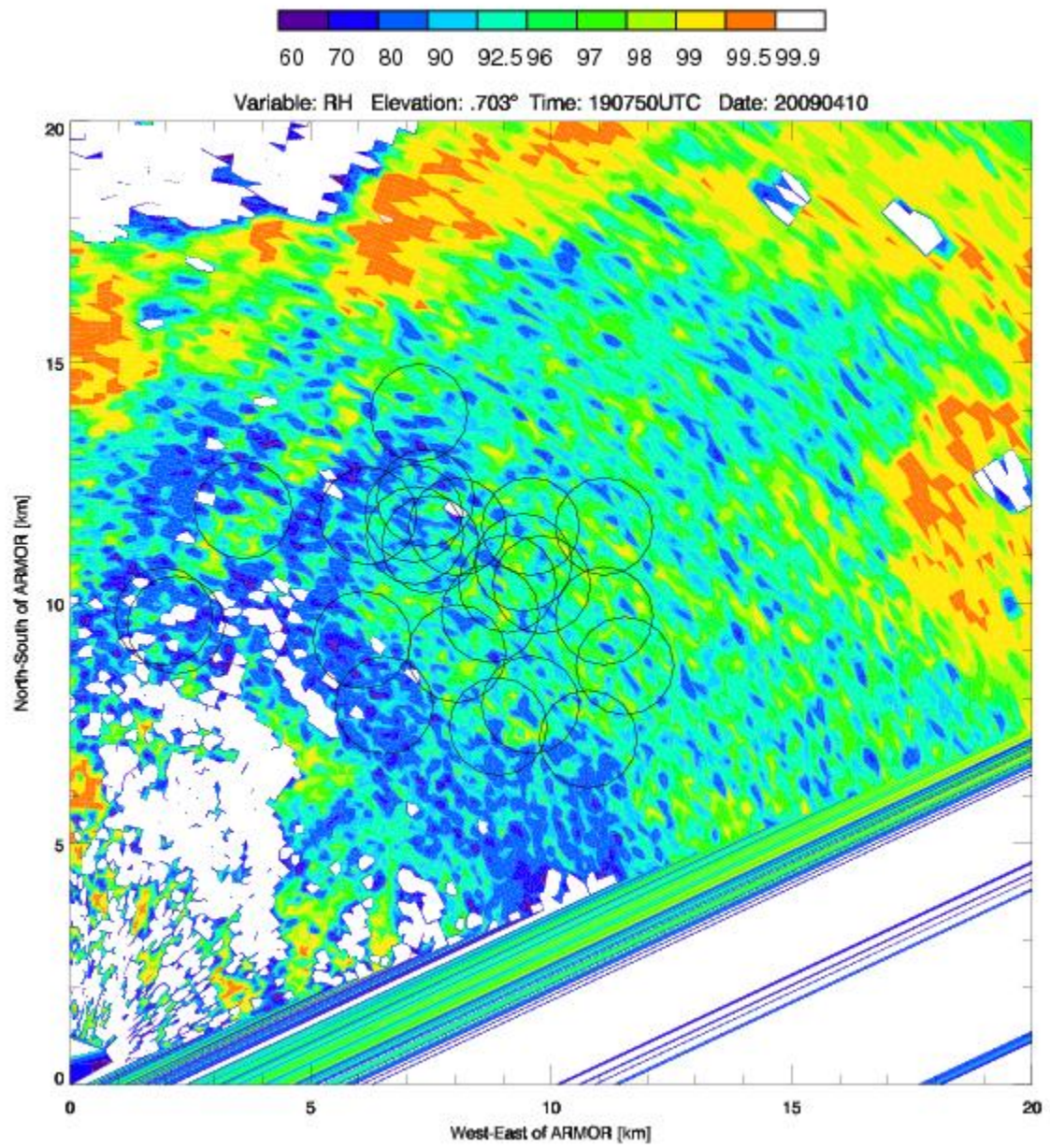
Figure 4.7: Same as Figure 4.2 except for contoured ρ_{hv}.

(2007). The PPI indicates low ρ_{hv} (< 0.95) for areas with high Z_h (> 50 dBZ) associated with a possible mixture of rain, hail, and melting hail that fall into the resonance sizes at the C-band (> 5 mm) (Figure 4.7). Overall, the PPI plot shows similar results to the joint frequency histogram analysis.   with a possible mixture of rain, hail, and melting hail that fall into the resonance sizes at C-band (> 5 mm) (Figure 4.7). Overall, the PPI plot shows similar results to the joint frequency histogram analysis.

4.1.2   Other Cases

February 21, 2005

Severe thunderstorms impacted the Southeast US as a weather system moved across the region. The areas most impacted by the system were north Alabama, north Georgia, and east Tennessee. Supercells developed early in the afternoon across northwest Alabama and southern Tennessee and moved towards the southeast as the day progressed. There were no tornadoes reported with the system across the Southeast, but there were over 100 reports of severe hail and 35 reports of damage caused by severe winds. Twenty-one of these hail reports, which passed the quality control metrics, were examined for this event to examine the C-band polarimetric signature of hail with sizes ranging from 0.75 – 1.75 inches (1.91 – 4.45 cm) with a mean of 0.95 inches (2.41 cm).

The Z_h and polarimetric variable joint frequency histograms reveal similar results to the April 10, 2009 case (Figure 4.8). The joint frequency histogram of Z_{dr} versus Z_h shows a mode of 3 dB near 48 dBZ, but there is an even higher mode of 5 dB near 58 dBZ (Figure 4.7a). In the Z_h bin from 55-57 dBZ, the 25th, 50th, and 75th percentiles of Z_{dr} are 3.73, 4.47, and 5.14 dB with a mean of 4.42 dB. It also can be seen in Figure 4.8a
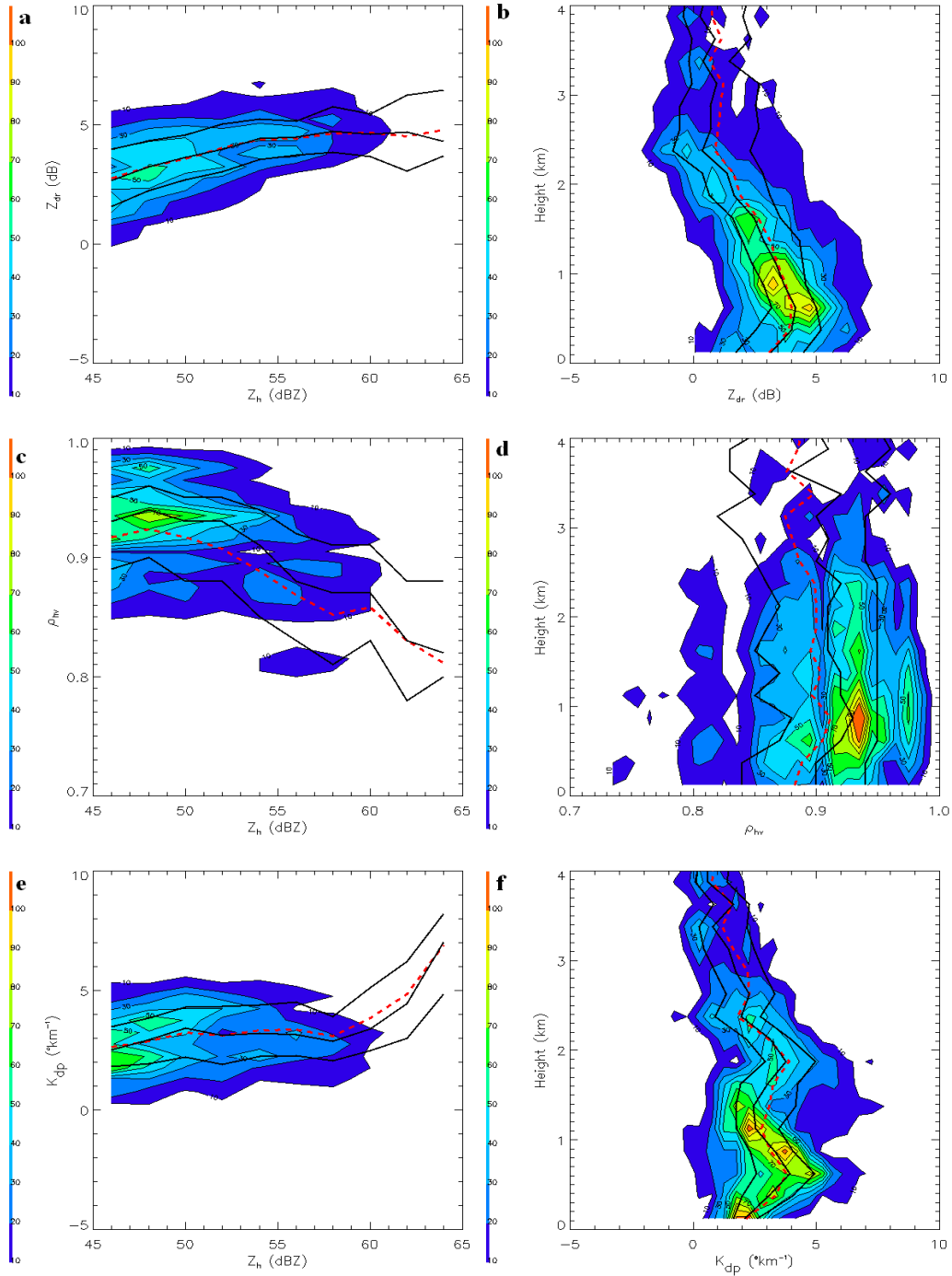
Figure 4.8: Same as Figure 4.1 except for the February 21, 2005 data set and an environmental 0 °C level near 3 km. Also H_{dr} not evaluated for (a).

that Z_{dr} tends to increase with increasing Z_h. This plot clearly shows the high Z_{dr} (3-8 dB) hail signature. The polarimetric variables and height joint frequency histograms present the vertical structure of the C-band polarimetric hail signature. The joint frequency histogram of Z_{dr} versus height plot shows a significant shift from Z_{dr} near 0 dB to positive values below 2 km (Figure 4.8b). The mode of Z_{dr} near the surface is near 4 dB. For the height bin from 0 to 250 m, the 25th, 50th, and 75th percentiles for Z_{dr} are 1.74, 3.16, and 4.47 dB with a mean of 3.10 dB while well above the 0 °C level at the 3.50 to 3.75 km bin, the 25th, 50th, and 75th percentiles for Z_{dr} are -0.05, 0.90, and 2.33 dB with a mean of 1.15 dB. The results suggest that melting along with resonance could be causing the shift to positive Z_{dr} below the 0 °C level which is found at 3 km.

The joint frequency histogram of ρ_{hv} versus Z_h indicates a mode of near 0.935 for Z_h values from 46 - 54 dBZ, but a clear lowering of the ρ_{hv} mode can be seen as Z_h increases (Figure 4.8c). In the Z_h bin from 55-57 dBZ, the 25th, 50th, and 75th percentiles of ρ_{hv} are 0.83, 0.88, and 0.92 with a mean of 0.87. The 25th, 50th, and 75th percentiles lines and the mean indicate that as Z_h increases, ρ_{hv} decreases. Irregular shaped hydrometeors, a mixture of rain, hail, and melting hail, and resonant sized particles (> 5 mm at the C-band) can all cause ρ_{hv} to be low. The joint frequency histogram of ρ_{hv} and height reveals a consistent mode of near 0.925 extending from near the surface up to 4 km with a minimum below 0.8 near the surface (Figure 4.8d). Again, this mode suggests a possible mixture of hydrometeors, irregular shaped hydrometeors, and resonant sized hydrometeors that are contributing to lowering ρ_{hv}. There appears to be no clear shift as seen in the joint frequency histogram of Z_{dr} versus height (Figure 4.8b). For the 0 – 250 m bin, the 25th, 50th and 75th percentiles of ρ_{hv} are 0.84, 0.90, and 0.94 with a

mean of 0.88 while well above the 0 °C level in the 3.50- 3.75 km bin, the 25th, 50th and 75th percentiles of ρ_{hv} are 0.83, 0.88, and 0.94 with a mean of 0.88. The lack of a significant change between above and below the 0 °C level in ρ_{hv} could be due to the fact that there is not a sufficient number of points above the 0 °C level to show how ρ_{hv} changes below the 0 °C level and the relatively small data set.

The joint frequency histogram of K_{dp} versus Z_h is slightly different than others analyzed because most of the values in the plot are positive. The mode of the plot remains nearly the same around 2.5 °km^{-1} for all values of Z_h (Figure 4.8e). In the Z_h bin from 55-57 dBZ, the 25th, 50th, and 75th percentiles of K_{dp} are 2.26, 3.16, and 4.51 °km^{-1} with a mean of 3.37 °km^{-1}. Since K_{dp} is not sensitive to isotropic (e.g., tumbling or spherical hail), this positive mode suggests that there maybe more anisotropic (e.g., raindrops) in the sample than other events. Again, the joint frequency histogram of K_{dp} versus height is rather noisy (Figure 4.8f). The mode is near 0 °km^{-1} above 3 km (the 0 °C level). Then the mode shifts towards positive values with a mode near 2 °km^{-1} near the surface. The values of K_{dp} vary widely from 0 to 7 °km^{-1} making it a rather noisy field. For the 0 – 250 m bin, the 25th, 50th and 75th percentiles of K_{dp} are 1.63, 2.08, and 2.61 °km^{-1} with a mean of 2.16 °km^{-1} while well above the 0 °C level in the 3.50- 3.75 km bin, the 25th, 50th and 75th percentiles of K_{dp} are 0.43, 1.45, and 2.47 °km^{-1} with a mean of 1.15 °km^{-1}. The positive values of K_{dp} may be due to the presence of a higher concentration of raindrops. The vertical structure histogram shows that significant changes occur below the 0 °C level in the C-band polarimetric signatures of hail. Overall, the polarimetric signatures are similar to others observed with high Z_{dr}, low ρ_{hv}, and noisy K_{dp}.

August 2, 2008

Pulse severe thunderstorms impacted the Southeastern US producing a large number of severe hail and wind reports across the region. Thunderstorms developed early in the afternoon along the Tennessee and Alabama border and pushed towards the south throughout the day ahead of a weak cold front. The threat for severe weather was not expected to be very high for the day so the ARMOR C-band radar was only in rain1 scan mode. This means the radar was only scanning the three lowest elevation scans because of this the vertical structure of the polarimetric signatures of hail cannot be evaluated. However, the storm system produced 19 reports of severe hail that met the storm report criteria with a range of sizes from 0.75 – 1.75 inches (1.91 – 4.45 cm) with a mean of 1.28 inches (3.25 cm).

The joint frequency histograms of Z_h and the polarimetric variables were still produced because they focus on the signatures below 1 km near the surface (Figure 4.9). The joint frequency histogram of Z_{dr} versus Z_h shows similar results to those previously observed. The Z_{dr} mode is near 4.5 dB for Z_h of 50 dBZ, and then increases to near 6 dB for Z_h of 55 dBZ (Figure 4.9a). In the Z_h bin from 55-57 dBZ, the 25th, 50th, and 75th percentiles of Z_{dr} are 4.81, 5.65, and 6.68 dB with a mean of 5.41 dB. As seen in Figure 4.4a, the mode of Z_{dr} increases as Z_h increases along with the 25th, 50th, 75th percentiles and the mean. Figure 4.9a clearly demonstrates that the high Z_{dr} associated with hail at the C-band does not resemble the "hail hole" signature routinely found at the S-band. The joint frequency histogram of ρ_{hv} versus Z_h indicates a ρ_{hv} mode of 0.92 for Z_h of 48 dBZ (Figure 4.9b). In the Z_h bin from 55-57 dBZ, the 25th, 50th, and

75th percentiles of ρ_{hv} are 0.82, 0.87, and 0.92 with a mean of 0.87. The mode of ρ_{hv}

dramatically decreases as Z_h increases. This again suggests irregular shaped
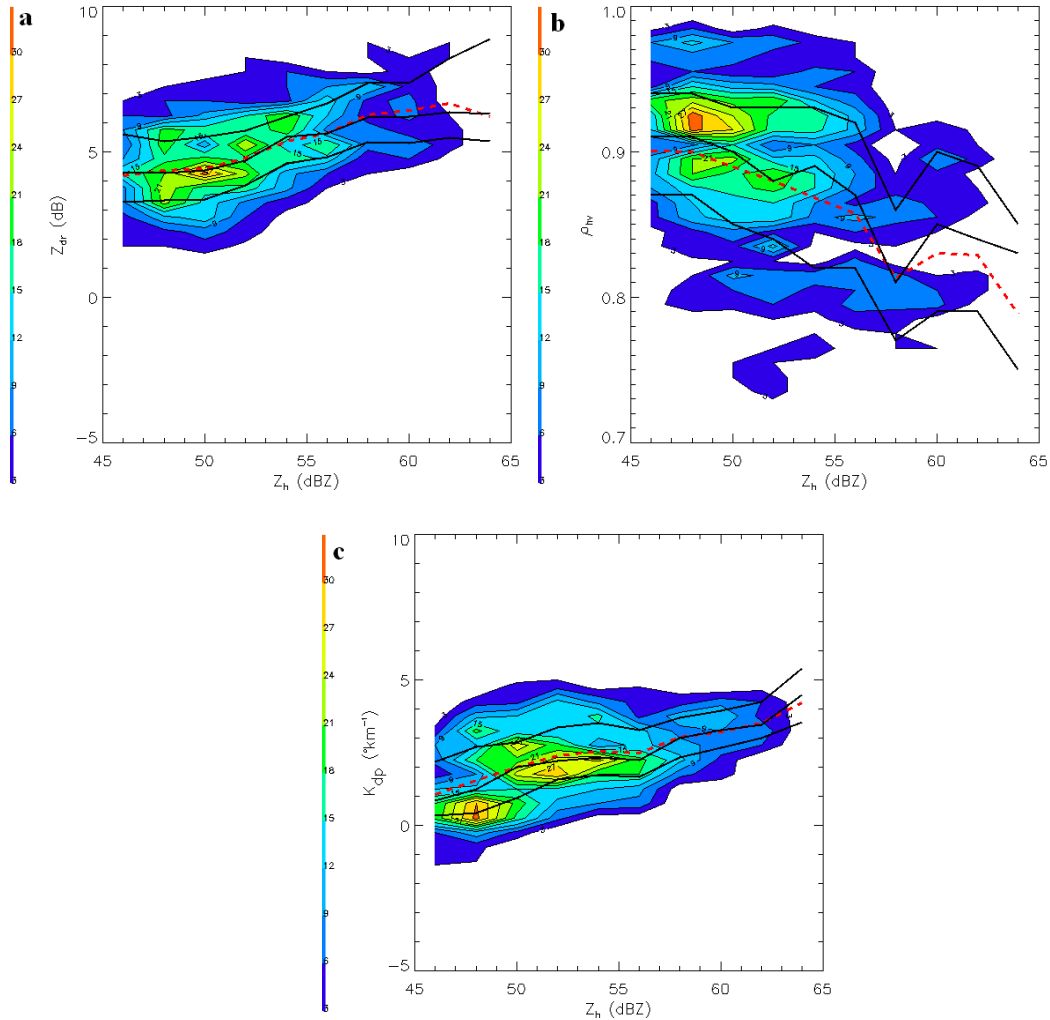
Figure 4.9: Joint frequency histograms of (a) Z_{dr} versus Z_h, (b) ρ_{hv} and Z_h, and (c) K_{dp} versus Z_h. All data is below 1 km and within a 1 km radius of a hail report from August 2, 2008 data set. The Z_h data is in 2 dB bins, the Z_{dr} is in 0.5 dB bins, the K_{dp} data is in 0.5 °km^{-1} bins, and the ρ_{hv} data is in 0.01 bins. The black lines from bottom to top are the 25th, 50th, and 75th percentile lines (a-c) and with the dashed red line is the mean (a-c).

hydrometeors, mixtures of rain, hail, and melting hail, and resonant sized hydrometeors (> 5mm at the C-band) near the surface. The joint frequency histogram K_{dp} versus Z_h shows similar results observed in the February 21, 2005 case. Most of the values in the plot are positive ranging from near 0 to 5 $^{\circ}$km^{-1} (Figure 4.9c). In the Z_h bin from 55-57 dBZ, the 25th, 50th, and 75th percentiles of K_{dp} are 1.66, 2.23, and 3.26 $^{\circ}$km^{-1} with a mean of 2.48 $^{\circ}$km^{-1}. Again, these positive values of K_{dp} suggest that the possibility of rain mixing with hail due the sensitivity of K_{dp} to anisotropic particle (e.g., raindrops). The idea of rain mixing with hail may be a good assumption because of the low ρ_{hv} as well. In addition, this event is a summer time event where large amounts of warm air are near the surface and promote melting of hailstones into large oblate raindrops. Even though the vertical structure of the polarimetric variable cannot be analyzed, the observations near the surface show that high Z_{dr} (3-8 dB), low ρ_{hv} (< 0.95), and positive K_{dp} (0-5 $^{\circ}$km^{-1}) are representative of the C-band polarimetric signature of hail at the surface for this event.

Additional Cases

The focus of this study is to carefully document the C-band polarimetric signatures of hail. The ρ_{hv} and K_{dp} signatures have been consistent in the first three events analyzed and produce similar results in the other cases as well. In this study, ρ_{hv} has been consistently low near the surface for locations of hail (< 0.95) and K_{dp} has been consistently near zero to slightly positive for areas of hail in the other events. Therefore, because of these similar signatures, ρ_{hv} and K_{dp} will not be explored in the minor events in this study. However, Z_{dr} produces surprising results in the previous three events when

compared to the S-band.   At the C-band, Z_{dr} produces more of a high Z_{dr} (3-8 dB) signature while at the S-band low Z_{dr} (-1 – 1 dB) is expected for hail.   Therefore, Z_{dr} will be further explored in the minor events in this study to see if the high Z_{dr} signature is the prevalent signature for hail at the C-band. The remaining events are not high impact events and are minor compared to the events addressed in the previous section.

The first case that will be presented in this section is the April 3, 2007 event.   The event produced widespread severe weather across the Midwest and Southeast.   This study uses nine reports of severe hail in the ARMOR study domain with sizes ranging from 0.75 – 1.75 inches (1.91 – 4.45 cm) with a mean of 0.95 inches (2.41 cm).   The joint frequency histogram of Z_{dr} versus Z_h indicates a mode of Z_h near 54 dBZ at a Z_{dr} of 4 dB (Figure 4.10a). The range for Z_{dr} is from 1.5 to 8.5 dB with no values near 0 dB. In the Z_h bin from 55-57 dBZ, the 25th, 50th, and 75th percentiles of Z_{dr} are 3.63, 5.05, and 6.47 dB with a mean of 5.09 dB. Z_{dr} does not exhibit a slope and the mean remains constant near 4 dB for all values of Z_h.   However, the 25th, 50th, 75th percentiles and mean values increase beyond 60 dBZ. This is most likely due to limited Z_{dr} data in this range.   In this case, a vertical profile of Z_{dr} is available because ARMOR was running volumes scans. The joint frequency histogram of Z_{dr} versus height shows that Z_{dr} increases from near 0 dB at 2 km to positive values below this point (Figure 4.10b).   The Z_{dr} mode is near 0 dB at 2 km and is near 4 dB at the surface. For the height bin from 0 to 250 m, the 25th, 50th, and 75th percentiles for Z_{dr} are 2.12, 3.31, and 4.43 dB with a mean of 4.37 dB while above the 0 °C level at the 3.75 to 4.00 km bin, the 25th, 50th, and 75th percentiles for Z_{dr} are -1.81, -1.12, and -0.25 dB with a mean of -0.25 dB. Clearly, a shift is occurring in the data as the hailstones melt below the height of the 0 °C level. The Z_{dr} is not as high as

76
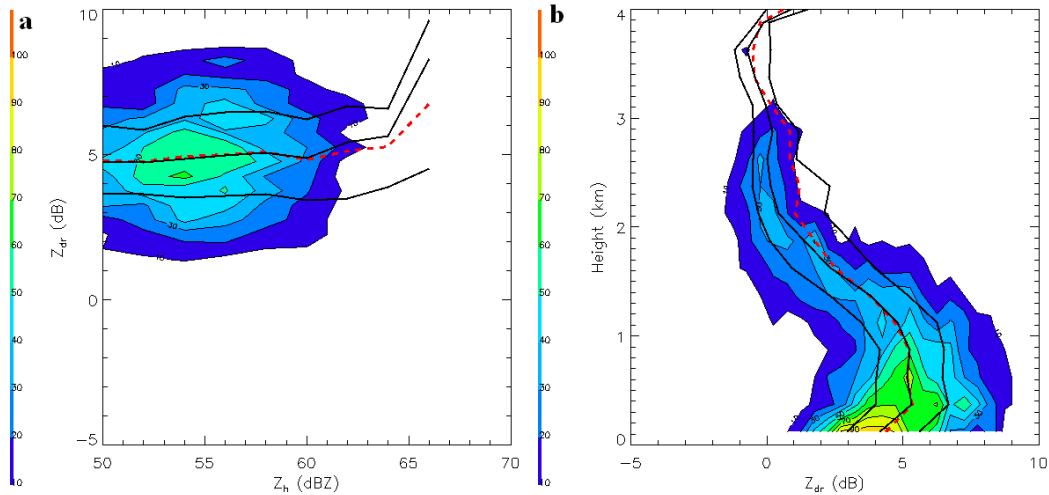
Figure 4.10: April 3, 2007 joint frequency histograms of (a) Z_{dr} versus Z_h and (b) Z_{dr} and height. Data is below 1 km for figure (a) and within a 1 km radius of a hail report from April 3, 2007 data set. The Z_h data is in 2 dB bins, the Z_{dr} is in 0.5 dB bins, the K_{dp} data is in 0.5 °km^{-1} bins, and the ρ_{hv} data is in 0.01 bins. The 0 °C level is at 3.7 km. The black lines from bottom to top are the 25th, 50th, and 75th percentile lines (a) and from left to right the 25th, 50th, and 75th percentiles (b) with the dashed red line as the mean (a,b).

observed in other cases (e.g., April 10, 2009) but does not resemble the "hail hole" signature either.

The next event occurred on March 15, 2008. The event produced widespread severe weather across the Southeast with the main areas of impact in Georgia and South Carolina. However, there were seven reports of severe hail that meet the criteria for this event near ARMOR with a range of sizes from 0.75 -0.88 inches (1.91 – 2.24 cm) with a mean of 0.84 inches (2.13 cm). The joint frequency histogram of Z_{dr} versus Z_h indicates a small sample of gates with a general increase in the Z_{dr} mode with increasing Z_h (Figure 4.11a). The mode increases from near 2.5 dB at 46 dBZ to 4.5 dB near 51 dBZ. This positive slope has been observed in other events as well (e.g., April 10, 2009). The
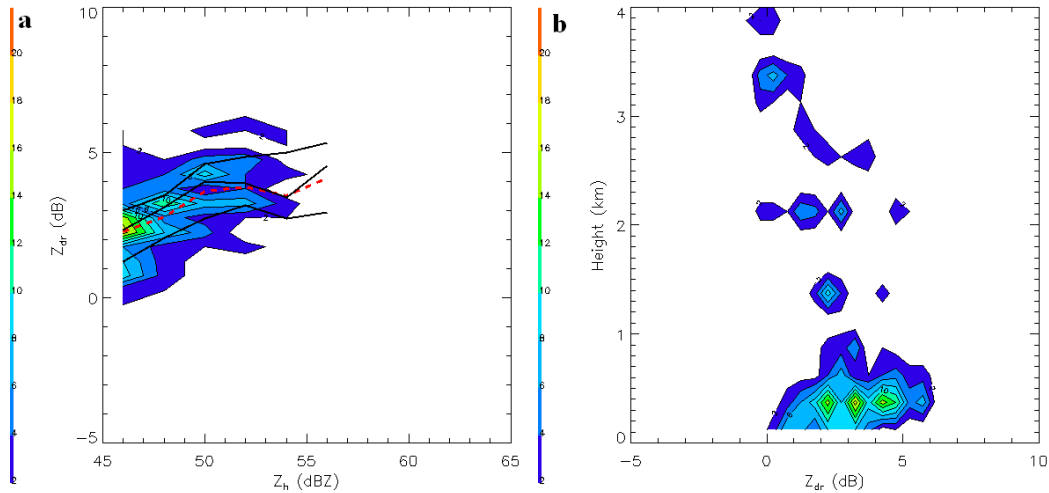
Figure 4.11: Same as Figure 4.10 except for March 15, 2008 data set and the 0 °C level is at 3.2 km.

Z_{dr} values range from near 0 to 6 dB. In the Z_h bin from 55-57 dBZ, the 25th, 50th, and 75th percentiles of Z_{dr} are 2.93, 4.55, and 5.32 dB with a mean of 4.12 dB. The joint frequency histogram of Z_{dr} versus height shows a Z_{dr} mode near 0 dB around 4 km with a steady increase to positive values from below 4 km to the surface with a 0 °C level of 3.2 km (Figure 4.11b). The mode of Z_{dr} near the surface is near 3.5 dB. Both of the plots have very few data points due to the distances from the radar to the reports. The 25th, 50th, and 75th percentiles were not analyzed with the joint frequency histogram of Z_{dr} versus height due to the lack of data of points in this event. Even so, the hail signatures observed near the surface during this event are characterized by high Z_{dr} (3-8 dB) and do not and are not consistent with the "hail hole" concept.

An even more limited sample is presented in the next event. The March 28, 2009 event produced a number of severe weather reports across the Southeast. However, the event only produced a limited number (4) of reports across the area that met the criteria

for this study with a range of sizes from 0.75 − 1.25 inches (1.91 − 3.18 cm) with a mean

of 1.00 inch (2.54 cm). The joint frequency histogram of Z_{dr} versus Z_h reveals a mode of

Z_{dr} near 3 dB at 46 dBZ (Figure 4.12a). Again, the Z_{dr} mode increases with increasing Z_h

producing a mode near 4 dB for 52 dBZ and 6 dB near 55 dBZ. In this case, Z_{dr} ranges

from 1 to 7.5 dB. In the Z_h bin from 53-55 dBZ, the 25th, 50th, and 75th percentiles of Z_{dr}

are 4.39, 6.47, and 7.14 dB with a mean of 5.84 dB. This indicates that 50% of the Z_{dr}

data in the 53-55 dBZ bin is found between 4.39 − 7.14 dB. Therefore, the hail signature

in this case again produces high Z_{dr}. The joint frequency histogram Z_{dr} versus height

shows similar results as seen in the other examples (e.g., April 10, 2009). At 4 km, the

Z_{dr} mode is near 0 dB but increasing to positive values below 4 km with a 0 °C level at

3.3 km (Figure 4.12b). The mode of Z_{dr} near the surface is 3.5 dB with a range of values

from 1 to 8 dB. The Z_{dr} versus height histogram shows that the Z_{dr} shifts dramatically

towards positive values below the 0 °C level of 3.3 km. The 25th, 50th, and

75th percentiles were not analyzed with the joint frequency histogram of Z_{dr} and height

due to the lack of data points in this event. Again, the signatures of hail near the surface

for this event are characterized by high Z_{dr} (3-8 dB) and are not consistent with the "hail

hole" concept.

The next event April 13, 2009 was a smaller event that only produced a limited

number of severe hail reports across the Tennessee Valley with a range of sizes from 0.75

− 1.00 inch (1.91 − 2.54 cm) with a mean of 0.91 inches (2.31 cm). The ARMOR C-band

radar was not operating in volume scan mode. Therefore, only the three lowest elevation

angles are available and a vertical structure of Z_{dr} cannot be evaluated. The joint

frequency histogram of Z_{dr} versus Z_h indicates that the Z_{dr} mode increases with increasing
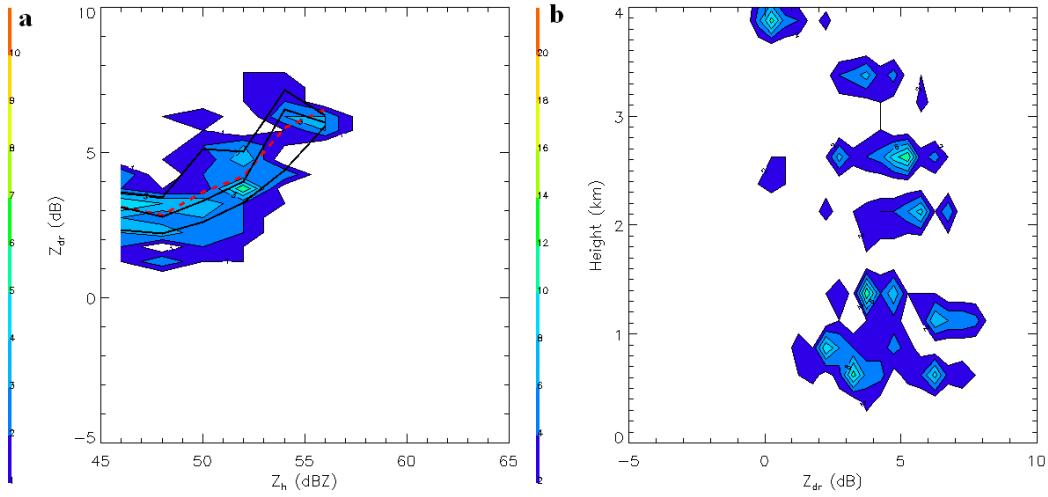
Figure 4.12: Same as Figure 4.10 except for March 28, 2009 data set and the 0 °C level is at 3.3 km
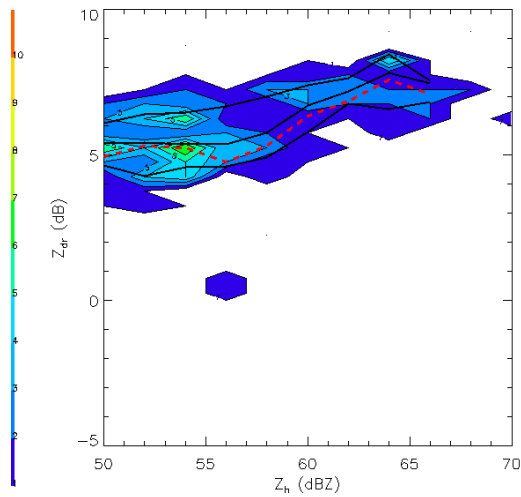
Figure 4.13: Joint frequency histograms of Z_{dr} versus Z_h. Data is below 1 km and within a 1 km radius of a hail report from April 13, 2009 data set. The Z_h data is in 2 dB bins and the Z_{dr} is in 0.5 dB bins. The black lines from bottom to top are the 25th, 50th, and 75th percentile lines and the dashed red line is the mean.

Z_h (Figure 4.13). The Z_{dr} mode is near 5 dB at 54 dBZ and then increases to 8 dB for

64 dBZ. The Z_{dr} values range from near 0 to 9 dB. The data near 0 dB appears to be an

outlier and not associated with the majority of the data from this event. In the Z_h bin from

57-59 dBZ, the 25th, 50th, and 75th percentiles of Z_{dr} are 4.90, 5.75, and 7.01 dB with a

mean of 5.30 dB. This indicates that 50% of the Z_{dr} data in the 57-59 dBZ bin is found

between 4.90 – 7.01 dB. Again, the signatures of hail near the surface at the C-band

suggest that hail is characterized by high Z_{dr} (3-8 dB) and are not consistent with the "hail

hole" concept.

The next event January 21, 2010 was a localized severe weather event that

affected the Tennessee Valley. There were a limited number of hail reports with the

event with a range of sizes from 0.50 – 2.75 inches (1.27 – 6.99 cm) with a mean of

1.31 inches (3.33 cm). However, an EF-2 tornado touched downed in downtown

Huntsville, AL, producing damage to homes and businesses. The joint frequency

histogram of Z_{dr} versus Z_h indicates a Z_{dr} mode near 3 dB at 48 dBZ for the limited

sample of reports for this event (Figure 4.14a). Again, an increase in the Z_{dr} mode can be

seen to 5 dB near 52 dBZ. The Z_{dr} values in this case range from 0 to 8 dB. In the Z_h bin

from 55-57 dBZ, the 25th, 50th, and 75th percentiles of Z_{dr} are 4.14, 4.52, and 5.08 dB with

a mean of 4.30 dB. Therefore, 50% of the Z_{dr} data in the 55-57 dBZ bin is found between

4.14 – 5.08 dB. The joint frequency histogram of Z_{dr} versus height is slightly different

than the other case because the mode of 0 dB extends down to 1 km. However, below

1 km a positive shift occurs in the data where the mode of Z_{dr} is near 4 dB near the

surface (Figure 4.14b). In this case, the 0 °C level was closer to the ground at 2.4 km

with surface temperature in the mid 60's. Therefore, the significant shift of Z_{dr} from near
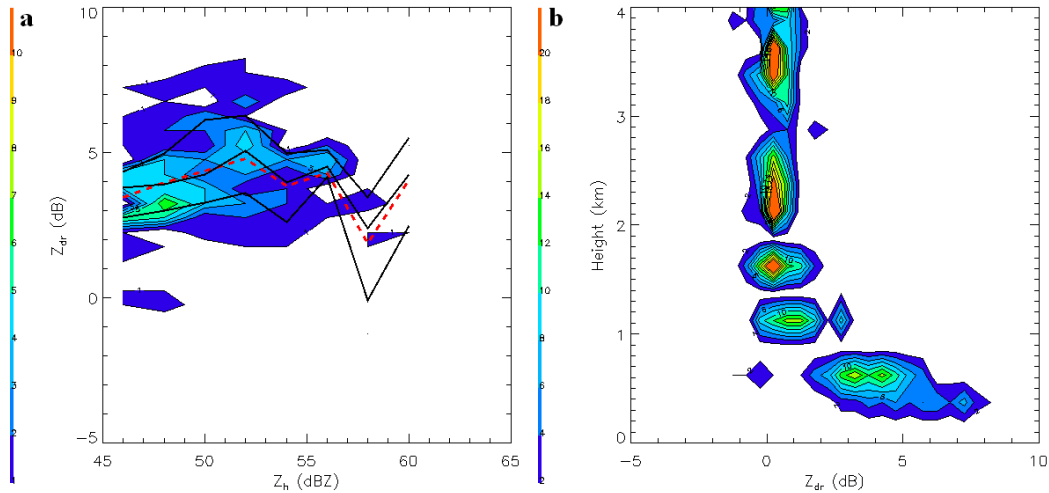
Figure 4.14: Same as Figure 4.10 except for January 21, 2010 data set and the 0 °C level is at 2.4 km

0 dB to positive values does not occur until near the surface. The 25th, 50th, and 75th percentiles were not analyzed with the joint frequency histogram of Z_{dr} and height due to the lack of data of points in this event. Again, the C-band polarimetric signatures of hail near the surface for this event are characterized by high Z_{dr} (3-8 dB) and are not consistent with the "hail hole" concept.

The March 12, 2010 produced a number of severe hail (21) reports across the Tennessee Valley associated with a line of severe hail producing supercells with hail sizes ranging from 0.75 − 1.75 inches (1.91 − 4.45 cm) with a mean of 1.13 inches (2.87 cm). The joint frequency histogram of Z_{dr} versus Z_h indicates a mode of Z_{dr} near 4 dB for 50 dBZ (Figure 4.15a). In the Z_h bin from 55-57 dBZ, the 25th, 50th, and 75th percentiles of Z_{dr} are 3.51, 5.10, and 6.15 dB with a mean of 4.76 dB. Therefore, 50% of the Z_{dr} data in the 55-57 dBZ bin is found between 3.51 − 6.15 dB. There is an

increase in Z_{dr} with Z_h and this is similar to what has been observed in other cases in this study.
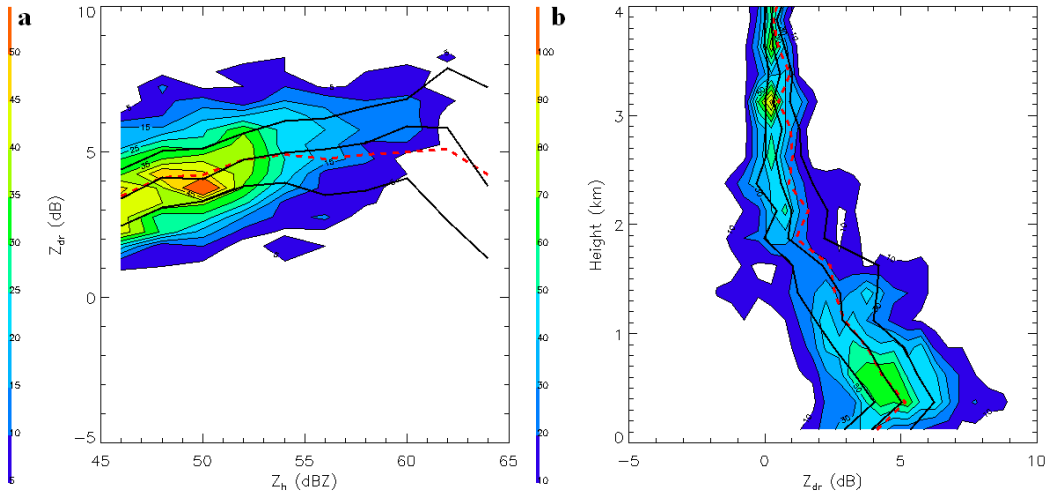
Figure 4.15: Same as Figure 4.10 except for March 12, 2010 data set and the 0 °C level is at 2.9 km

However, there is a clear difference where Z_h is greater than 60 dBZ. The 25th, 50th, and 75th percentile lines in this region decrease and are the best example of a "hail hole" signature that have been addressed, so far, in this study. This example will be addressed further in Section 4.2. Despite the few points that exhibit more of a "hail hole" signature, the majority of the gates in the case are more representative of the high Z_{dr} signature. The joint frequency histogram of Z_{dr} versus height shows a gradual increase from near 0 dB Z_{dr} above 2 km to a mode of 4.5 dB near the surface (Figure 4.15b). For the height bin from 0 to 250 m, the 25th, 50th, and 75th percentiles for Z_{dr} are 2.94, 3.93, and 5.36 dB with a mean of 4.12 dB while above the 0 °C level at the 3.75 to 4.00 km bin the 25th, 50th, and 75th percentiles for Z_{dr} are 0.01, 0.25, and 0.44 dB with a mean of

0.29 dB. Again, a significant shift occurs from near 0 dB to positive values of Z_{dr} below

the 0 °C level of 2.9 km.

4.1.3   Composite Analysis

Due to the large number of events in the study, composite plots are made from all

events to characterize the overall polarimetric signature of hail from the ARMOR C-band

radar. However, in this section the analysis uses joint relative frequency distribution of

Z_h versus polarimetric variables and contoured frequency by altitude diagrams of

polarimetric variable versus height outlined in Chapter 3. The composite images consist

of nine hail events observed by the ARMOR C-band radar.

The joint relative frequency distribution of Z_{dr} versus Z_h reveals a high Z_{dr} mode

of 5 dB with Z_h between 51 to 57 dBZ (Figure 4.16a). Table 4.1 indicates the 25th, 50th,

and 75th percentiles for the Z_h bin from 55 to 57 dBZ are 3.99, 5.47, and 6.90 dB with a

mean of 5.34 dB. Therefore, 50 % of the data in the 55 to 57 dBZ bin is in between 3.99

to 6.90 dB. In addition to the high Z_{dr} mode, an increase in Z_{dr} occurs as Z_h increases

(Table 4.1). The high Z_{dr} may be due to melting, stably oriented hailstones that fall into

the resonance regime at the C-band (Meischner et al. 1991, Vivekanandan et al. 1991,

Ryzhkov et al. 2007). The contoured frequency by altitude diagram of Z_{dr} versus height

indicates a clear shift in Z_{dr} from near zero and shifts dramatically below 1.5 km to

positive Z_{dr} values (Figure 4.16b). For the height bin from 0 to 250 m, the 25th, 50th, and

75th percentiles for Z_{dr} are 3.74, 5.21, and 6.71 dB with a mean of 5.20 dB while above

the 0 °C level for most cases from 4.00 to 4.25 km bin the 25th, 50th, and 75th percentiles

for Z_{dr} are -0.17, 0.19, and 0.62 dB with a mean of 0.37 dB. The shift towards positive

values will not always occur at the same altitude due to the variation of the 0 °C level.

However, Figure 4.16b suggests that significant microphysical changes are occurring to

cause the sudden increase in Z_{dr} near the surface.
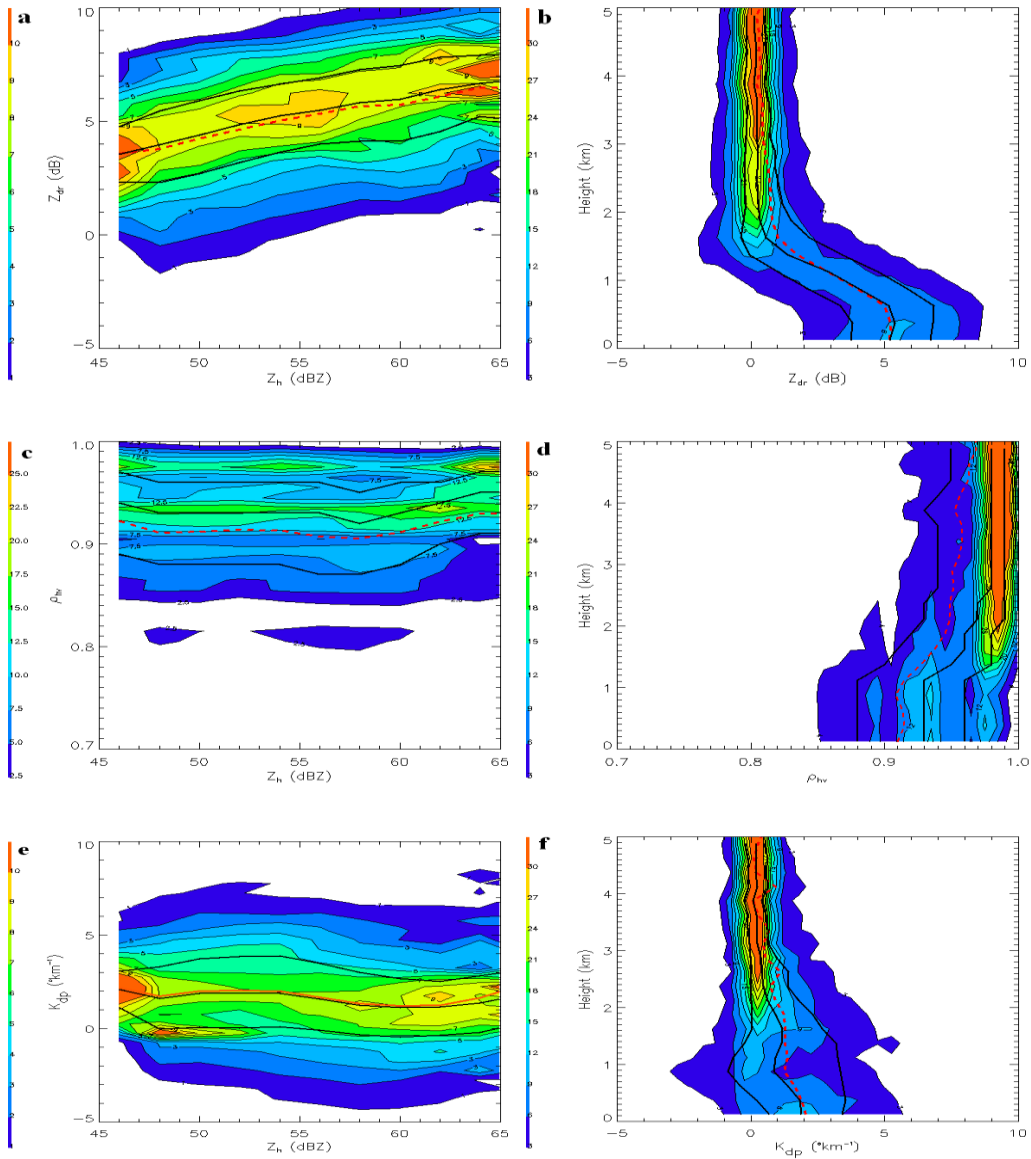
Figure 4.16: Composite joint relative frequency histograms in percent of polarimetric variables vs. Z_h (left) and height (right) (a) Z_{dr} vs. Z_h (b) Z_{dr} vs. height (c) ρ_{hv} vs. Z_h (d) ρ_{hv} vs. height (e) K_{dp} vs. Z_h (f) K_{dp} vs. height. All data points taken within 1 km of hail reports where Z_h is > 45 dBZ and all data in plots on left taken from below 1 km. The Z_h data is in 2 dB bins, the Z_{dr} is in 0.5 dB bins, the K_{dp} data is in 0.5 °km^{-1} bins, the ρ_{hv} data is in 0.05 bins, and the height data is in 250 m bins. The black lines from bottom to top are the 25th, 50th, and 75th percentile lines (a,c,e) and from left to right the 25th, 50th, and 75th percentiles (b,d,f) with the dashed red line as the mean (a-f).

85

Table 4.1: Statistical Analysis of Composite Data below 1 km.

Z_h bin (dBZ)	Z_{dr} 25th Percentile dB	Z_{dr} 50th Percentile dB	Z_{dr} 75th Percentile dB	K_{dp} 25th Percentile $^\circ$km^{-1}	K_{dp} 50th Percentile $^\circ$km^{-1}	K_{dp} 75th Percentile $^\circ$km^{-1}	ρ_{hv} 25th Percentile	ρ_{hv} 50th Percentile	ρ_{hv} 75th Percentile
45-47	2.31	3.54	4.77	1.12	2.09	3.06	0.89	0.94	0.97
47-49	2.31	3.96	5.45	-0.02	1.62	3.30	0.88	0.93	0.96
49-51	2.70	4.40	5.92	0.07	1.87	3.74	0.88	0.93	0.96
51-53	3.19	4.85	6.33	0.02	1.89	3.86	0.88	0.93	0.96
53-55	3.65	5.23	6.65	0.10	1.89	3.88	0.88	0.93	0.96
55-57	3.99	5.47	6.90	-0.10	1.59	3.47	0.87	0.93	0.96
57-59	4.11	5.82	7.26	-0.34	1.25	3.00	0.87	0.92	0.95
59-61	4.12	5.96	7.44	-0.44	1.12	2.67	0.88	0.93	0.96
61-63	4.54	6.38	7.81	-0.36	1.15	2.51	0.90	0.94	0.96
63-65	5.22	6.67	7.92	-0.20	1.35	2.81	0.91	0.95	0.97

The joint relative frequency distribution of ρ_{hv} versus Z_h indicates two distinct modes (Figure 4.16c). The first mode can be seen with a ρ_{hv} of 0.975 for all values of Z_h and the second mode is at a ρ_{hv} of 0.935 for all values of Z_h. Table 4.1 indicates the 25th, 50th, and 75th percentiles for the ρ_{hv} bin from 55 to 57 dBZ are 0.87, 0.93, and 0.96 with a mean of 0.91. Therefore, 50 % of the data in the 55 to 57 dBZ bin is in between 0.87 to 0.96. The lower mode of ρ_{hv} suggests a possibility of a mixture of hydrometeors (e.g.,

rain, hail, and melting hail), irregular hydrometeors (e.g., lumps and lobes), and resonant sized hydrometeors. The contoured frequency by altitude diagram of ρ_{hv} and height reveals a clear shift in mode just above the surface. The mode in the composite analysis is near 0.985 at 1.5 km above the surface and broadens substantially with a mode of 0.975 and 0.935 near the surface (Figure 4.16d). This high value 1.5 km and above the surface suggests that a consistent hydrometeor type exist above the 1.5 km level. In this case, the consistent hydrometeor type is most likely hail. For the height bin from 0 to 250 m, the ρ_{hv} 25th, 50th, and 75th percentiles for are 0.88, 0.93, and 0.96 with a mean of 0.91 while above the 0 °C level for most cases from 4.00 to 4.25 km bin the 25th, 50th, and 75th percentiles for ρ_{hv} are 0.94, 0.98, and 0.99 with a mean of 0.96. The shift towards lower ρ_{hv} values near the surface suggests melting is occurring causing a mixture of hydrometeors below this level along with resonant sized hydrometeors. As observed in the Z_{dr} and height joint frequency histograms, a clear shift in mode occurs in the polarimetric data below the 0 °C level even in hail producing thunderstorms.

The last composite comparisons that will be made are the K_{dp} analysis. The joint relative frequency distribution of K_{dp} and Z_h reveals a rather noisy distribution of data (Figure 4.16e). Figure 4.11e reveals varies modes. The first mode occurs near 2 °km^{-1} with Z_h of 46-48 dBZ. A second mode occurs at 0 °km^{-1} with Z_h of 48-53 dBZ. At higher Z_h (> 60 dBZ), the mode is 1-2 °km^{-1}. Table 4.1 indicates the 25th, 50th, and 75th percentiles for the K_{dp} bin from 55 to 57 dBZ are -0.10, 1.59, and 3.47 °km^{-1} with a mean of 1.68 °km^{-1}. Therefore, 50 % of the data in the 55 to 57 dBZ bin is in between -0.10 to 3.47 °km^{-1}. The mode near 0 °km^{-1} suggests isotropic hydrometeors such as hail while the positive mode suggest a possible mixture of isotropic and anisotropic

hydrometeors (e.g., rain and hail mixture). The values of K_{dp} in this composite analysis range from -4 to 8 °km^{-1}. This large spread in the data indicates that estimated K_{dp} varies significantly in hail at the C-band. The contoured frequency by altitude diagram of K_{dp} and height histogram reveals a mode near 0 °km^{-1} above 1.5 km with a shift to 1.5 °km^{-1} near the surface (Figure 4.16f). For the height bin from 0 to 250 m, the K_{dp} 25th, 50th, and 75th percentiles are 0.68, 1.88, and 3.40 °km^{-1} with a mean of 2.04 °km^{-1} while above the 0 °C level for most cases from 4.00 to 4.25 km bin, the 25th, 50th, and 75th percentiles for K_{dp} are -0.09, 0.25, and 0.63 °km^{-1} with a mean of 0.93 °km^{-1}. The data also becomes rather noisy below 1.5 km values of K_{dp} below this level as the distribution broadens. K_{dp} is the one-half range derivative of the already noisy field Φ_{dp} (Bringi and Chandrasekar 2001. p.548-550). Therefore, K_{dp} can be a particularly noisy field. Again, there is a significant shift in mode and range of values below 1.5 km suggesting clearly that the melting of resonant sized hydrometeors causes obvious shifts in polarimetric data.

May 25, 2009 (Rain Case)

For comparison, a rain case was analyzed in the same manner as the hail cases. Similarly, histogram plots are produced in the same manner as the hail histogram plots. During this case, the ARMOR C-band radar was only operating in rain1 mode. Therefore, the height plots will not have as much detail. The case was carefully evaluated to make sure no hail was reported which would have contaminated the sample for comparison. The joint frequency histograms were made from one single radar volume that contains no evidence of hail falling at the ground. The comparison should be useful in making distinctions in polarimetric signatures from rain and hail.
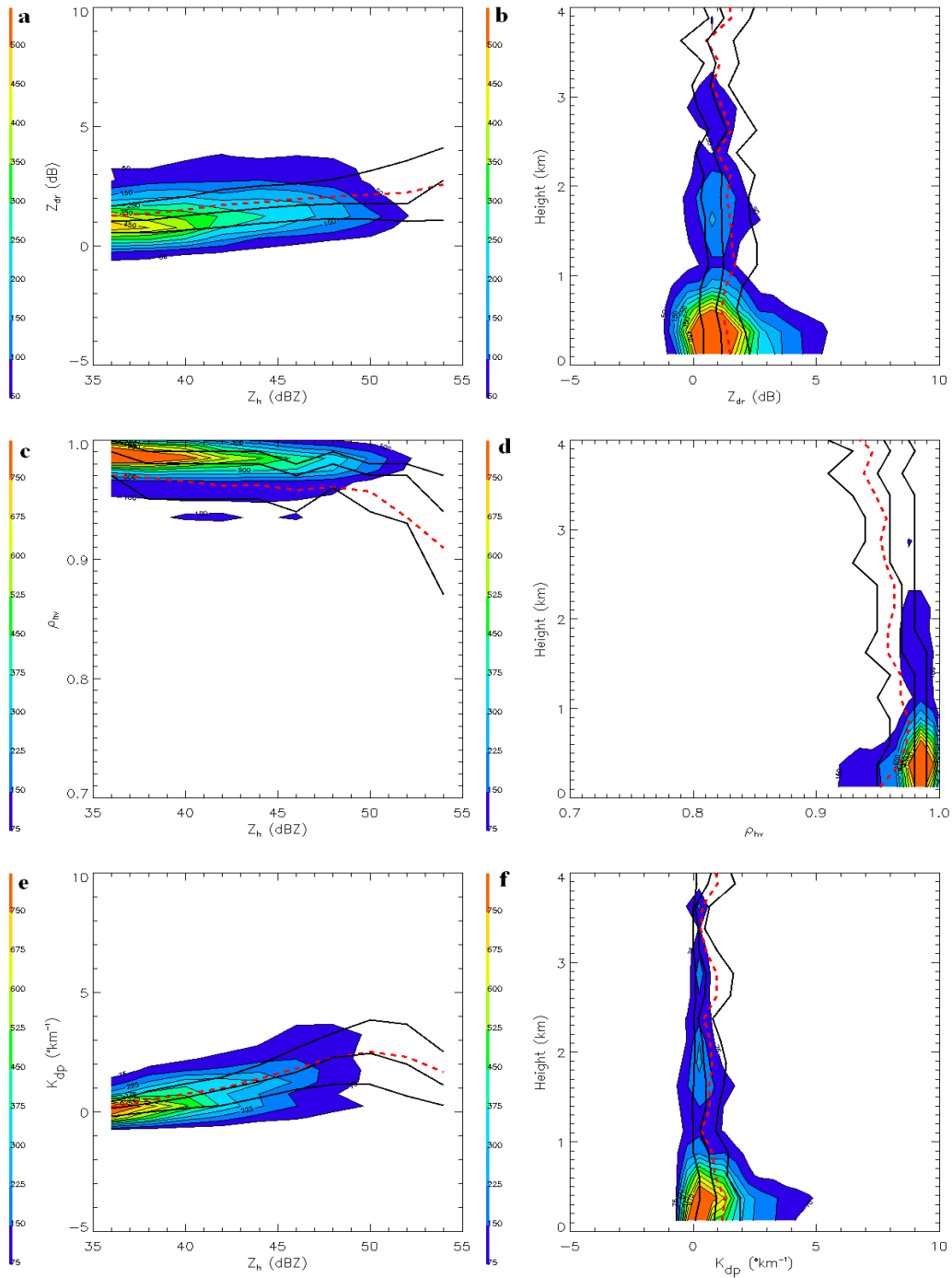
Figure 4.17: Same as Figure 4.8 except for the May 25, 2009 rain case data set and the 0 °C level near 4.3 km.

The joint frequency histogram of Z_{dr} and Z_h for rain reveals a mode of Z_{dr} near 1 dB for Z_h values from 36 to 38 dBZ (Figure 4.17a). The mode slightly increases as Z_h increases. However, this mode remains low (< 3 dB) compared to the hail cases. The range of Z_{dr} values for the rain case is only from -0.5 to 4 dB. This range is rather small when compared to the hail cases that can range from -1 dB to 10 dB. In the Z_h bin from 49-51 dBZ, the 25th, 50th, and 75th percentiles of Z_{dr} are 1.11, 1.77, and 3.16 dB with a mean of 2.14 dB. The joint frequency histogram of Z_{dr} and height reveals a mode of near 0 dB around 2 km with a gradual shift to 1 dB near the surface (Figure 4.17b). However, a range of Z_{dr} exists between -0.5 to 5 dB. The vertical structure of Z_{dr} does not exhibit anomalously high values Z_{dr} like those observed for the hail case. For the height bin from 0 to 250 m, the 25th, 50th, and 75th percentiles for Z_{dr} are 0.43, 1.18, and 2.31 dB with a mean of 1.50 dB. The statistical distribution of the rain case shows that Z_{dr} is lower in this case than the other hail cases. The analysis is different than the hail cases that exhibit high Z_{dr} (3-8 dB) near the surface. However, these Z_{dr} values are similar to those by other studies for rain at the C-band (e.g., Bringi et al. 1991, Aydin and Giridhar 1992, Carey et al. 2000).

The joint frequency histogram of ρ_{hv} and Z_h indicates a mode of near 0.985 for Z_h values from 36 to 39 dBZ with a slight decrease in ρ_{hv} toward high Z_h (Figure 4.17c). The high mode in this case suggests that only rain is occurring in the sample. For the Z_h bin from 43 to 45 dBZ, the 25th, 50th, and 75th percentiles for ρ_{hv} are 0.95, 0.98, and 0.99 with a mean of 0.96 while for higher Z_h in the 51 to 53 dBZ bin the 25th, 50th, and 75th percentiles for ρ_{hv} are 0.93, 0.97 and 0.98 with a mean of 0.94. This lowering in ρ_{hv} could be due to larger sized raindrops (> 5 mm) that fall into the resonant region (Zrnic

et al. 2000). The joint frequency histogram of ρ_{hv} and height indicates a fairly consistent profile from 2 km to the surface with a mode of 0.98 (Figure 4.17d). However, at the surface there is a wider range of ρ_{hv} values from 0.92 to 1.00. For the height bin from 0 to 250 m, the 25th, 50th, and 75th percentiles for ρ_{hv} are 0.95, 0.98, and 0.99 with a mean of 0.95 while for higher up in the 3 to 3.25 km bin, the 25th, 50th, and 75th percentiles for ρ_{hv} are 0.94, 0.96 and 0.98 with a mean of 0.96. Overall, there is not much variation in ρ_{hv} with height because the profile is taken below the 0 °C level of 4.3 km. However, the 25th percentile line is rather low (0.89 – 0.94) and could be due to resonant sized drops that cause ρ_{hv} to lower significantly (Zrnic et al. 2000). Overall, the ρ_{hv} results for the rain case are similar to those observed in other rain studies at the C-band (e.g., Bringi et al. 1991, Aydin and Giridhar 1992, Carey et al. 2000). The hail cases in this study differ because they show a clear decrease in ρ_{hv} with height as melting occurs.

The joint frequency histogram of K_{dp} and Z_h reveals a clear mode of near 0 °km[-1] for values of Z_h from 36 to 39 dBZ. Beyond this a clear increase in K_{dp} can be seen with increasing Z_h (Figure 4.17e). This has been observed by many other rain studies at the C-band (e.g., Bringi et al. 1991, Aydin and Giridhar 1992, Carey et al. 2000). The raindrops with larger diameters produce large Z_h (> 40 dBZ) and positive K_{dp}. For the Z_h bin from 43 to 45 dBZ, the 25th, 50th, and 75th percentiles for K_{dp} are 0.62, 1.26, and 1.98 °km[-1] with a mean of 1.38 °km[-1] while for higher Z_h in the 51 to 53 dBZ bin, the 25th, 50th, and 75th percentiles for K_{dp} are 0.68, 2.00 and 3.66 °km[-1] with a mean of 2.30 °km[-1]. The values of K_{dp} range from -1 to 4 °km[-1], while the range of K_{dp} values for hail case could be as large as -5 to 8 °km[-1]. Clearly, K_{dp} for hail is much noisier than the K_{dp} for rain. The joint frequency histogram of K_{dp} and height indicates a mode of 0 °km[-1] for all

height levels (Figure 4.17f). For the height bin from 0 to 250 m, the 25th, 50th, and

75th percentiles for K_{dp} are 0.07, 0.85, and 1.90 $^{\circ}$km^{-1} with a mean of 1.19 $^{\circ}$km^{-1} while for

higher up in the height bin of 3 to 3.25 km, the 25th, 50th, and 75th percentiles for K_{dp} are

0.03, 0.25, and 1.00 $^{\circ}$km^{-1} with a mean of 0.54 $^{\circ}$km^{-1}. The range of values increases

significantly below 1 km from -1 to 1 $^{\circ}$km^{-1} above 1 km to -1 to 5 $^{\circ}$km^{-1} below 1 km.

This broadening of K_{dp} near the surface is also seen in the hail cases. However, in the

hail case the broadening can range from $-$ 5 to 8 $^{\circ}$km^{-1}. Clearly, K_{dp} is noisier for the hail

cases. This is most likely due to the large variations in Φ_{dp} for the hail cases due to

resonant scattering.

4.1.4   Small and Large Hail

In this study, hail is also separated into small and large categories and histogram

plots were made from the data. The Storm Prediction Center's (SPC) definition of large

hail is any hailstone above 2.00 inches (5.08 cm). However, in this study, small hail in

the plots is anything that is less than 1.75 inches (4.44 cm) and large hail is anything

equal to or greater than 1.75 inches (4.44 cm). The hailstone sizes in this study range

from 0.635 to 10.8 cm with a mean of 3.30 cm and median of 2.54 cm. The number of

hail reports in the small category is 108 with 64 reports in the large hail category. These

values were chosen because in this study hail larger than 2.00 inches rarely occurs in

northern Alabama. It is important to study the different signatures of large and small hail

because Bringi and Chandrasekar (2001) (p.451-452). Ryzhkov et al. (2009),

Vivekanandan et al. (1990) suggest that the hail hole (large Z_h (> 50 dBZ) and $|Z_{dr}|$

$<$ 1.0 dB) should be observed at the C-band when hailstones are large (> 1.5 cm) and

numerous enough to dominate the reflectivity and appear as effective spheres. Therefore, the larger hail in this study should produce signatures similar to the "hail hole."

Because the focus of this study is on the Z_{dr} C-band polarimetric signatures of hail, the Z_{dr} small and large joint relative frequency distributions will be addressed first. The small hail joint relative frequency distribution of Z_{dr} and Z_h indicates a mode of Z_{dr} near 4 dB for values of Z_h from 48 to 52 dBZ (Figure 4.18a). An overall increase in Z_{dr} with Z_h is observed as seen in other events. The values of Z_{dr} range significantly from - 1 dB from 47 to 52 dBZ to almost 10 dB from 54 to 57 dB. In the Z_h bin from 55-57 dBZ, the 25th, 50th, and 75th percentiles of Z_{dr} are 3.84, 5.33, and 6.83 dB with a mean of 5.27 dB. The large hail joint relative frequency distribution of Z_{dr} and Z_h shows similar results to the small hail. The mode of Z_{dr} is near 5 dB at 50-55 dBZ (Figure 4.18b). There is an overall increase of Z_{dr} with Z_h. The values of Z_{dr} range significantly from -1 dB from 48 to 52 dBZ to 10 dB from 57 to 61 dB. In the Z_h bin from 55-57 dBZ, the 25th, 50th, and 75th percentiles of Z_{dr} are 4.31, 5.83, and 7.24 dB with a mean of 5.67 dB. Both small and large hail categories are rather similar; the only difference exists where Z_{dr} is slightly higher for a given Z_h in the large hail category. Contrary to Bringi and Chandrasekar (2001) (p.451-452) and Ryzhkov et al. (2009), the large hail minimum, mode, and maximum values of Z_{dr} are slightly larger than the small hail. Similarly, the contoured frequency by altitude diagram of Z_{dr} and height were produced for both small and large hail (Figure 4.19). Table 4.2 indicates the statistical distribution of small hail data and Table 4.3 indicates the statistical distribution of large hail data. The small hail contoured frequency by altitude of Z_{dr} and height indicates a mode of Z_{dr} near 0 dB for all locations above 1.5 km with a dramatic shift toward positive
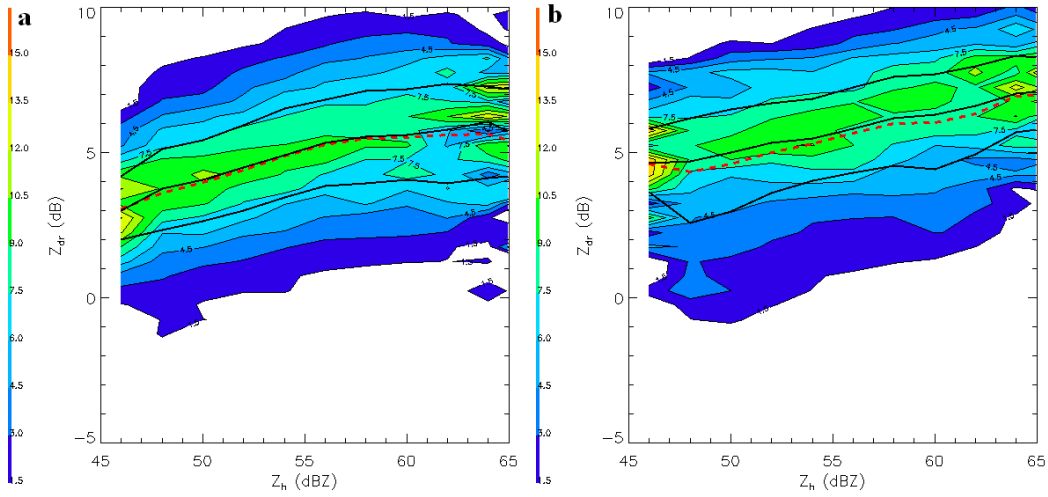
Figure 4.18: Joint relative frequency distributions in percent of (a) Small and (b) Large hail of Z_{dr} vs. Z_h. All data points taken within 1 km of hail reports where Z_h is > 45 dBZ and all data in plots are taken from below 1 km. The black lines from bottom to top are the 25th, 50th, and 75th percentile lines and the dashed red line is the mean.
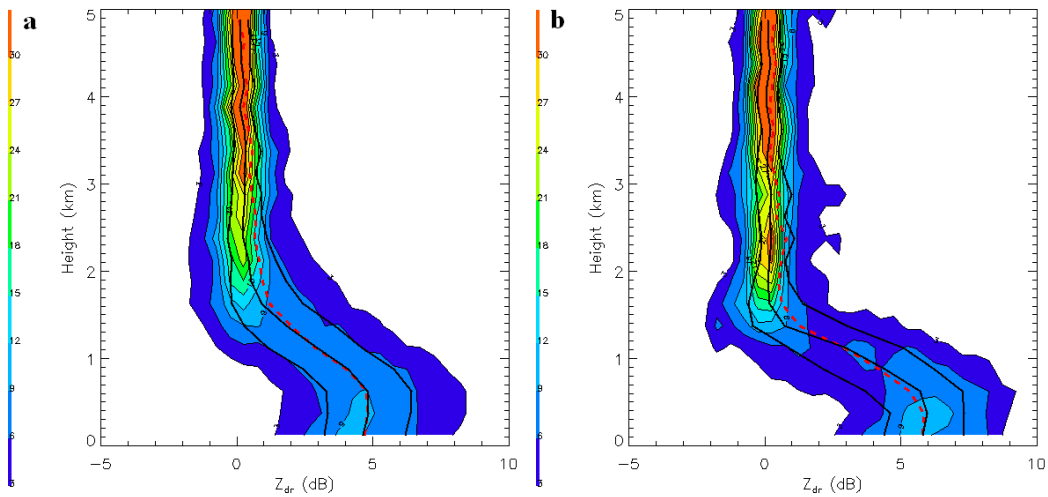
Figure 4.19: Contoured frequency by altitude diagram in percent of (a) Small and (b) Large hail of Z_{dr} vs. height. All data points taken within 1 km of hail reports where Z_h is > 45 dBZ. The black lines from left to right are the 25th, 50th, and 75th percentiles and the dashed red line is the mean.

Table 4.2 Statistical Analysis of Small Hail Data below 1 km

Z_h bin (dBZ)	Z_{dr} 25th Percentile dB	Z_{dr} 50th Percentile dB	Z_{dr} 75th Percentile dB	K_{dp} 25th Percentile $°km^{-1}$	K_{dp} 50th Percentile $°km^{-1}$	K_{dp} 75th Percentile $°km^{-1}$	ρ_{hv} 25th Percentile	ρ_{hv} 50th Percentile	ρ_{hv} 75th Percentile
45-47	2.00	2.99	4.19	1.14	1.99	2.77	0.90	0.94	0.96
47-49	2.32	3.76	5.12	0.00	1.71	3.24	0.88	0.93	0.96
49-51	2.63	4.05	5.42	0.03	1.87	3.64	0.88	0.93	0.96
51-53	3.00	4.49	5.94	0.02	2.09	3.95	0.88	0.93	0.96
53-55	3.44	4.91	6.50	0.28	2.34	4.15	0.86	0.92	0.96
55-57	3.84	5.33	6.83	0.15	2.26	4.01	0.85	0.91	0.95
57-59	3.93	5.55	7.11	0.05	2.14	4.00	0.86	0.91	0.95
59-61	4.05	5.62	7.19	-0.10	1.90	3.90	0.88	0.93	0.96
61-63	3.93	5.79	7.37	0.07	2.03	3.97	0.90	0.94	0.96
63-65	4.13	6.05	7.27	0.46	2.82	5.19	0.88	0.94	0.96

values below 1.5 km with a mode of 4 dB near the surface (Figure 4.19a). The range of

Z_{dr} values above 1.5 km is between -1 to 1 dB while near the surface the range increase to

1.5 to 8 dB. In the height bin from 0 - 250 m, the 25th, 50th, and 75th percentiles of Z_{dr} are

3.21, 4.63, and 6.20 dB with a mean of 4.71 dB while above the 0 °C level for most cases

from 4.00 to 4.25 km bin, the 25th, 50th, and 75th percentiles for Z_{dr} are -0.10, 0.26, and

0.66 dB with a mean of 0.42 dB. The large hail contoured frequency by altitude diagram

Table 4.3 Statistical Analysis of Large Hail Data below 1 km

Z_h bin (dBZ)	Z_{dr} 25th Percentile dB	Z_{dr} 50th Percentile dB	Z_{dr} 75th Percentile dB	K_{dp} 25th Percentile °km⁻¹	K_{dp} 50th Percentile °km⁻¹	K_{dp} 75th Percentile °km⁻¹	ρ_{hv} 25th Percentile	ρ_{hv} 50th Percentile	ρ_{hv} 75th Percentile
45-47	3.63	4.65	5.82	0.61	1.07	2.25	0.87	0.90	0.94
47-49	2.58	4.69	6.18	-0.21	1.04	3.04	0.88	0.93	0.96
49-51	2.98	5.00	6.47	-0.07	1.61	3.75	0.88	0.93	0.96
51-53	3.61	5.34	6.69	-0.09	1.60	3.73	0.89	0.94	0.96
53-55	4.02	5.49	6.85	-0.14	1.41	3.53	0.89	0.94	0.96
55-57	4.31	5.83	7.24	-0.58	0.94	2.57	0.88	0.93	0.96
57-59	4.55	6.19	7.60	-0.81	0.66	1.98	0.8	0.93	0.96
59-61	4.42	6.30	7.69	-0.67	0.64	1.95	0.88	0.93	0.96
61-63	4.94	6.60	7.97	-0.56	0.72	1.90	0.90	0.94	0.96
63-65	5.69	7.03	8.32	-0.46	0.76	2.02	0.92	0.95	0.97

of Z_{dr} and height shows a mode of Z_{dr} near 0 dB for all locations above 1.5 km with an even more dramatic shift towards positive values with a mode near the surface of 5.5 dB (Figure 4.19b). The range of Z_{dr} values above 1.5 km is between -1 to 1 dB while near the surface the range increases to 2.5 to 9 dB. In the height bin from 0 - 250 m, the 25th, 50th, and 75th percentiles of Z_{dr} are 4.38, 5.80, and 7.30 dB with a mean of 5.81 dB while above the 0 °C level for most cases from 4.00 to 4.25 km bin, the 25th, 50th, and

75th percentiles for Z_{dr} are -0.23, 0.07, and 0.50 dB with a mean of 0.28 dB. From this analysis, large hail actually produces slightly larger Z_{dr} than small hail. This analysis is seemingly contradictory to the conclusions of Vivekanandan et al. (1990), Bringi and Chandrasekar (2001) (p.451-452) and Ryzhkov et al. (2009).

In addition, all polarimetric variables were analyzed to determine the different signatures between small and large hail. The first that will be addressed is the small hail joint relative frequency distribution of ρ_{hv} and Z_h. There are two modes one occurs for ρ_{hv} of 0.975 for all values of Z_h and the other occurs at ρ_{hv} of 0.935 for all values of Z_h (Figure 4.20a). For the Z_h bin from 55 to 57 dBZ, the 25th, 50th, and 75th percentiles for ρ_{hv} are 0.85, 0.91, and 0.95 with a mean of 0.90. The large hail joint relative frequency distribution of ρ_{hv} and Z_h reveals two modes of ρ_{hv} (Figure 4.20b). The first mode occurs at a ρ_{hv} of 0.975 for all values of Z_h while the second mode occurs at 0.935 for all values of Z_h. For the Z_h bin from 55 to 57 dBZ, the 25th, 50th, and 75th percentiles for ρ_{hv} are 0.88, 0.93, and 0.96 with a mean of 0.91. The only difference between small and large is that the statistics of ρ_{hv} are slightly higher for large hail. The small hail contoured frequency by altitude diagram of ρ_{hv} and height reveals a mode of near 0.985 above 2 km (Figure 4.21a). There are two modes near the surface of 0.975 and 0.935 with a range of values from 0.80 – 1.00. For the height bin from 0 - 250 m, the 25th, 50th, and 75th percentiles for ρ_{hv} are 0.87, 0.92, and 0.95 with a mean of 0.90 while above the 0 °C level for most cases from 4.00 to 4.25 km bin, the 25th, 50th, and 75th percentiles for ρ_{hv} are 0.93, 0.98, and 0.99 with a mean of 0.95. The contoured frequency by altitude diagram of large hail ρ_{hv} and height indicates a mode of near 0.98 above 1.5 km (Figure 4.21b).
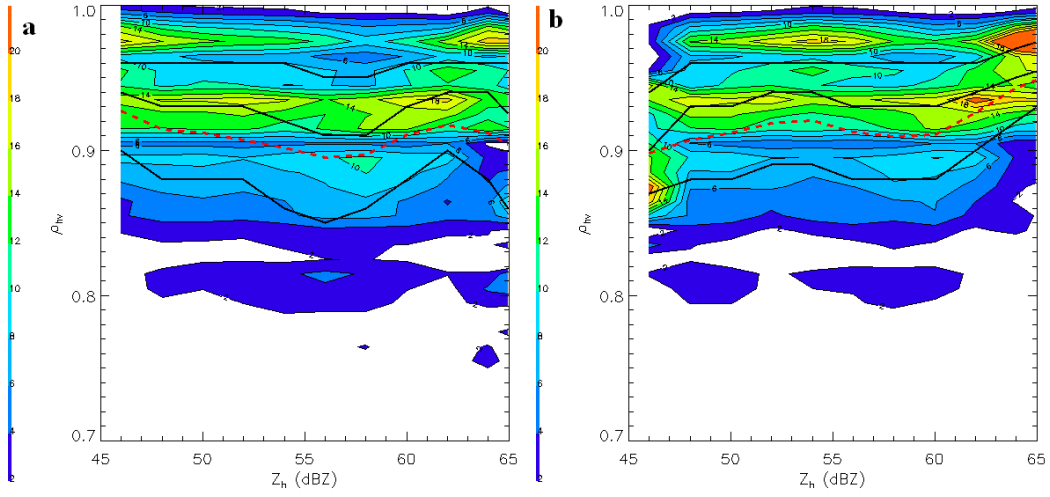
Figure 4.20: Same as Figure 4.18 except ρ_{hv} vs. Z_h.
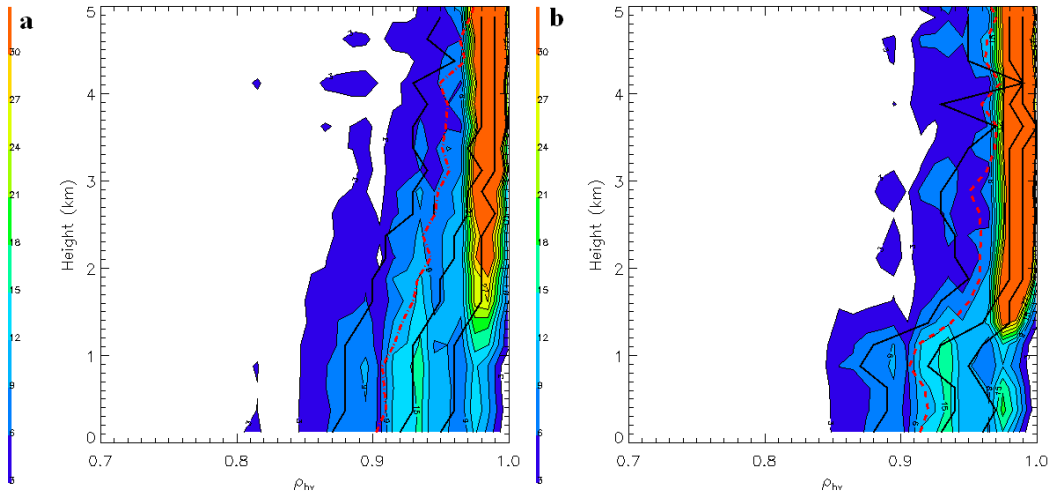
Figure 4.21: Same as Figure 4.19 except ρ_{hv} vs. height.

Near the surface, there are two modes at 0.975 and 0.935. For the height bin from 0 –

250 m, the 25th, 50th, and 75th percentiles for ρ_{hv} are 0.88, 0.93, and 0.96 with a mean of

0.91 while above the 0 °C level for most cases from 4.00 to 4.25 km bin the 25th, 50th,

and 75th percentiles for ρ_{hv} are 0.95, 0.98, and 0.99 with a mean of 0.97. Overall, both the

small and large appear to be similar in nature showing a decrease in ρ_{hv} as melting begins

to occur.

The small hail joint relative frequency distribution of K_{dp} and Z_h is bimodal with

the first mode of 0 °km^{-1} for values of Z_h from 48 to 52 dBZ and the second of 2 °km^{-1} for

values of Z_h from 46 to 55 dBZ (Figure 4.22a). K_{dp} ranges significantly from -4 to

7 °km^{-1}. For the Z_h bin from 55 to 57 dBZ, the 25th, 50th, and 75th percentiles for K_{dp} are

0.15, 2.26, and 4.01 °km^{-1} with a mean of 2.08 °km^{-1}. The large hail joint relative

frequency distribution K_{dp} and Z_h has multiple modes with the first mode of 0 °km^{-1} for

values of Z_h from 48 to 50 dBZ (Figure 4.22b). The second mode can be seen near

1 °km^{-1} for Z_h values of 46-48 dBZ. For higher Z_h (> 55 dBZ), the mode is near 1 °km^{-1}

for values of Z_h greater than 55 dBZ. For the Z_h bin from 55 to 57 dBZ, the 25th, 50th, and

75th percentiles for K_{dp} are -0.58, 0.94, and 2.57 °km^{-1} with a mean of 1.13°km^{-1}. There is

also a large range of K_{dp} values from -4 to 8 °km^{-1}, but the range becomes small with

increasing Z_h. Overall, the small hail K_{dp} is slightly higher than the large hail K_{dp}. The

small hail contoured frequency by altitude of K_{dp} and height reveals a mode of 0 °km^{-1}

above 2 km (Figure 4.23a). Then the mode shifts toward 2 °km^{-1} near the surface. Below

2 km, the plot becomes rather noisy with a broader distribution of K_{dp} values ranging

from -3 to 6 °km^{-1}. For the height bin from 0 - 250 m, the 25th, 50th, and 75th percentiles

for K_{dp} are 1.14, 2.25, and 3.91 °km^{-1} with a mean of 2.45 °km^{-1} while above the 0 °C
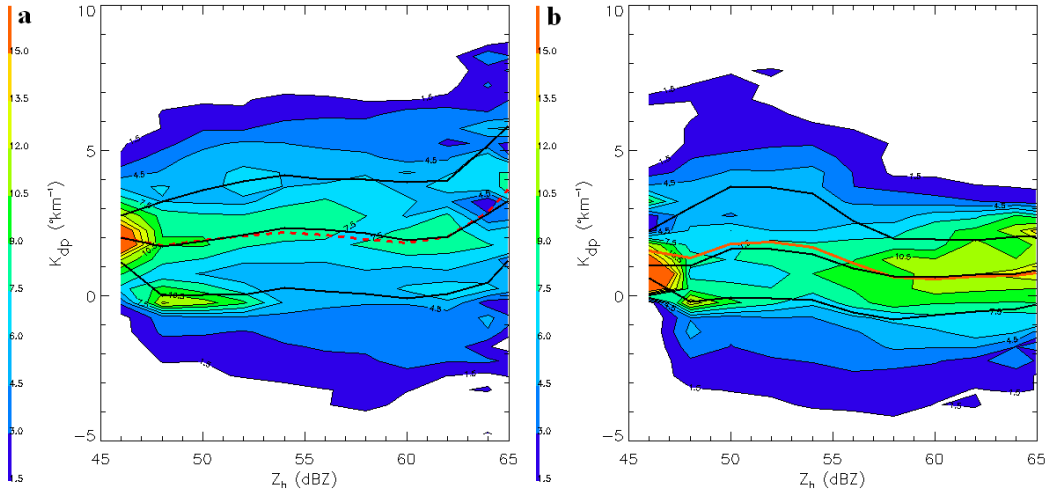
Figure 4.22: Same as Figure 4.18 except K_{dp} vs. Z_h.
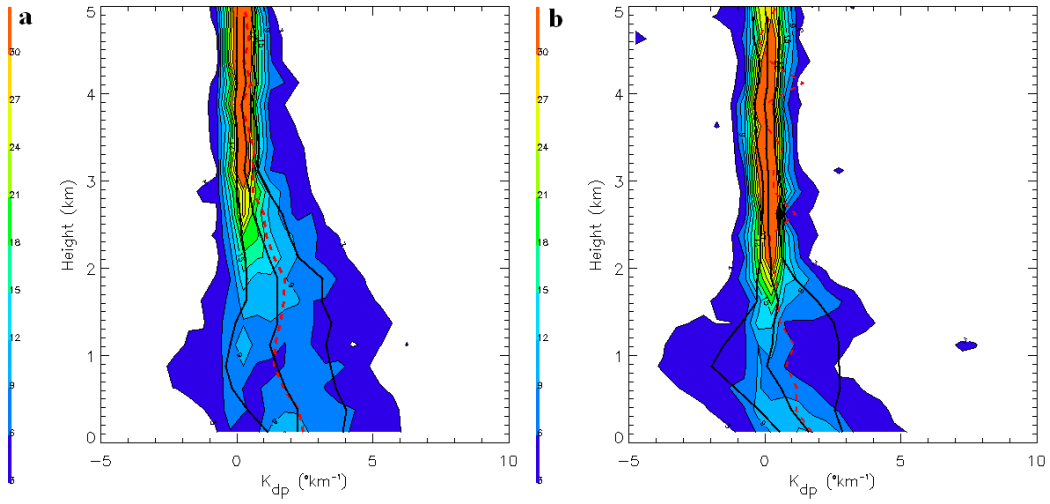
Figure 4.23: Same as Figure 4.19 except K_{dp} vs. height

100

level for most cases from 4.00 to 4.25 km bin, the 25th, 50th, and 75th percentiles for K_{dp} are 0.01, 0.33, and 0.74 $^{\circ}$km^{-1} with a mean of 0.53 $^{\circ}$km^{-1}. The large hail contoured frequency by altitude diagram of K_{dp} and height indicates a mode of near 0 $^{\circ}$km^{-1} above 1.5 km (Figure 4.23b). However, the mode shifts gradually towards 1 $^{\circ}$km^{-1} near the surface. For the height bin from 0 - 250 m, the 25th, 50th, and 75th percentiles for K_{dp} are 0.56, 1.65, and 2.86 $^{\circ}$km^{-1} with a mean of 1.74 $^{\circ}$km^{-1} while above the 0 $^{\circ}$C level for most cases from 4.00 to 4.25 km bin, the 25th, 50th, and 75th percentiles for K_{dp} are -0.25, 0.10, and 0.50 $^{\circ}$km^{-1} with a mean of -0.01 $^{\circ}$km^{-1}. The K_{dp} values near the surface are relatively noisy with values ranging from -4 to 5 $^{\circ}$km^{-1}. Overall, the signatures of K_{dp} of hail for both small and large hail are similar with near 0 $^{\circ}$km^{-1} above the 0 $^{\circ}$C level and become rather noisy below the 0 $^{\circ}$C level.

4.2   Potential "Hail Hole" Cases

Even though the majority of cases show the high Z_{dr} signature, there are a few cases that suggest a possible "hail hole" may sometimes exist. In this section, two of these examples will be addressed. One of the examples (April 7, 2005) does not meet the storm report criteria while the other does (March 12, 2010). Possible reasons for the signature will be discussed and analyzed.

April 7, 2005

A strong upper level low produced a few reports of severe weather in the Southeast US on April 7, 2005. Early in the afternoon a storm developed in central Alabama and tracked towards the northeast throughout the day. Due to the lack of

widespread organized convection, only one cell produced severe hail within 100 km of the ARMOR C-band radar. This report was from a storm in Marshall County that produced penny sized hail (1.9 cm). The report was carefully analyzed to see if it met the storm report criteria for this study and it did not due to the inaccuracy of the location of the report. However, the storm was still analyzed at the time of the report using contoured ARMOR data and a 1 km circle to denote the location of the storm report.

A cursory examination of the PPI images from ARMOR reveals a key difference between the current (Figures 4.24-4.29) and earlier examples. The first and most obvious difference is the clear lowering of Z_{dr} (~0 dB) associated with the highest Z_h (~ 55 dBZ) (Figures 4.24-4.25). This behavior in Z_{dr} is contrary to what has been observed in the previous case study examples and more similar to the "hail hole" concept than the high Z_{dr} (3-8 dB) concept. The PPI is from the lowest elevation angle and should be most representative of what is occurring at the surface. The PPI is also taken from well below the 0 °C level of 2.4 km such that melting hail and rain are likely present within the storm. This example shows that both the corrected and uncorrected Z_{dr} are low and slightly negative for the strongest part of the storm (Figures 4.25-4.26). The PPI reveals that K_{dp} is rather large (> 5 °km^{-1}) in the strongest areas of the storm (Figure 4.27). The storm exhibits low ρ_{hv} (< 0.95) with the area of higher Z_h (~ 55 dBZ) suggesting a mixture of hydrometeors and resonant sized hydrometeors (Figure 4.28). The PPI also indicates that large amounts of Φ_{dp} (> 80°) are occurring within the strongest part of the cell (Figure 4.29). This example must be viewed with caution because it does not meet the storm report criteria for a more detailed analysis. However, this example is one of the
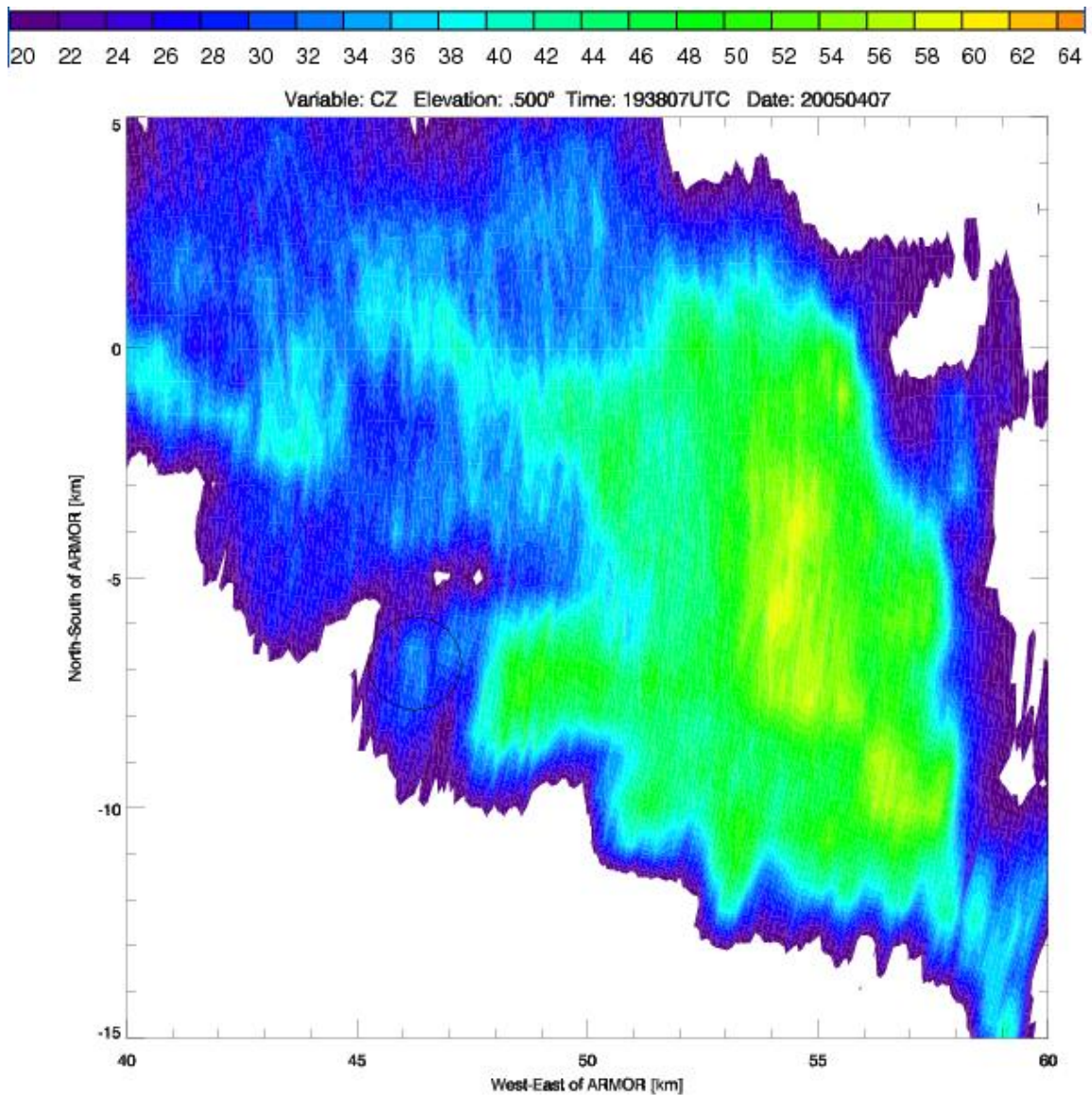
Figure 4.24: Plan Position Indicator (PPI) of contoured corrected Z_h (dBZ) on April 7, 2005 at 1938 UTC at 0.5° elevation angle. The circle is from a hail report within 1 minute of the time of the scan. The circles represent the 1 km radius from the hail report. Horizontal east-west distance from ARMOR (km) versus north-south distance from ARMOR (km) is shown. The potential hail hole is found at x = 54 km and y = -6 km.
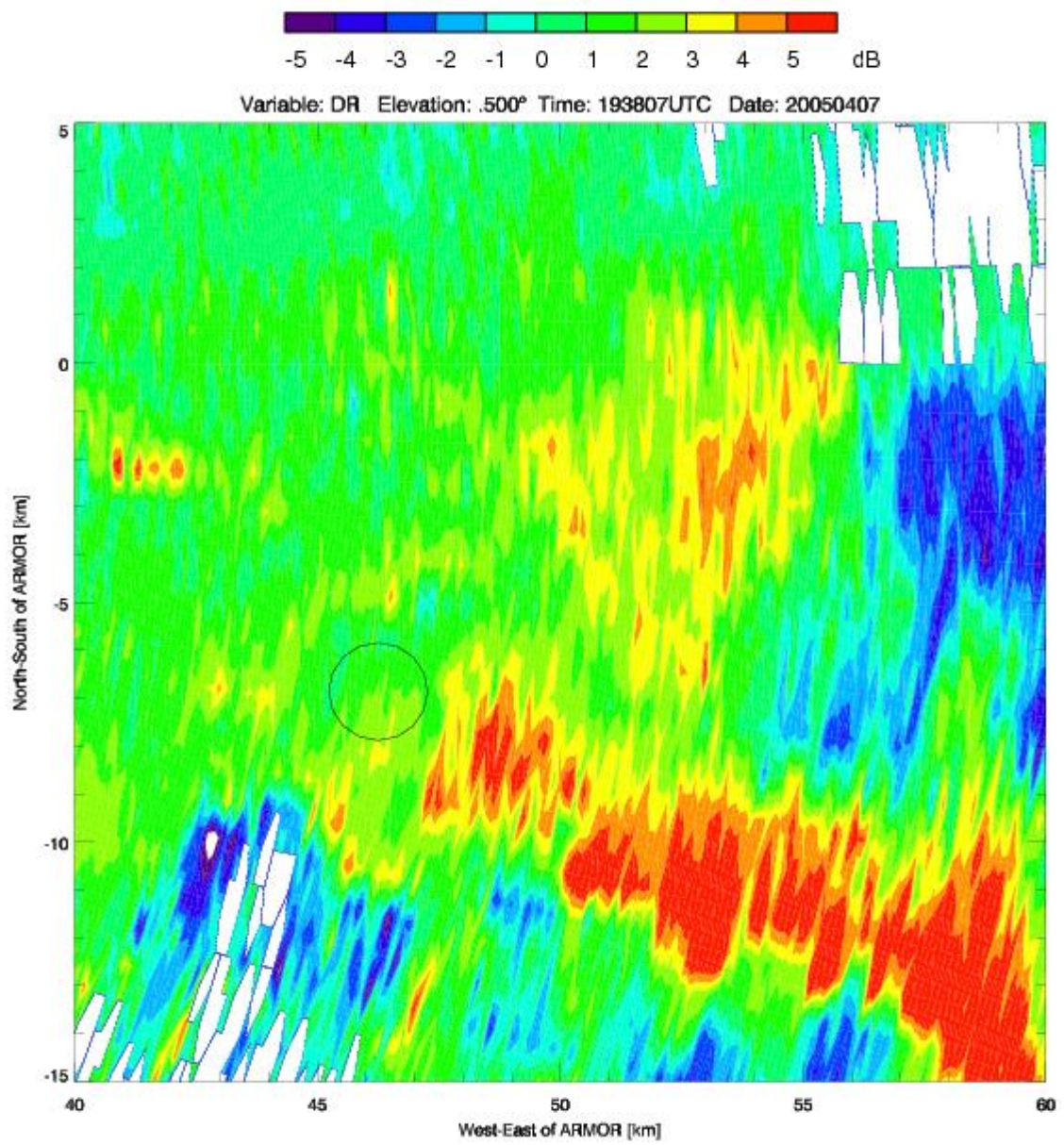
Figure 4.25: Same as Figure 4.24 except contoured corrected Z_{dr} (dB).
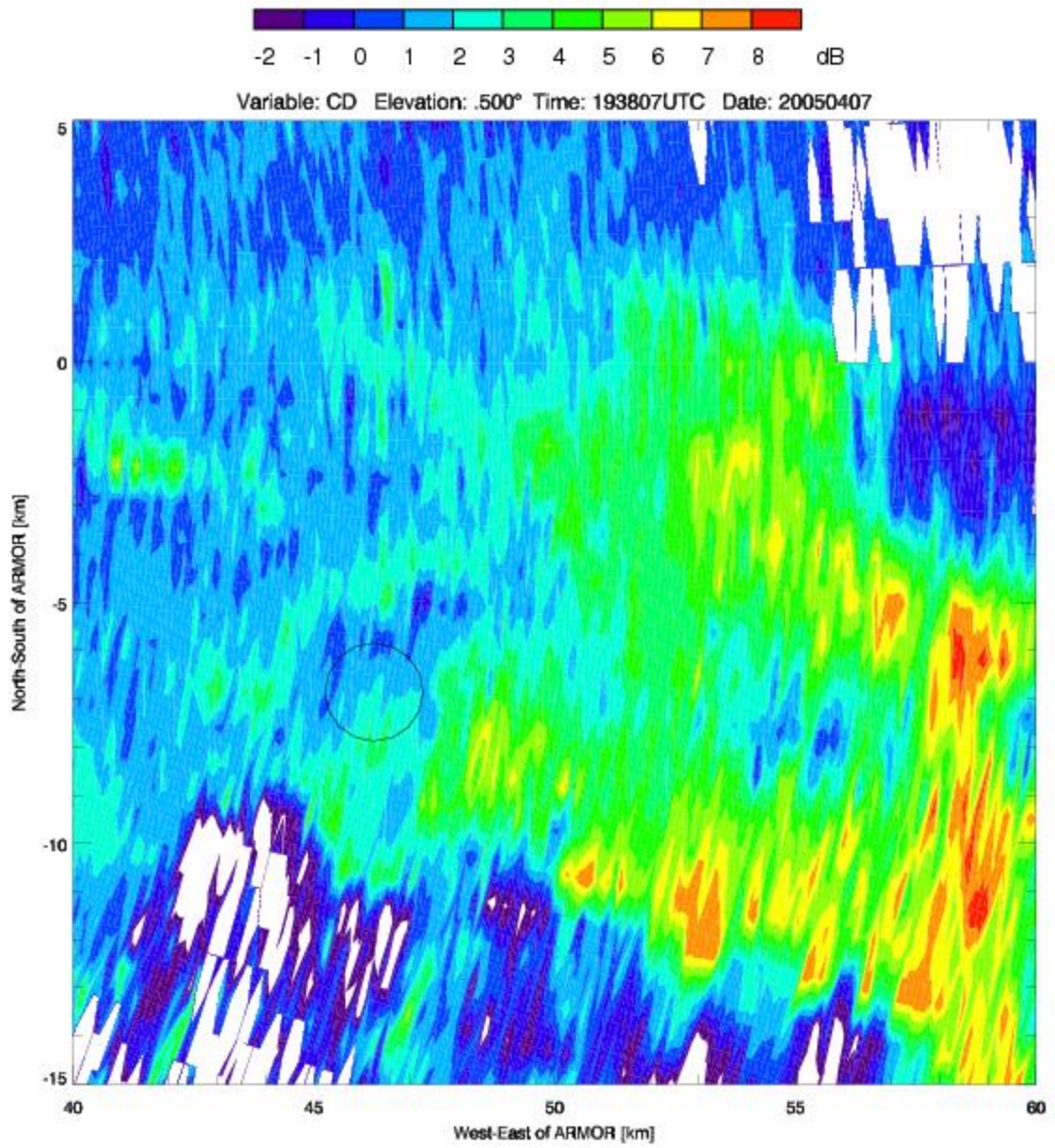
Figure 4.26: Same as Figure 4.24 except contoured uncorrected Z_{dr} (dB).
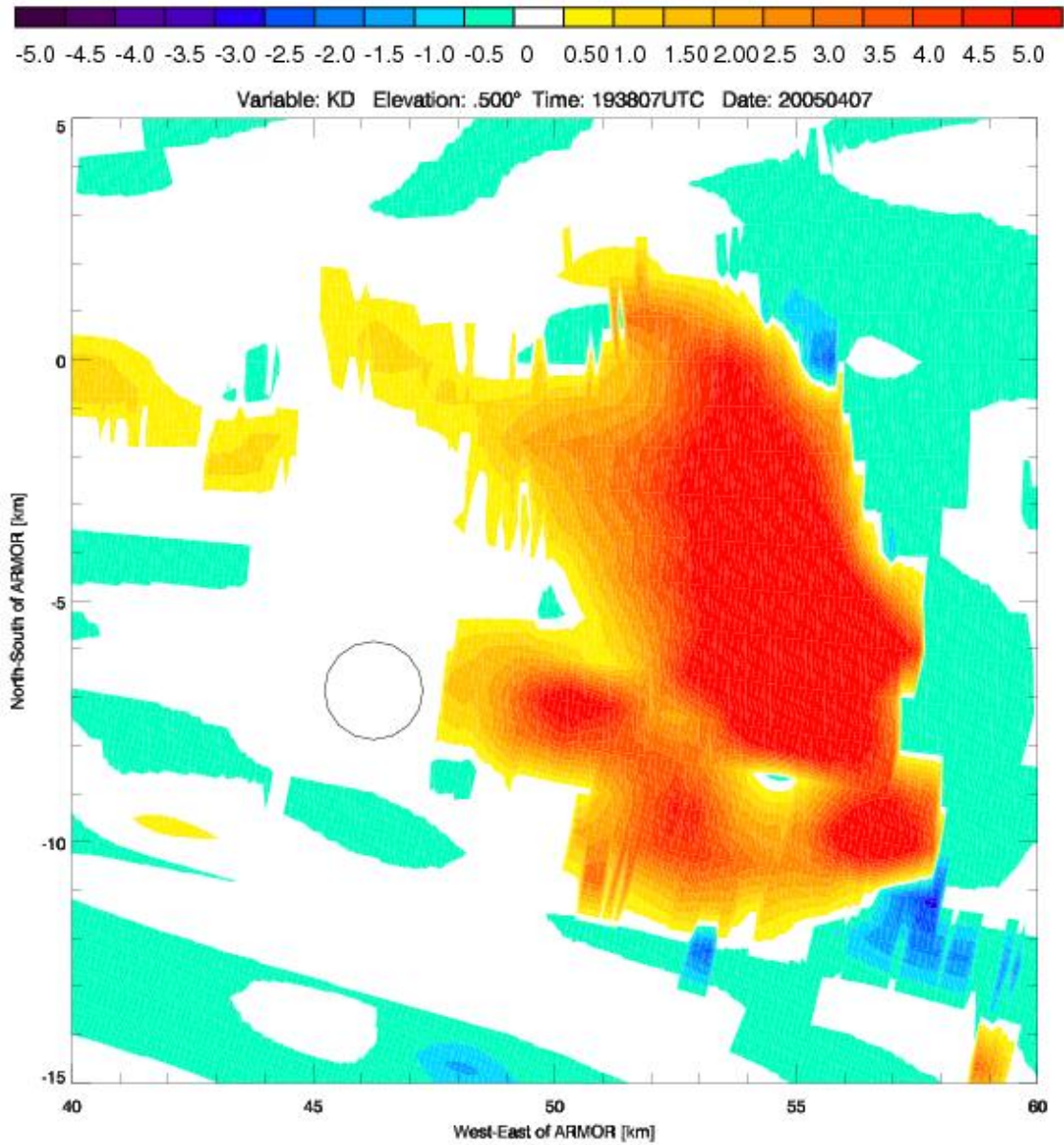
Figure 4.27: Same as Figure 4.24 except contoured K_{dp} (°km^{-1}).
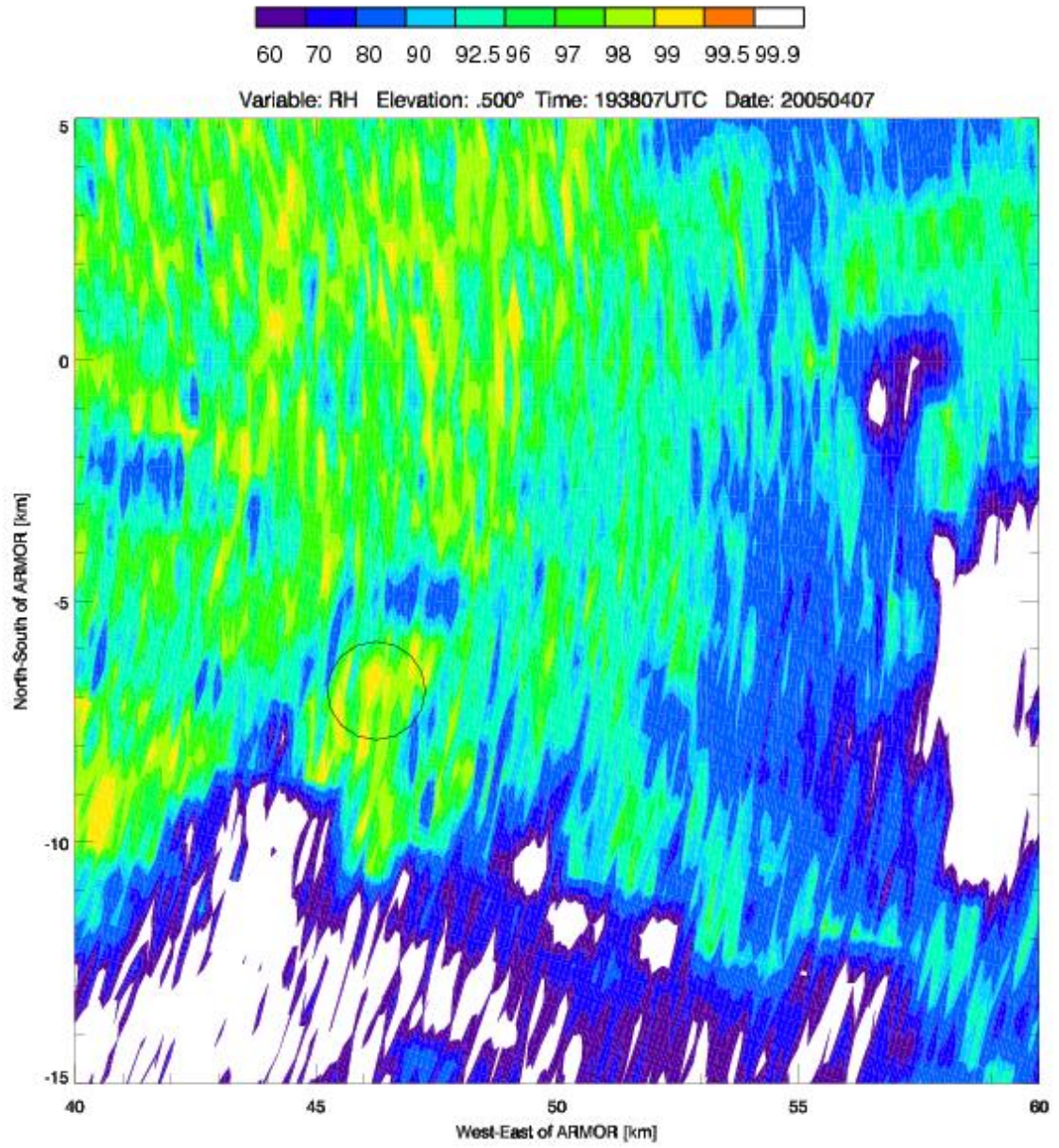
Figure 4.28: Same as Figure 4.24 except contoured ρ_{hv}.
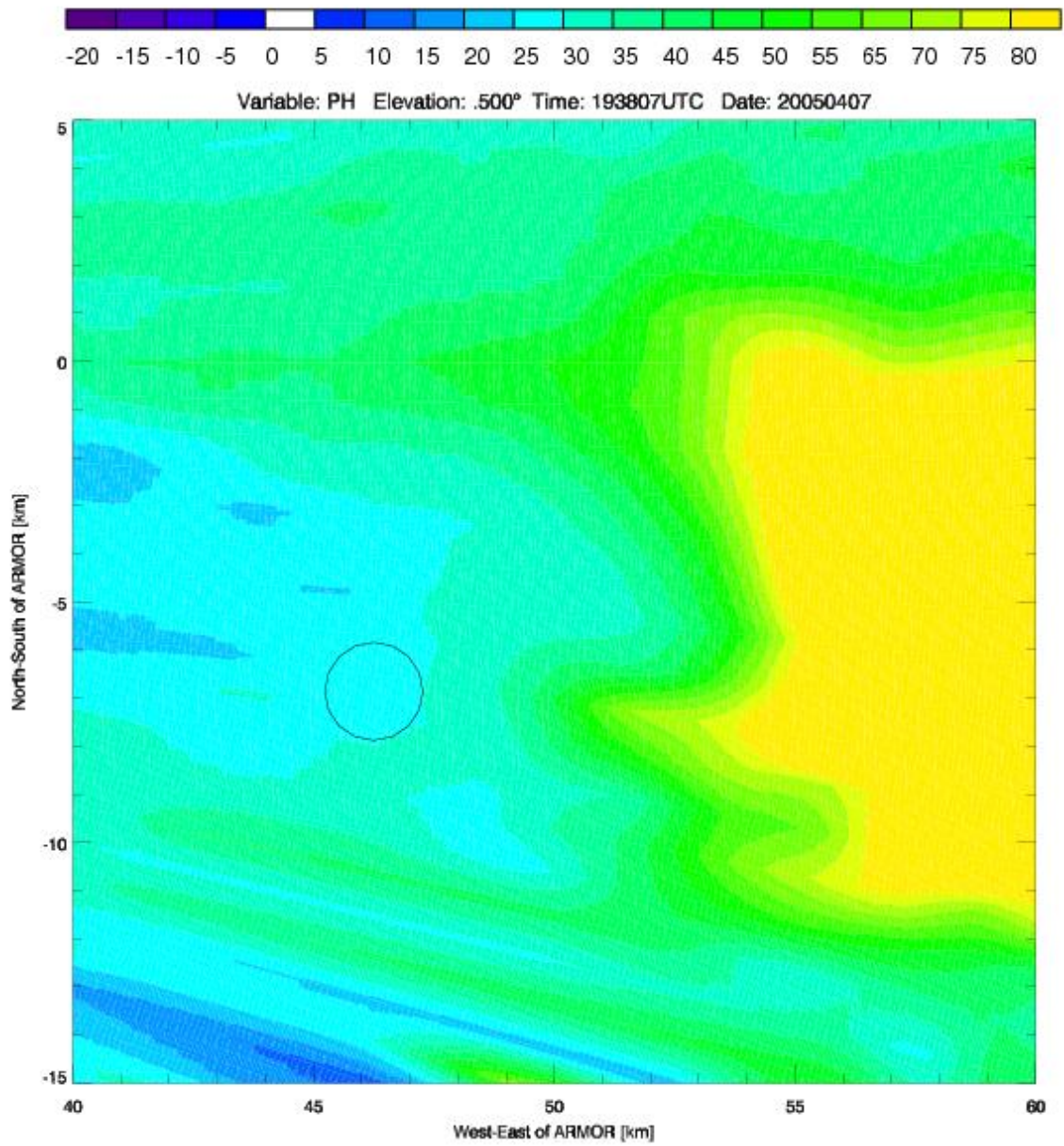
Figure 4.29: Same as Figure 4.25 except for contoured Φ_{dp} (°).

best potential examples of a "hail hole," but the data must be carefully evaluated before declaring the signature as a "hail hole."

March 12, 2010

A strong upper level system produced numerous reports of severe weather that occurred across the Southeast US. Supercell thunderstorms developed along the Mississippi and Alabama border early in the morning hours and progressed across the state of Alabama throughout the morning. As the line of severe thunderstorms crossed north Alabama, over 21 reports of severe hail were received that met the storm report criteria. Of these reports, one of them will be analyzed in this section to see if it meets the criteria for a "hail hole" signature. The report was examined carefully, and for this case, the report does meet the storm report criteria for this study with a 50 dBZ gate within 1 km in 15 minutes of the report.

The PPI image for this case is taken at the lowest elevation angle (0.7°) to give the best representation of the C-band polarimetric signatures at the surface (Figures 4.30-4.35). The circle marks the location of the hail report and the 1 km radius within the location of the reports (Figures 4.30-4.35). The location of the hail report is found within the area of high Z_h (> 50 dBZ) and low Z_{dr} (< 2 dB) on the northwestern edge of the line of storms (Figures 4.30-4.31). The Z_h data in the region of the hail report looks to be inconsistent in the cell and may have some errors in the data (Figure 4.30). In addition, multiple negative values of Z_{dr} can be seen down range of the hail report suggesting that large amounts of differential attention is occurring in this location (Figures 4.31-4.32). There are also obvious differences between the corrected and uncorrected Z_{dr} suggesting
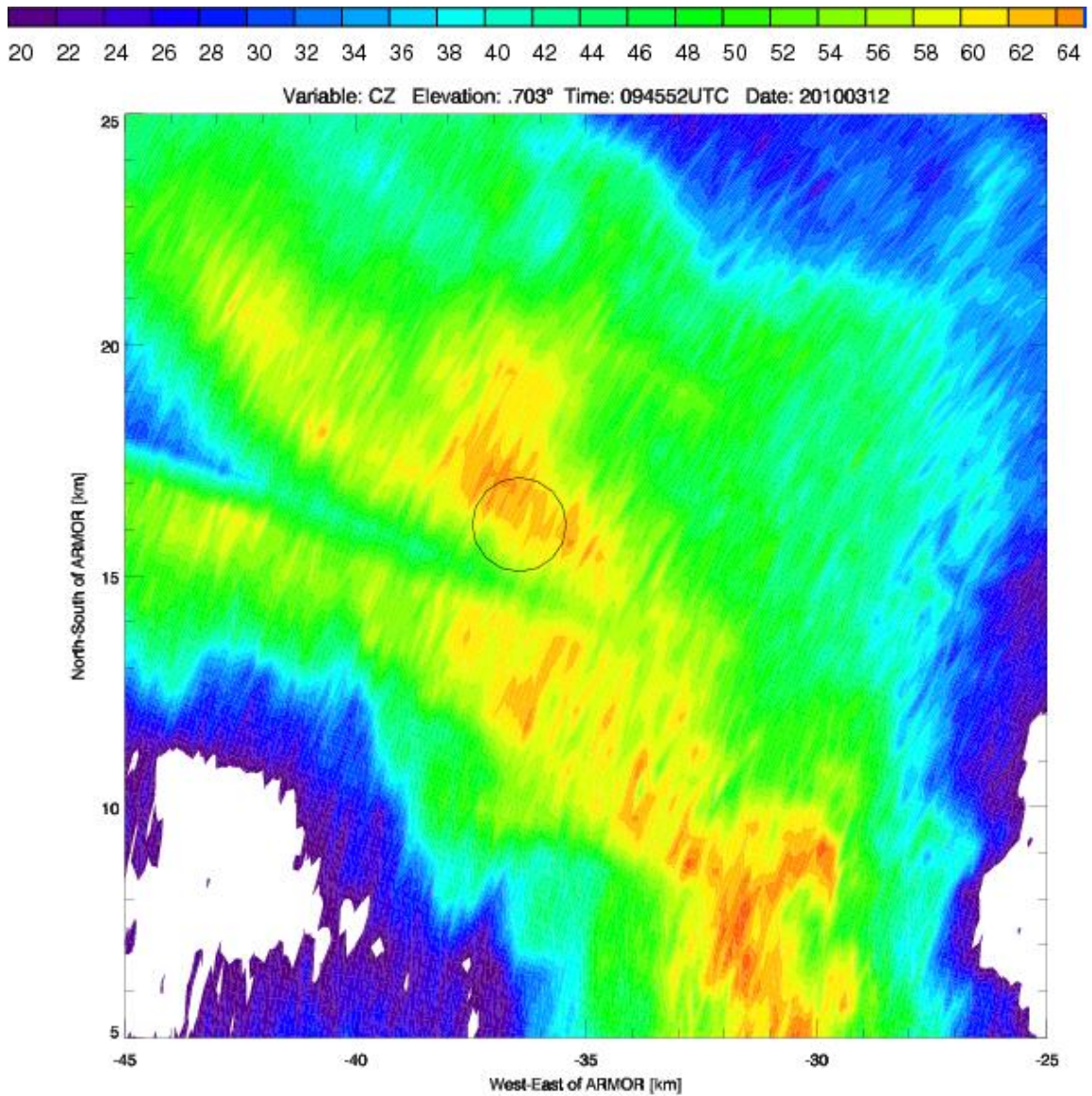
Figure 4.30: Plan position indicator of contoured Z_h (dBZ) on March 12, 2010 at
0945 UTC at 0.7° elevation angle. The circle is from a hail report within 1 minute of the
time of the scan. The circles represent the 1 km radius from the hail report. Horizontal
east-west distance from ARMOR (km) versus north-south distance from ARMOR (km) is
shown.
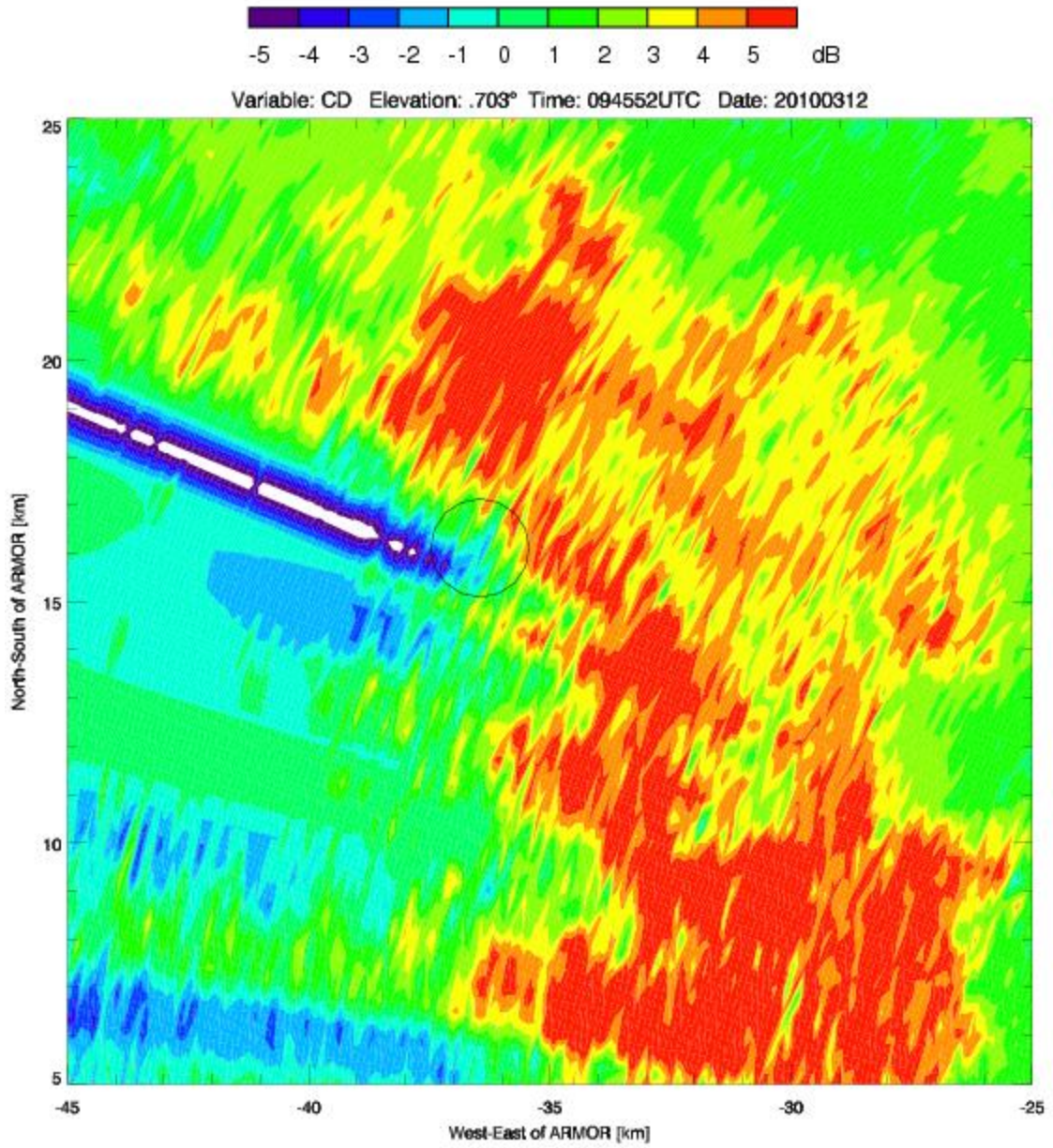
Figure 4.31: Same as Figure 4.30 except contoured corrected Z_{dr} (dB).
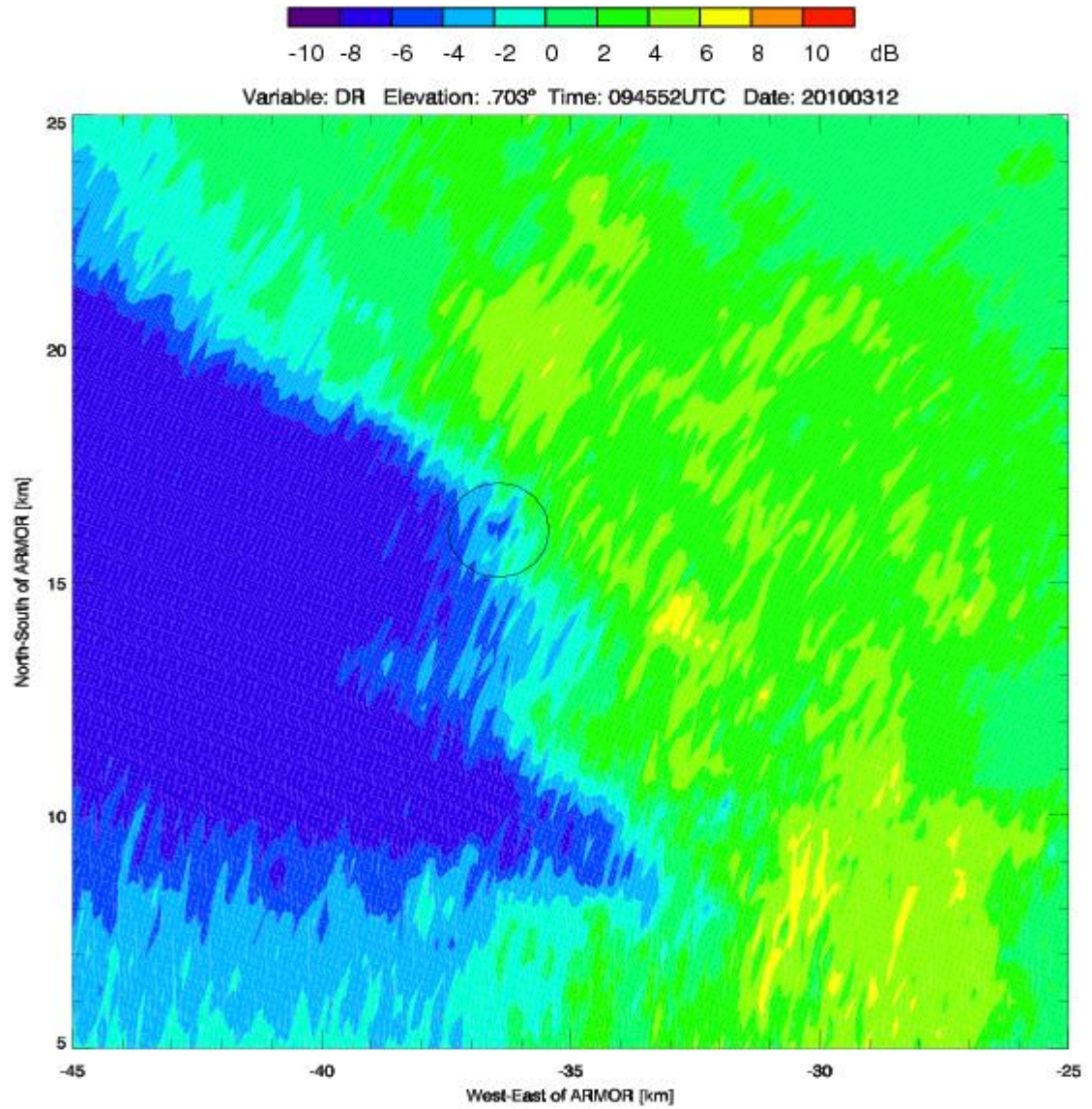
Figure 4.32: Same as Figure 4.30 except contoured uncorrected Z_{dr} (dB).
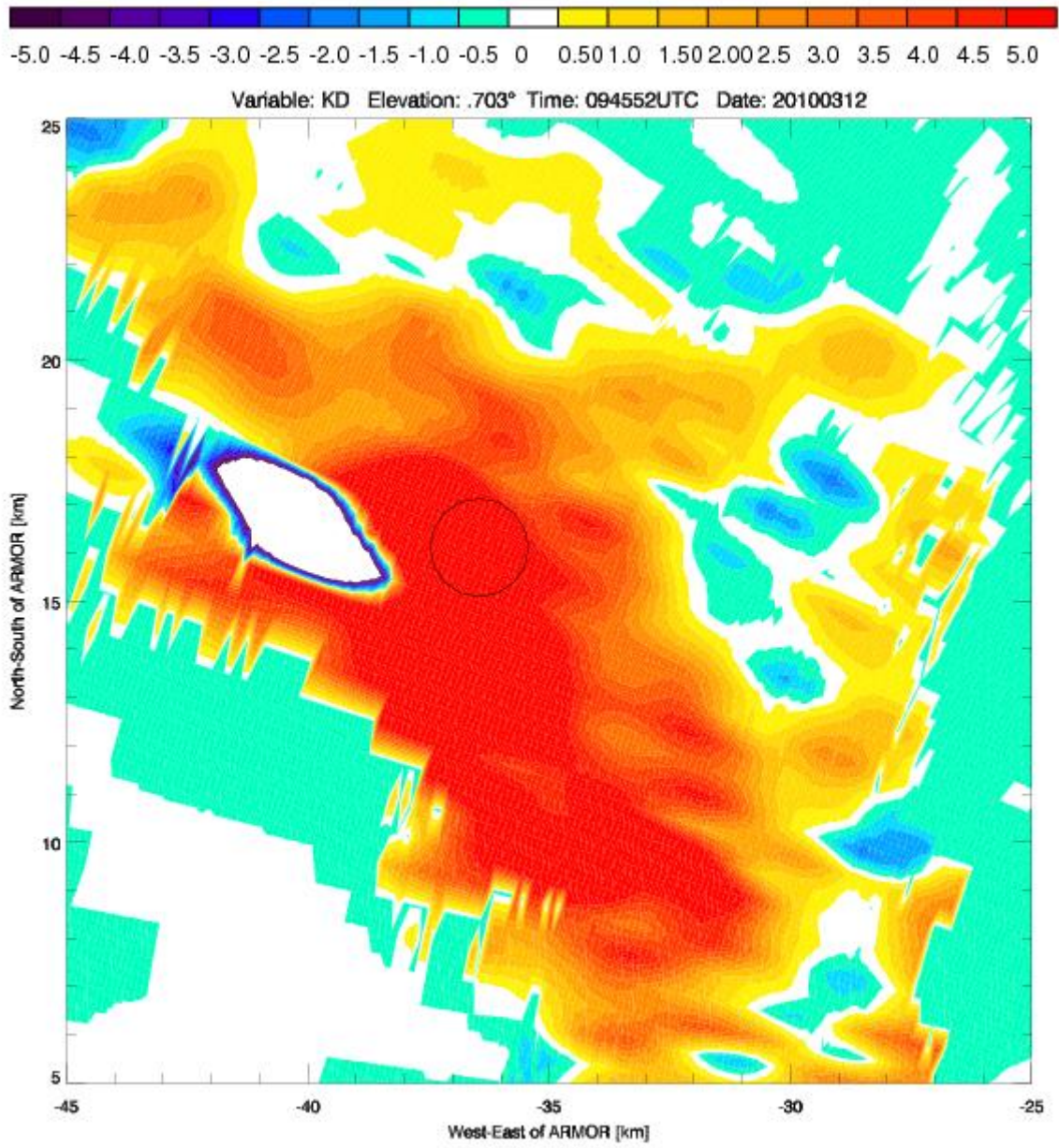
Figure 4.33: Same as Figure 4.30 except contoured K_{dp} (°km^{-1}).
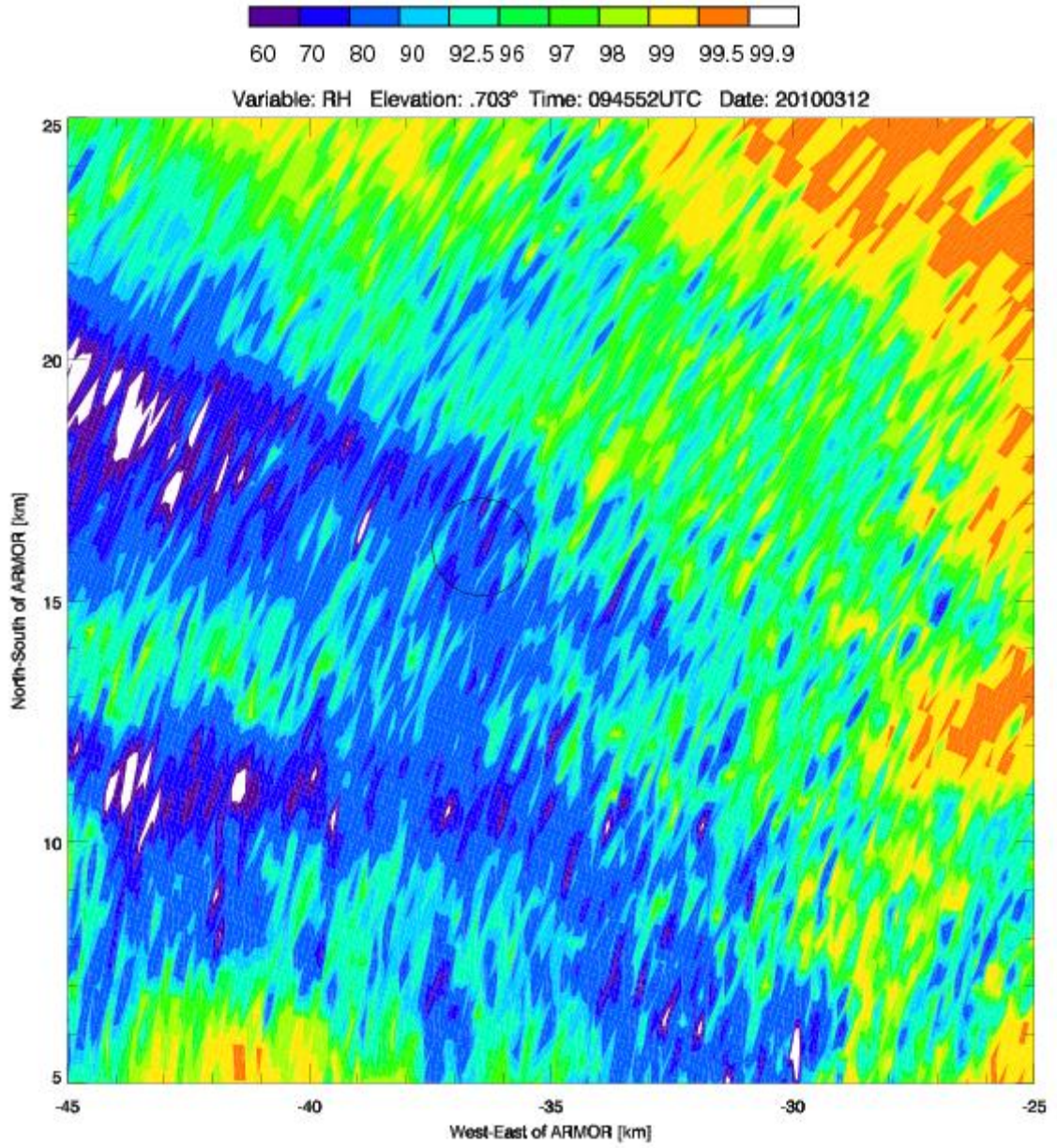
Figure 4.34: Same as Figure 4.30 except contoured ρ_{hv}.
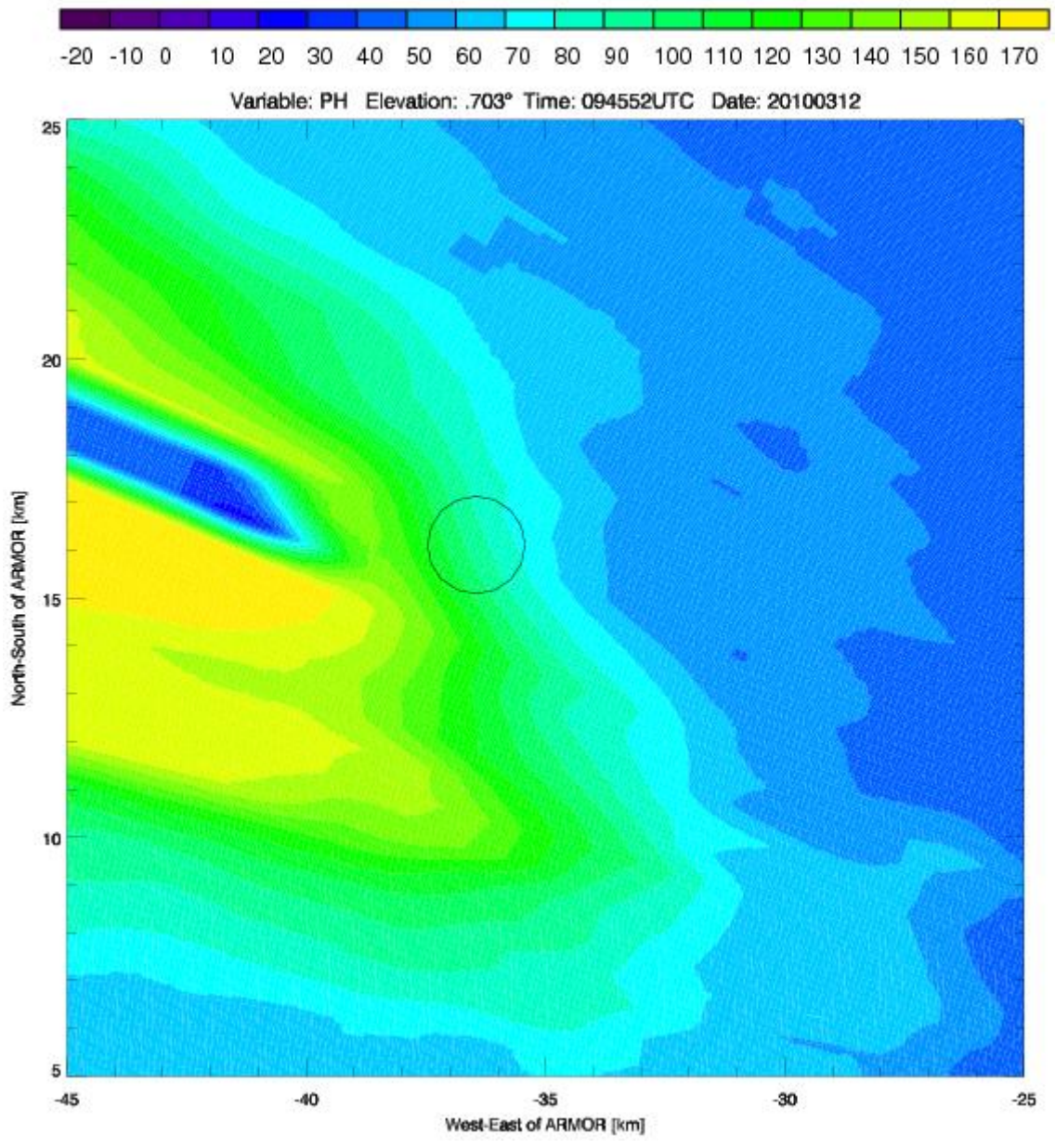
Figure 4.35: Same as Figure 4.30 except contoured Φ_{dp} (°).

high amounts of differential attenuation (Figures 4.31-4.32). The low Z_{dr} (< -5 dB) values in the uncorrected Zdr are unrealistic and due to differential attenuation that can be seen in Φ_{dp} (Figure 4.35). The K_{dp} in the location of the hail report is high (> 5 °km^{-1}) with negative values to the west of the hail report location (Figure 4.33). In addition, low values of ρ_{hv} are observed within the 1 km radius of the hail report (Figure 4.34). This suggests large amounts of resonant sized particles that can lead to enhanced attenuation and differential attenuation (Tabary et al. 2009). Values of Φ_{dp} in the PPI are as high as 180° suggesting large amounts of differential phase (Figure 4.35). Additionally, there are abrupt changes in the Φ_{dp} field suggesting the possibility of phase folding or improper filtering of the backscatter differential phase (δ) that can effect the estimation of Φ_{dp} which is consistent with large hail. Since there are large amounts of differential attenuation, the attenuation correction algorithm may have failed in this case. Under correction of Z_{dr} is one likely reason for the possible "hail hole" in this example or these cases could be examples of "hail holes" at the C-band.

CHAPTER 5

RADAR MODELING RESULTS

This section of the study focuses on the modeling of hailstones to arrive at the expected dual-polarimetric radar variables of hail. Questions about what type of hydrometeor causes the high Z_{dr} (3-8 dB) signature at the C-band still remain from Chapter 4. Other studies at the S-band have shown that lower ρ_{hv} (< 0.95) and zero to slightly positive K_{dp} can be expected in hail and rail and hail mixtures (e.g., Balakrishnan and Zrnic 1990a,b). There still is no clear explanation behind what is producing the signature. Other studies suggest that the signature is produced by small melting hailstones and rain mixed with hail (e.g., Vivekanandan et al. 1990, Meischner et al. 1991, Ryzhkov et al. 2009). These studies used the T-matrix to model melting hailstones, but the main focus of the studies was on small hail with initial diameters less than 1 cm. In some of these studies (Vivekanandan et al. 1990, Meischner et al. 1991), the hail almost completely melts before reaching the ground. In the study herein, large (> 4.45 cm) hail is present at the ground through reports and observations. The following section will model hail of all sizes and not just focus on the smaller hail (< 1 cm). The

section will address differences in polarimetric signatures of hail based on variation in the hailstone size distribution, orientation, canting angle, size and reflectivity fraction.

5.1   Hailstone Orientation

As discussed in the background, there is still uncertainty about hail fall mode behavior. Therefore, this study models hail falling with its major axis both horizontal and vertical. Figure 5.1 illustrates polarimetric results from melting hail using the T-matrix assuming a monodisperse distribution and an outer water torus of 0.5 mm (Depue et al. 2007). The figure shows the expected Z_{dr} results for melting hail as a function of the standard deviation of the canting angle. The images on the left are for hailstones modeled with their major axis horizontal, while the images on the right are for hailstones modeled with their major axis vertical. It can be seen from Figure 5.1 that hailstones with their major axis horizontal tend to produce positive Z_{dr} and hailstones with their major axis vertical tend to produce negative Z_{dr}, as might be expected based on physical shape despite some non-Rayleigh-Gans scattering. However, as the standard deviation of the canting angle increases (e.g., more tumbling), Z_{dr} approaches 0 dB. This is an expected result because as the melting hailstone tumbles, it would appear to the radar as an effective sphere producing near 0 dB. Zrnic et al. (1993) observed negative Z_{dr} associated with a hail producing storm and concluded that the radar was observing hail with its major axis vertical. In Chapter 4, no observations were made of negative Z_{dr} associated with the hail reports; only positive Z_{dr} was observed. Therefore, based on these simple simulations, it is assumed that hail in this study most likely fell with its major axis horizontal.
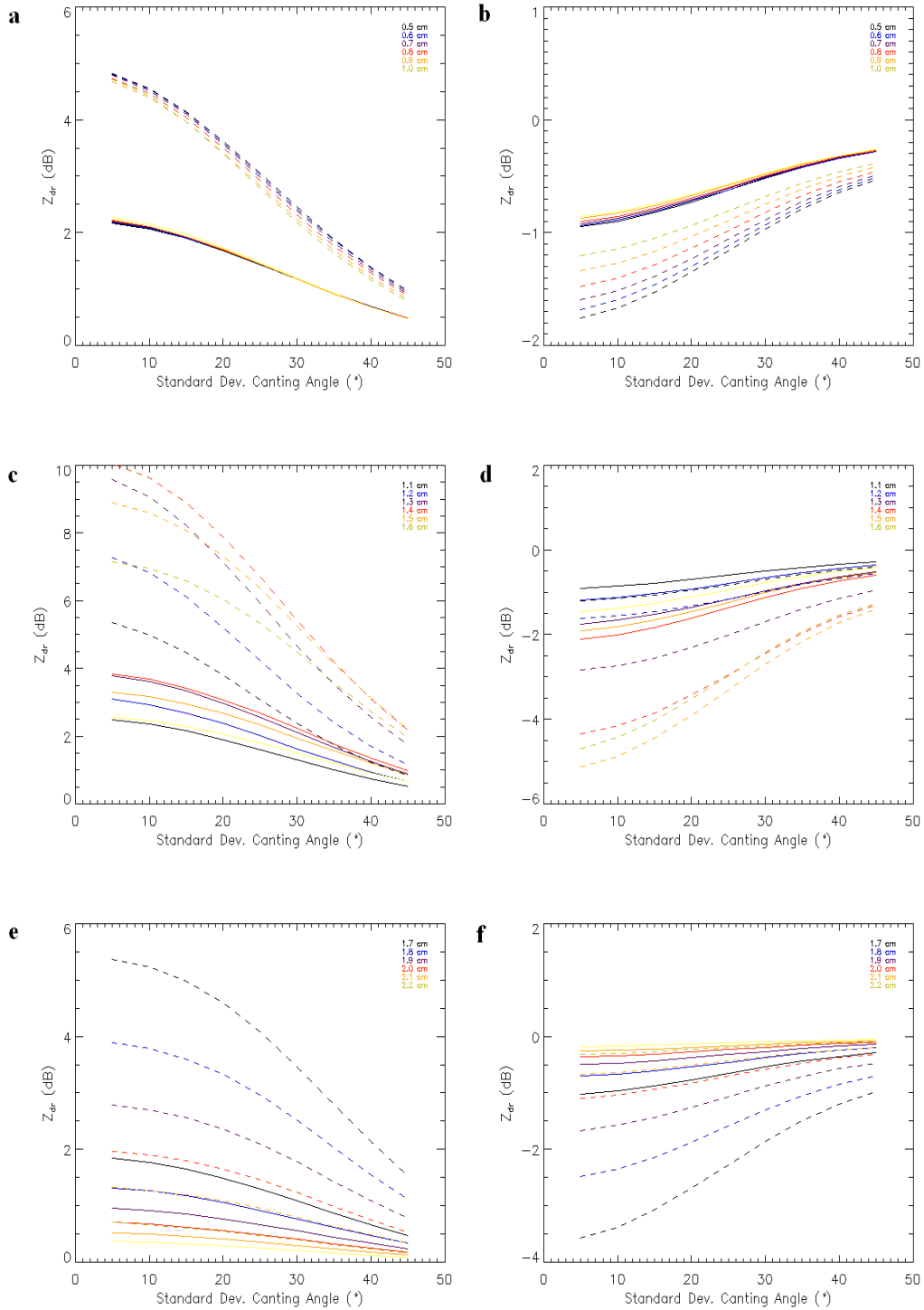
Figure 5.1: Z_{dr} (dB) versus standard deviation of the hail canting angle (°) for various diameters of monodisperse hail (a-f). Figures on the left assume the major axis of the hailstone is horizontal (a,c,e) and the figures on the right assume the major axis of the hailstone is vertical (b, d, f). Axis ratio of 0.6 dashed lines and 0.8 solid lines. The water coat is assumed to be 0.5 mm with a temperature of 20 °C.

5.2   Hailstone Size Distributions

The study also examines the possible difference in the C-band polarimetric hail signature due to variations in the hailstone size distribution. From the background, it is clear that uncertainty exists in the preferred size distribution for hail. Ulbrich (1983) shows that the differences in the hydrometeor size distribution lead to different values for reflectivity. Since Z_{dr} is dependent upon reflectivity in both the horizontal and vertical, different size distribution should lead to different simulated values of Z_{dr}. In this study monodisperse, exponential, and gamma distribution are simulated.

5.2.1   Monodisperse Distribution

The first of these hail stone size distributions that will be discussed is the monodisperse distribution.   Auer and Marwitz (1972) suggest that the monodisperse distribution is a good assumption for the hailstone size distribution. Figure 5.1 indicates the results from the monodisperse simulations for melting hailstone run by the T-matrix. The results show positive Z_{dr} of 10 dB for a monodisperse melting hailstone size of 1.4 cm and 0.6 axis ratio with a standard deviation of the canting angle of 5°, indicating that the melting hailstone falls rather stable. Vivekanandan et al. (1990) and Meischner et al. (1991) both have shown through modeling that small (< 1 cm) melting hailstones can produce high Z_{dr} (> 5 dB) at the C-band, but the studies did not include polarimetric results from melting hailstones greater than 1 cm. These studies focused on the first peak of resonance that occurs near 5 to 8 mm (e.g., Meischner et al. 1991, Zrnic et al. 2000). However, there are multiple peaks in resonance at the C-band for hydrometeor greater than 5 mm. The advantage of Vivekanandan et al. (1990) and Meischner et al. (1991) is

120

that the melting hail stone size and shape varied because both studies used the Rasmussen and Heymsfield (1987a) hail melting model. This study is at a relative disadvantage because the melt model was not used and the water torus remained constant at 0.5 mm. However, the simplified approach used herein has been used successfully in other studies (Depue et al. 2007). The monodisperse simulations in Figure 5.1 show that a wide variety of Z_{dr} values can be expected depending on the assumptions about the melting hailstone shape, size, orientation, and canting angle. From the simulations, in order to produce high Z_{dr} (3-8 dB), the melting hailstone must be assumed to be fairly oblate (e.g., 0.6 axis ratio), small standard deviation of the canting angle (rather stable), fall with major axis horizontal, and size between 1.1-1.7 cm.

5.2.2   Exponential Distribution

The second hailstone size distribution that will be simulated by the Mueller matrix is the exponential size distribution. Cheng and English (1983) suggest that the exponential size distribution is the best fit for hailstone size distributions. Figure 5.2 shows the T-matrix and Mueller matrix simulations for melting hailstones assuming an exponential hailstone size distribution with a 0.5 mm water coat with a minimum diameter of 0.5 cm and a maximum diameter of 4.0 cm. The figures on the left side are simulated hailstone with their major axis horizontal and on the right with their major axis vertical. Again, it can be seen as the standard deviation of the canting angle increases (e.g., more tumbling), Z_{dr} approaches 0 dB because it appears to the radar as an effective sphere. In addition, the more oblate the melting hailstone is, the higher the Z_{dr}. These are both expected results and are similar to the monodisperse simulations. However, there is

121
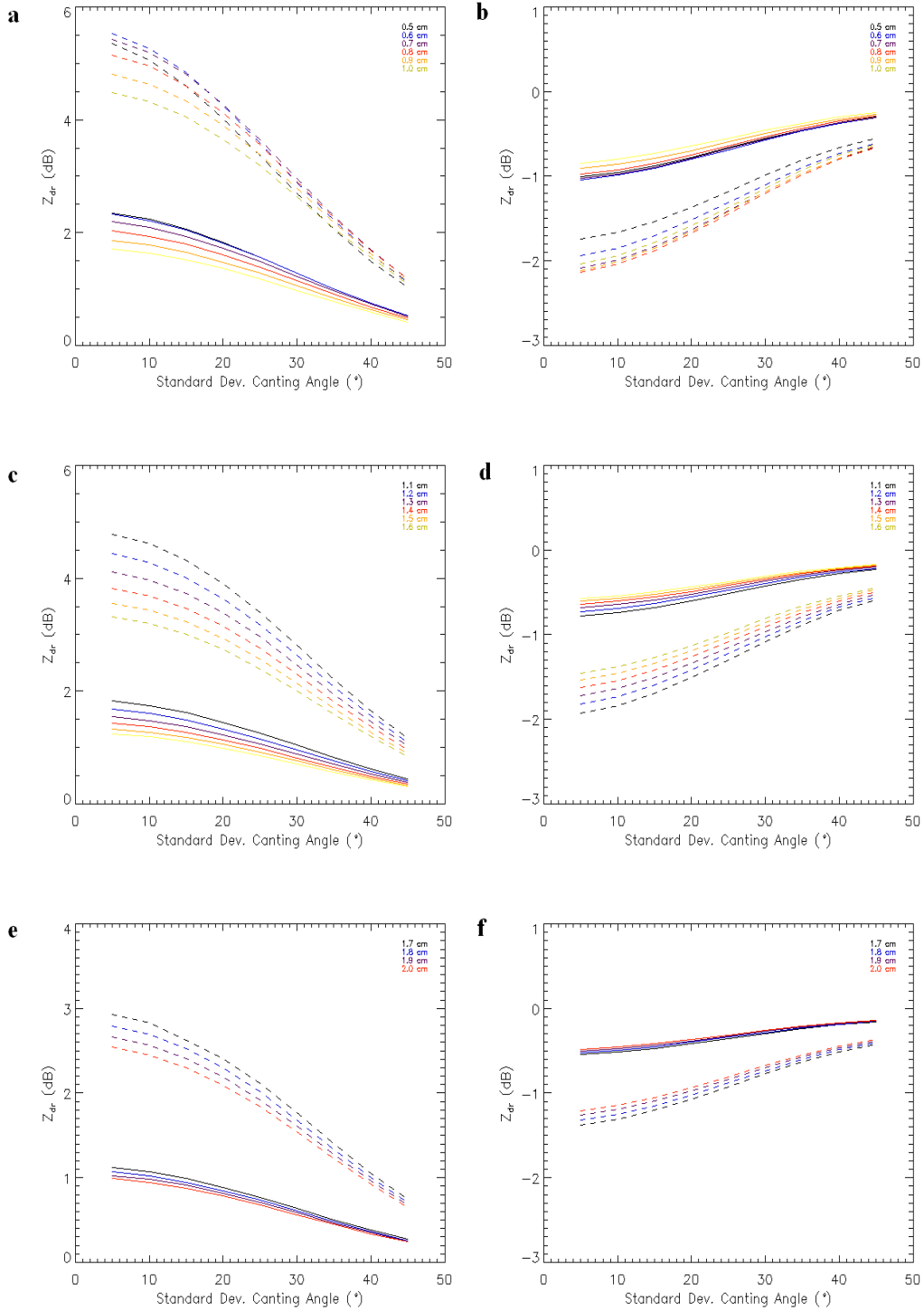
Figure 5.2: Same as Figure 5.1 except an exponential distribution.

a clear difference between where the maximum Z_{dr} occurs. Figure 5.2 indicates for the exponential hailstone size distribution the maximum Z_{dr} is 5.5 dB for a melting hailstone with a median volume diameter of 6 mm, oriented with its major axis horizontally, and a 5° standard deviation of the canting angle (e.g., stable). This Z_{dr} maximum is closer to first resonant region for the C-band radar. Zrnic et al. (2000) indicates that there is a peak in resonance for the C-band between 5-7 mm that can cause anomalously high Z_{dr}. These results from the simulation assuming an exponential distribution seem to match the finding of Zrnic et al. (2000) for large raindrops and Vivekanandan et al. (1990) and Meischner et al. (1991) for small melting (or melted) hail. It can be seen beyond this peak of resonance how Z_{dr} lowers with increasing median volume diameter. However, if the melting hailstone falls stable with is major axis horizontal and is rather large (e.g., 1.5-2.0 cm), then Z_{dr} is still $2.5 - 3.5$ dB. This is consistent with past modeling studies that show that resonant peaks seen in individual monodisperse diameters are smoothed by using a wide variety of sizes. It is clear from the limited simulations that the Z_{dr} results are highly dependent upon the assumptions made about the size distribution, shape, fall mode, and orientation of the melting hailstone.

5.2.3 Gamma Distribution

The third distribution hailstone size distribution examined in this study is the gamma distribution. Ziegler et al. (1983) found that the gamma distribution is the best fit for the size distribution of large hailstones observed in Oklahoma. Figure 5.3 shows the T-matrix model results assuming a gamma hailstone size distribution where μ=2. Hailstones are orientated with their major axis horizontal on the left and vertical on the
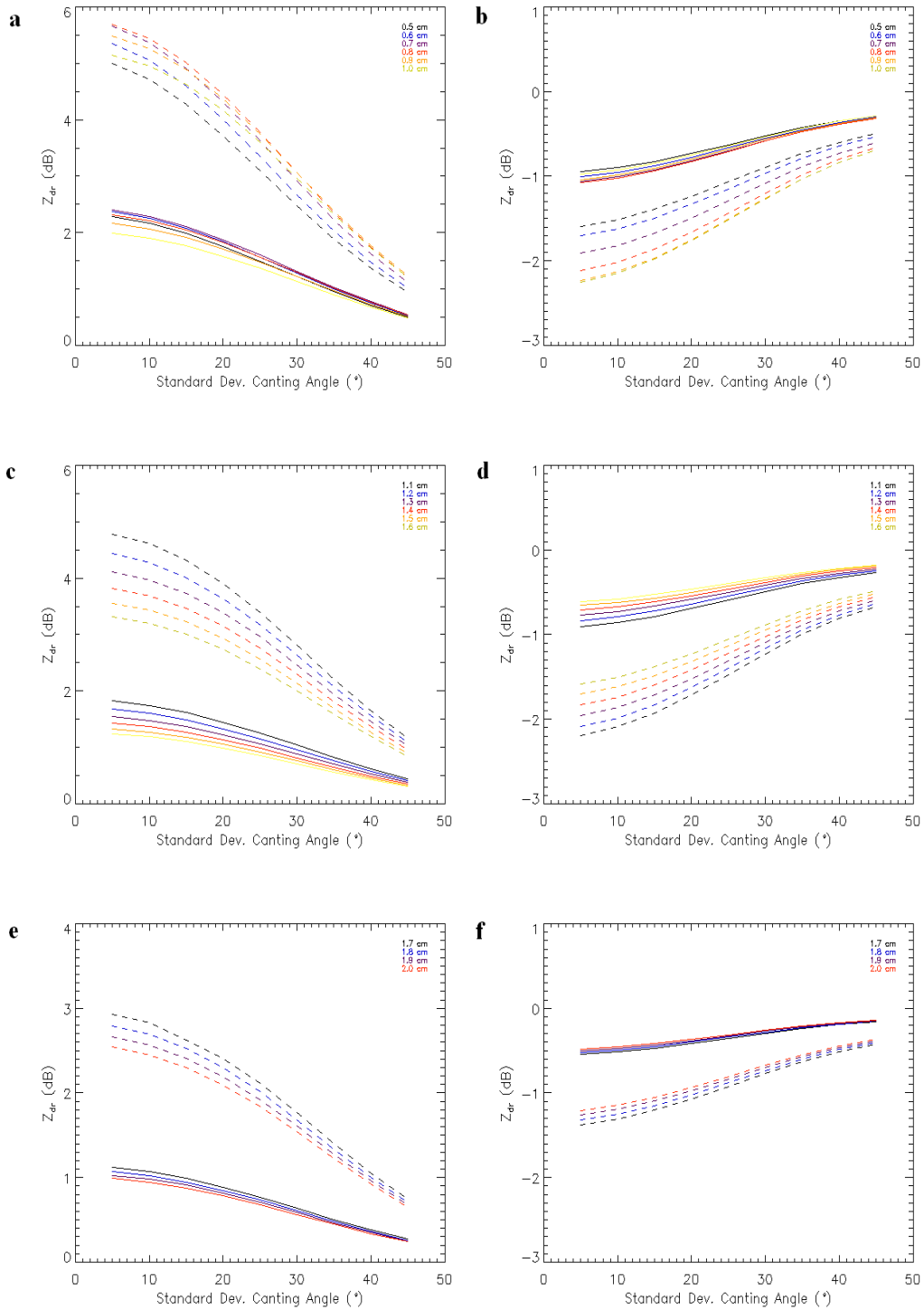
Figure 5.3: Same as Figure 5.1 except a gamma distribution with a shape parameter of two.

124

left (Figure 5.3). Again, both orientations show that as the standard deviation of the canting angle increases (e.g., more tumbling), the expected Z_{dr} approaches 0 dB. The results show that hailstones with their major axis horizontal produce positive Z_{dr} and hailstones with their major axis vertical produce negative Z_{dr}. Overall, the gamma distribution for a shape parameter of two (Figure 5.3) produces similar results to the exponential distribution (Figure 5.2). The maximum Z_{dr} simulated by the T-matrix for the gamma distribution is 5.7 dB for a melting hailstone at 8 mm. This maximum is found well into the resonant regime that starts near 5 mm for the C-band (Zrnic et al. 2000). Z_{dr} is still rather larger (2.5 – 4.0 dB) for melting hailstones with a median volume diameter up to 2 cm. However, certain assumptions must be made that the hailstone is fairly oblate (e.g., axis ratio 0.6) and must fall with a low standard deviation of the canting angle (< 15°).

For a more in depth study of the gamma hailstone size distribution, simulations were run of the T-matrix using a variety of shape parameters. Figure 5.4 shows the results from the simulations running a range of μ values from -4 to 20. The results assume that the melting hailstones fall with their major axis horizontal, the standard deviation of the canting angle is 5°, and the axis ratio is 0.6. Figure 5.4 indicates that as μ increases, Z_{dr} increases. The maximum value of Z_{dr} is at 6.94 dB with μ=20. This maximum is found at a median volume diameter of 1.1. cm which is in between the median volume diameters found for exponential (6 mm) and monodisperse (1.4 cm). It appears from the plot that as μ increases, the results become more similar to the monodisperse results (Cohen and McCaul 2005). However, Ziegler et al. (1983) only found μ values up to nine for hailstone size distributions. Therefore, these higher μ
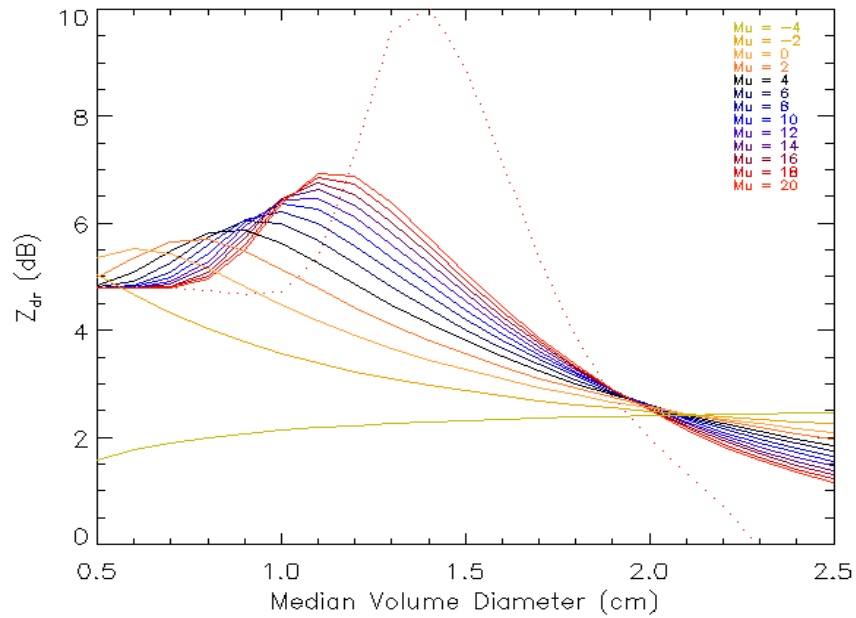
Figure 5.4: Z_{dr} (dB) versus median volume diameter (cm) for various shape parameters of the gamma size distribution. The dashed line assumes a monodisperse distribution. All assume a standard deviation of the canting angle of 5° with an axis ratio of 0.6. The water coat is assumed to be 0.5 mm with a temperature of 20 °C. All hailstones in the simulation fall with their major axis horizontal.

values (> 10) may be unrealistic. In addition to the positive μ values, negative μ values were simulated as well. The results indicate that these negative μ's produce lower maximum values and overall values of Z_{dr}. It is easy to see from the model simulations that if melting hail falls rather stable and is fairly oblate (e.g., axis ratio 0.6) large Z_{dr} (> 3 dB) can be easily simulated.

In addition to modeling melting hail alone, melting hail is modeled with rain to determine what values of Z_{dr} can be expected in a mixture of rain and melting hail. The mixture involves rain using the Andsager et al. (1999) axis ratios for rain, with the major axis orientated horizontally, a standard deviation of the canting angle of 5°, and an

exponential distribution and gamma distribution ($\mu = 0, 2, 4$) (Ulbrich 1983) with a D_{min}

of 0.8 mm and D_{max} of 8 mm. The mixture also contains melting hail and assumes an axis

ratio of 0.6, major axis is orientated horizontally, a standard deviation of the canting

angle of 5°, and an gamma distribution (Zeigler et al. 1983) $\mu = 5-9$ with a D_{min} of 0.5 cm

and D_{max} of 5.0 cm. Figure 5.5 shows the resulting Z_{dr} from a mixture of melting hail and

rain compared to the median volume diameter of the melting hailstone in a gamma size

distribution. Overall, the resulting Z_{dr} is similar to what is observed in Figure 5.4 with

peaks of Z_{dr} occurring for median volume diameters between 0.9-1.2 cm depending on

the shape parameter of the melting hailstone size distribution. The maximum Z_{dr} in this
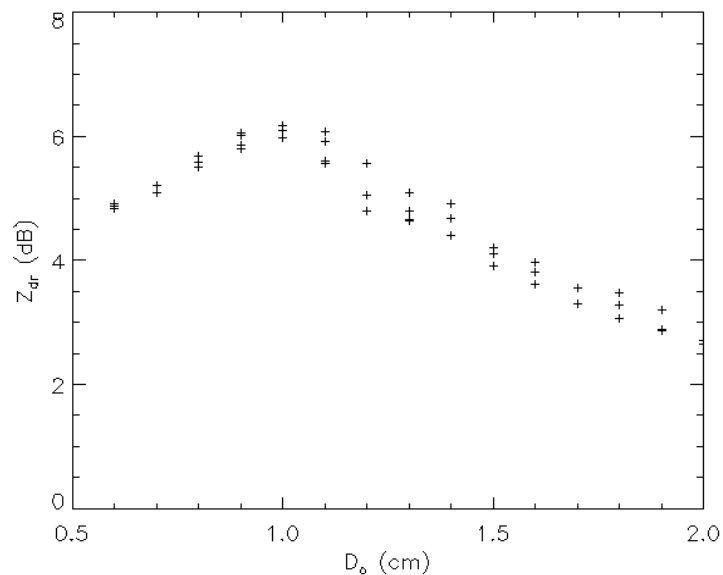
Figure 5.5: Overall Z_{dr} of rain and melting hail mixture versus median volume diameter
of melting hail. The size distribution of melting hail is assumed to be a gamma
distribution with a shape parameter of 5-9. The melting hail has a water coat of 0.5 mm
with an axis ratio of 0.6. The melting hailstones fall with their major axis horizontal and
a standard deviation of the canting angle of 5°. The axis ratios for rain are used from
Andsager et al. (1999) with a standard deviation of the canting angle of 5°. Rain also is
assumed to fall with its major axis horizontal. Both hydrometeors assume a temperature
of 20 °C.

127

simulation is observed at 6.17 dB for a melting hailstone with a median volume diameter of 1.00 cm and a shape parameter of nine. Figure 5.5 shows that in a mixture of rain and melting hail Z_{dr} as high as 4-6 dB is not uncommon if the assumptions made about size distribution, fall mode, shape, orientation, and canting angle are true.

5.3   Reflectivity Fraction

Vivekanandan et al. (1991) and Ryzhkov et al. (2007) suggest that when large hail (> 1.2-1.5 cm) is dominant in the radar volume, then Z_{dr} should be near 0 dB at the C-band. However, these studies along with modeling from this study suggest that if hail is not tumbling and in the resonant sized region, then non-zero Z_{dr} can easily be produced. To test this hypothesis, T-matrix simulations are run in this study to determine what happens to the C-band polarimetric signature of hail when large hail tumbling (> 1.2-1.5 cm) becomes dominant in the radar volume in a mixture of hydrometeors. The mixture involves rain using the Andsager et al. (1999) axis ratios for rain, with the major axis orientated horizontally, a standard deviation of the canting angle of 5°, and an exponential distribution (Ulbrich 1983) with a D_{min} of 0.8 mm and D_{max} of 8 mm. The mixture also contains melting hail and assumes an axis ratio of 0.6, major axis is orientated horizontally, a standard deviation of the canting angle of 5°, and an exponential distribution (Ulbrich 1983) with a D_{min} of 0.5 cm and D_{max} of 4.0 cm. The final hydrometeor in the mixture is large tumbling hail and assumes an axis ratio of 0.6, the major axis is orientated horizontally, a standard deviation of the canting angle of 45°, and an exponential distribution (Ulbrich 1983) with a D_{min} of 1.0 cm and a D_{max} of 7.0 cm. Figure 5.6 illustrates the results of the reflectivity fraction of large tumbling hail
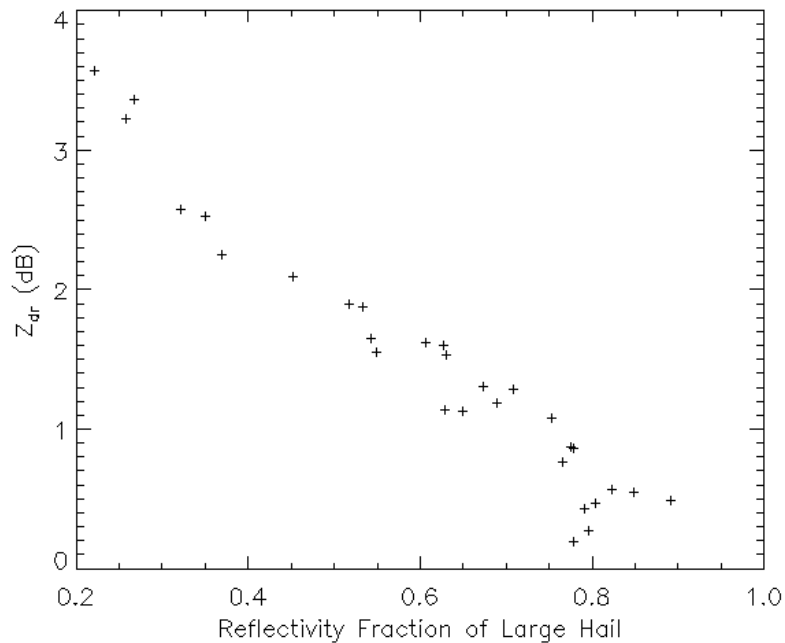
Figure 5.6: Z_{dr} (dB) versus the radar reflectivity fraction of large hail. The results of the reflectivity fraction include a mixture of rain, small stable melting hail with mean volume diameters of 0.6-0.9 cm, and large dry tumbling hail with mean volume diameters of 1.5-2.7 cm. All assume an exponential size distribution. The axis ratio of hail and melting hail is assumed to be 0.6 with axis ratios of rain from Andsager et al. (1999). The water coat for melting hail is 0.5 mm with a temperature of 20° C for all hydrometeor types. The hailstones fall with their major axis horizontal with a standard deviation of the canting angle of 45°, melting hailstone with a standard deviation of the canting angle of 5°, and rain with a standard deviation of the canting angle of 5°.

as many different combinations of these mixtures of these hydrometeor types are used.

Reflectivity fraction of large tumbling hail is the fraction that large tumbling hail

contributes to the overall reflectivity value of the mixture. It can be seen from Figure 5.6,

large dry tumbling hail contributes more to the reflectivity Z_{dr} decrease to near 0 dB.

However, when large dry tumbling hail only contributes 0.2 – 0.3 to the overall

reflectivity, Z_{dr} can be between 3-4 dB. From the T-matrix simulations of the

hydrometeor mixtures, it appears the hypothesis is accepted that as large tumbling hail becomes dominant Z_{dr} will decrease towards 0 dB.

In addition, another mixture was modeled of rain and stably oriented (i.e., not tumbling) melting hail to examine the Z_{dr}'s of this mixture. The assumptions made in the mixture are the same as the rain and stably oriented melting hail mixture described in Section 5.3.3 and Figure 5.5. Figure 5.7 shows the overall Z_{dr} versus the reflectivity fraction of melting hail. It can be seen that the reflectivity fraction of stably oriented large hail does not lead to significant changes in the overall Z_{dr}. Overall, Z_{dr} is between 2.5-6.5 dB, independent of the reflectivity fraction of melting hail. Therefore, high Z_{dr} (3-8 dB) as observed in the empirical observations in this study could be produced by a
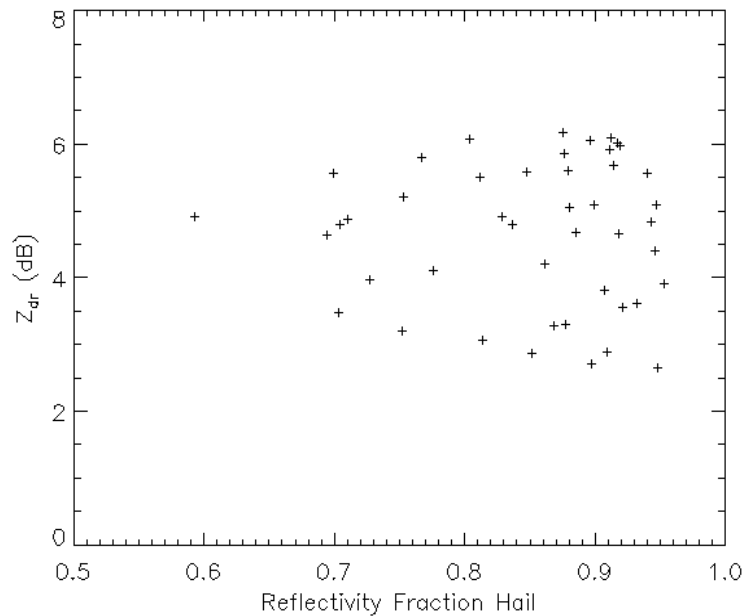
Figure 5.7: Same assumptions as Figure 5.5 except overall Z_{dr} of mixture versus reflectivity fraction of melting hail.

combination of rain and stably oriented melting hail based on the assumptions made in this simulation.

Overall, in order to produce high Z_{dr} (> 5 dB) as observed in Chapter 4, a few key assumptions have to be made. One of those assumptions is that the melting hailstones must have a small (< 15°) standard deviation of the canting angle (e.g., fall stable). Other studies suggest that melting hail falls rather stably as the melt water acts to stabilize the drop (e.g., Rasmussen and Heymsfield 1987a, Aydin and Zhao 1990). Another assumption is the melting hailstone must be fairly oblate (e.g., axis ratio 0.6). Studies using the Rasmussen and Heymsfield (1987a) melt model have shown that melting hailstone become this oblate (e.g., Vivekanandan et al. 1990). Another key assumption is that the melting hailstones fall with their major axis horizontally. List et al. (1973) used wind tunnel experiments and found that hailstones fall with their major axis horizontally. If these assumptions are met, then it can be shown through the T-matrix simulations that high Z_{dr} (> 3 dB) can be produced. In addition, this section has shown that if large dry tumbling hail dominants the reflectivity, then Z_{dr} will be near 0 dB. From these simulations, it appears that the hydrometeor type that is most likely produce high Z_{dr} is oblate stable melting hailstones. The modeling results suggest that two possible situations are possible. The first is that large tumbling hail is always accompanied by stable melting hail and rain, which dominates the reflectivity, can produce Z_{dr} (3 − 6 dB) as seen in the simulation in this chapter. The second is that large hail melts and does not tumble producing higher Z_{dr} than tumbling hail. However, there is still no clear concise conclusion in the literature if hailstones tumble or fall stable. Overall, the results from

the modeling are consistent with the results in Chapter 4 if large hail is stably oriented

(i.e., not tumbling).

CHAPTER 6

MELTING HAIL IDENTIFICATION AT LOW-LEVELS

One of the key advantages of polarimetric radar is its ability to distinguish one hydrometeor type from another. Studies have been done at the S-band that can discriminate hail from rain (e.g., Aydin et al. 1986) and rain from snow (e.g., Ryzhkov and Zrnic 1998). If polarimetric radar is able to distinguish these hydrometeor types, then better forecasts can be made about hail, rainfall, and snowfall amounts. However, the S-band hydrometeor detection algorithms cannot be directly transferred over to use at the C-band. Marzano et al. (2006) suggest that using S-band membership functions at the C-band leads to a poor classification of accuracy because of resonant effects at the C-band, which can be significant in melting hail that is sometimes mixed with large raindrops. Therefore, the membership functions for ARMOR need to be tested against the observations from Chapter 4 and, to a lesser degree, the knowledge obtained in the modeling in Chapter 5. The following chapter will evaluate the current membership functions of the C-band NCAR PID for melting hail detection at low levels during the April 10, 2009 severe weather event. A few sensitivity tests will be conducted with adjustments to the membership and weighting functions. This chapter hopes to lead to

suggestions for potential future modifications of the C-band NCAR PID for melting hail detection at low levels (< 1 km) in severe convection.

6.1   C-band NCAR PID

The NCAR PID uses a fuzzy logic approach to identify hydrometeor types from polarimetric radar inputs.   In a fuzzy logic algorithm, boundaries between each hydrometeor type in polarimetric radar parameter space are fuzzy and not rigid (as in Boolean logic). The fuzzy logic method is preferred in this study over Boolean logic because of the short comings of Boolean logic and advantages of fuzzy logic discussed in Chapter 2.

The fuzzy logic approach employed herein was developed by Vivekanandan et al. (1999) at NCAR for hydrometeor identification at the S-band.   More specifically, this study uses a modified version of the NCAR PID adapted by Deierling et al. (2008) for radar-lightning studies at the C-band.   In the C-band NCAR PID fuzzy logic approach, two-dimensional (2-D) membership functions of each polarimetric variable $(X=Z_{dr}, K_{dp}, \rho_{hv})$ and Z_h are used to determine to what extent each (X, Z_h) pair belongs to a particular fuzzy set or hydrometeor type.   The value (0-1) from all the 2-D membership functions for each fuzzy set are then aggregated together with a weighting function applied to each.   The fuzzy set with the maximum aggregation value is declared the most likely hydrometeor type.

The C-band NCAR PID is applied to the ARMOR polarimetric data from the April 10, 2009 widespread severe hail event.   The resulting PID hydrometeor types below

1 km in height and within 1 km of a hail report are analyzed in order to determine the effectiveness of the C-band NCAR PID for indentifying melting hail at low levels.

Table 6.1 shows the observed percentage of each hydrometeor type in the C-band NCAR PID from above the 0 °C level of 3 km. The most observed hydrometeor types by the algorithm are graupel and small hail (61.58 %) and hail (31.81 %). The sample used for these results are data within 1 km of a hail report below 3 km (the 0 °C level) from the April 10, 2009 hail event. Therefore, the most likely hydrometeor type above the 0 °C level for this event should be hail and graupel and small hail. Overall, the algorithm does a good job at identifying these dominant hydrometeor types above the 0 °C level in hail producing supercells from the April 10, 2009 hail event. However, it is not certain if these results will transfer to the detection of hail and melting hail at the surface.

Table 6.2 shows the observed percentage of each hydrometeor type in the C-band NCAR PID. The most observed hydrometeor types by the algorithm are graupel and rain (29.34 %), hail (23.33 %), heavy rain (21.88 %), and rain-hail mix (15.84%). The sample used for these results are data within 1 km of a hail report below 1 km from the April 10, 2009 hail event. Therefore, the most likely hydrometeor type for this sample should be melting hail or a rain hail mixture, but instead graupel and rain is the most likely hydrometeor type. In addition, an example low-level PPI image of the C-band NCAR PID is shown (Figure 6.1). The image shows a variety of hydrometeor types (e.g., heavy rain, rain and hail mix, hail, and graupel and rain) within the most intense parts of the thunderstorm. The membership functions for each hydrometeor type will be explored to help determine why certain hydrometeor types may be favored over others. In the next

Table 6.1: Percent Occurrence of various hydrometeor types for all radar gates below

3 km (the 0 °C level) in height and within 1 km of a hail report on April 10, 2009 using

C-band NCAR PID

Hydrometeor ID	Percent of Occurrence (%)
Cloud	0.00
Drizzle	0.00
Light Rain	0.00
Moderate Rain	0.00
Heavy Rain	0.00
Hail	31.81
Rain Hail	2.06
Graupel and Small Hail	61.58
Graupel and Rain	4.40
Dry Snow	0.00
Wet Snow	0.01
Ice Crystals	0.00
Irregular Ice Crystals	0.00
Supercooled Liquid Drops	0.00
Flying Insects	0.00
Second Trip	0.00
Ground Clutter	0.14

Table 6.2: Percent Occurrence of various hydrometeor types for all radar gates below

1 km in height and within 1 km of a hail report on April 10, 2009 using the C-band

NCAR PID

Hydrometeor Type	Percent of Occurrence (%)
Cloud	0.00
Drizzle	0.00
Light Rain	0.04
Moderate Rain	0.63
Heavy Rain	21.88
Hail	23.23
Rain Hail	15.84
Graupel and Small Hail	8.33
Graupel and Rain	29.34
Dry Snow	0.00
Wet Snow	0.00
Ice Crystals	0.00
Irregular Ice Crystals	0.00
Supercooled Liquid Drops	0.00
Flying Insects	0.00
Second Trip	0.00
Ground Clutter	0.71
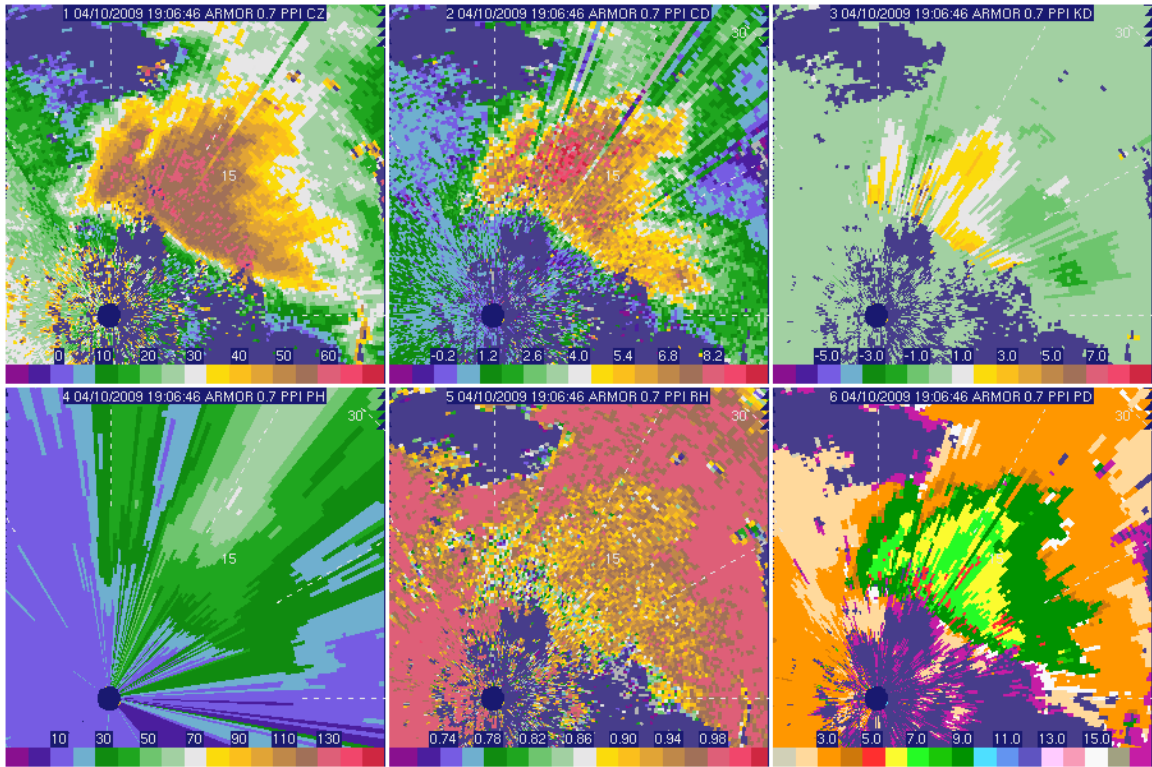
Category	Color	NCAR PID
1		Cloud
2		Drizzle
3		Light Rain
4		Moderate Rain
5		Heavy Rain
6		Hail
7		Rain and Hail
8		Graupel and Small Hail
9		Graupel and Rain
10		Dry Snow
11		Wet Snow
12		Ice Crystals
13		Irregular Ice Crystals
14		Supercooled Liquid Drops
15		Flying Insects
16		2nd Trip
17		Ground Clutter

Figure 6.1: Above is the PPI image from ARMOR at 1906 UTC on April 10, 2009 at 0.5 elevation angle. To the left is the chart for the NCAR PID, (a) Corrected Z_h (b) Corrected Z_{dr} (c) K_{dp} (d) Φ_{dp} (e) ρ_{hv} (f) NCAR PID.

section, suggestions will be made to adjust these membership and weighting functions to better detect hail at low-levels using C-band polarimetric radar observations.

The following images (Figures 6.2-6.5) display the histogram data from below 1 km from the April 10, 2009 hail reports with the 2-D membership functions of the most likely hydrometeor types overlain. Overlaying the current 2-D membership functions (Deierling et al. 2008) can potentially explain why some hydrometeor types may be preferred by the algorithm. Figure 6.2 shows all 2-D membership functions for graupel
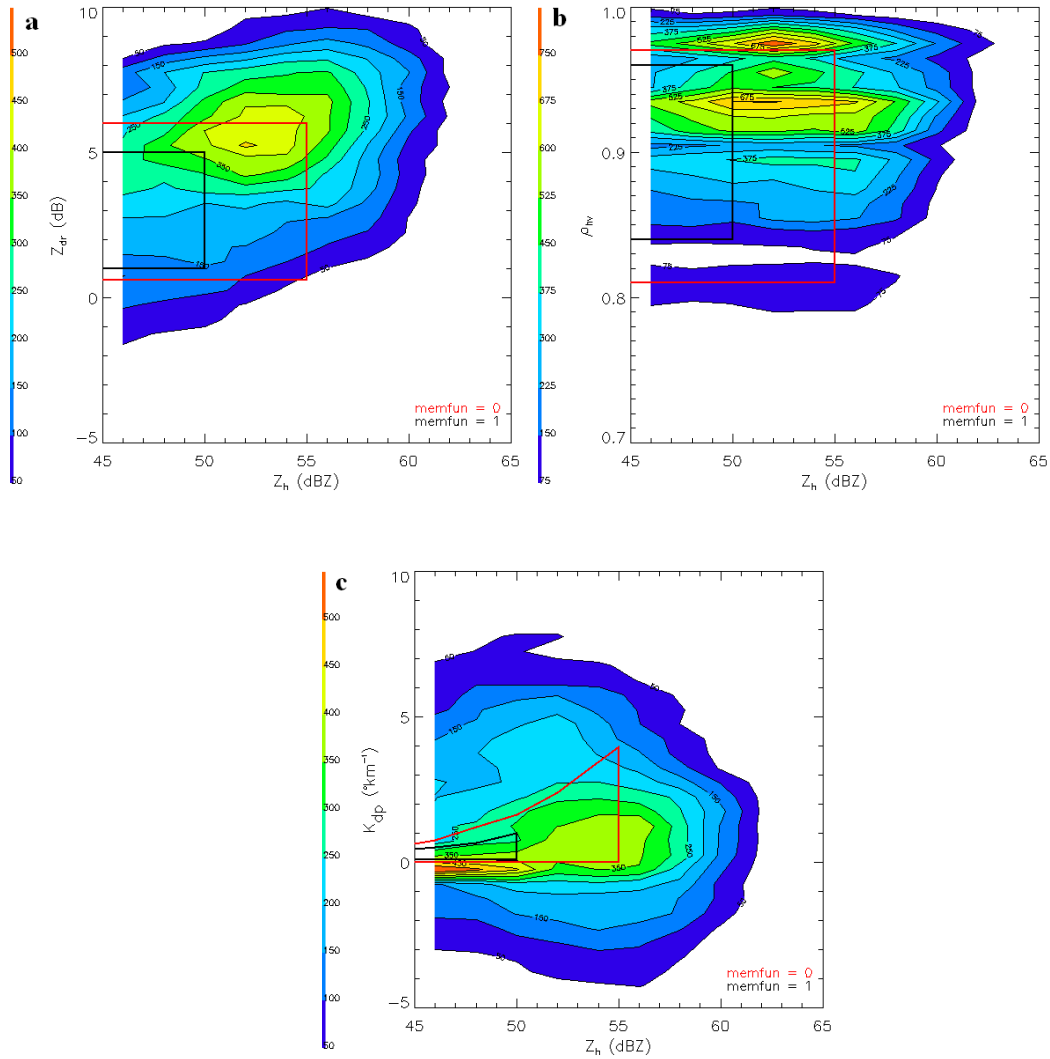
Figure 6.2: Joint frequency histograms of (a) Z_{dr}, (b) ρ_{hv}, and (c) K_{dp} versus Z_h. All data is below 1 km and within a 1 km radius of a hail report from April 10, 2009. The red and black lines represent the membership function for graupel and rain mix. The black line is where the membership function is equal to one and the red line is where the membership function is equal to 0. The Z_h data is in 2 dBZ bins, the Z_{dr} is in 0.5 dB bins, the K_{dp} data is in 0.5 $°km^{-1}$ bins, and the ρ_{hv} data is in 0.05 bins.

and rain. The Z_h and Z_{dr} membership function for graupel and rain shows the mode of the plot in the "fuzzy" region (between 0.0 – 1.0) of the membership function (Figure 6.2a). The plot shows that data above 6 dB and 55 dBZ fall completely outside of the range of the membership function.   The Z_h and ρ_{hv} membership function for graupel and rain shows that the mode of the plot falls into the high certainty near 1.0 category (Figure 6.2b). Data above 0.97 and 55 dBZ is outside of the range of the membership functions. However the mode of the plot 0.925 and 50 dBZ is completely within the range of values for the membership function. The Z_h and K_{dp} membership functions for graupel and rain show that the mode of the plot is just below the membership function (Figure 6.2c). However, the membership function increases and broadens with increasing Z_h. The mode of K_{dp} from 50 to 55 dBZ is within the "fuzzy" area of the membership function. Overall, all of the membership functions for each polarimetric variable contain large amounts of data below 55 dBZ within the "fuzzy" area of the membership functions.

Hail was the second most likely outcome for the data that was analyzed using the NCAR PID. The first hail membership function that will be examined is the Z_h and Z_{dr} membership functions. The plot of the membership functions overlaid on the Z_h and Z_{dr} histogram shows that only a few data points fall into the "fuzzy" category for hail (Figure 6.3a). In fact, the membership function looks more like what values would be expected for hail at the S-band. Possible adjustments may need to be made to this membership functions based on results from this study and will be discussed later. However, the Z_h and ρ_{hv} membership functions indicate the mode of the plot falls into the area of high certainty for hail (Figure 6.3b). In addition, the majority of the plot falls into
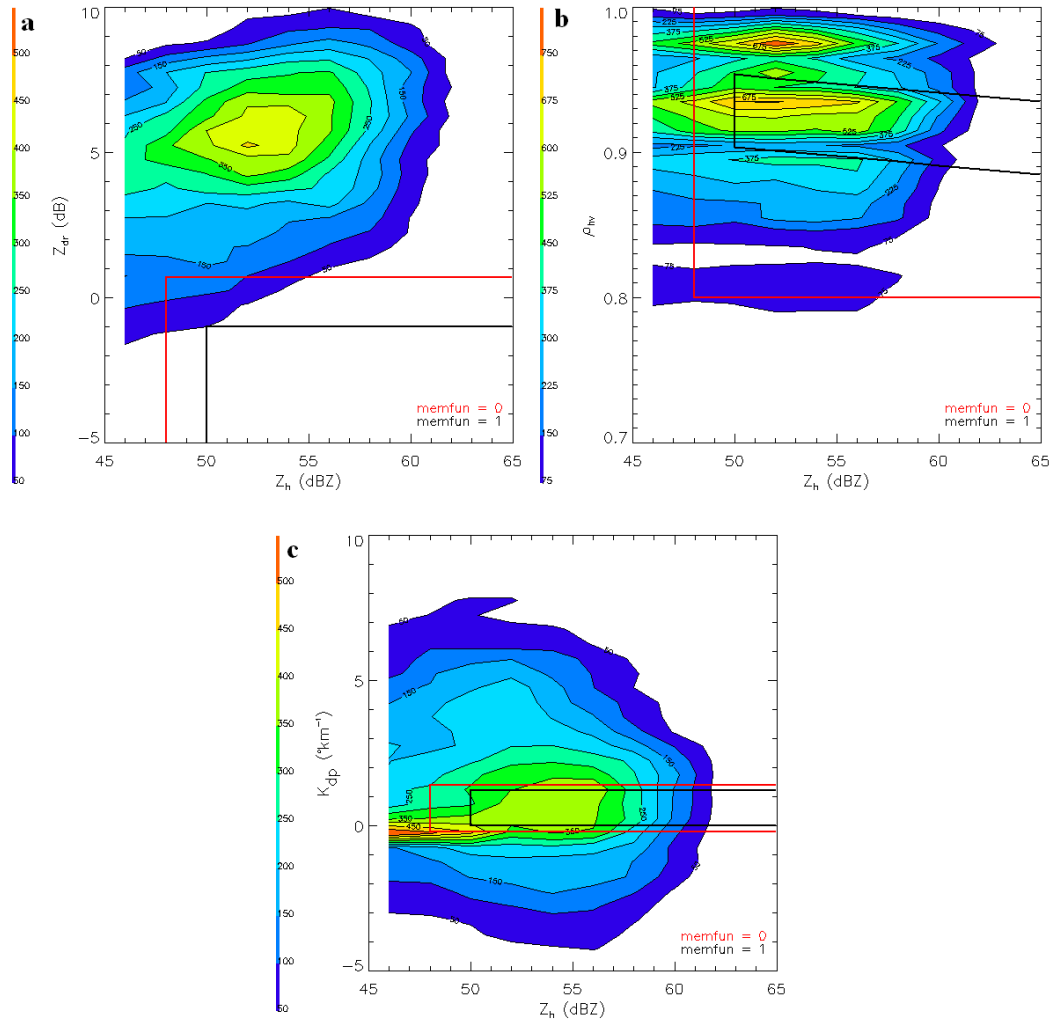
Figure 6.3: Same as in Figure 6.2 except hail membership functions.

the "fuzzy" category of the membership function from 0.8 – 1.0 to 48 to 65 dBZ. The Z_h

and K_{dp} membership function for hail shows the mode of K_{dp} from 50 to 57 dBZ falls

within the high certainty for hail category (Figure 6.3c). However, the mode of K_{dp} near

0 °km^{-1} for Z_h is completely outside of the membership function. Overall, hail is one of

the more likely outcomes from this data set. This is mostly due to the modes of ρ_{hv} and

K_{dp} falling into areas where the membership function for hail is equal to one even though

the majority of data in the Z_h and Z_{dr} histograms falls outside of the hail membership

function.

Heavy rain was one of the more common hydrometeor types observed by the C-

band NCAR PID. Therefore, the membership functions for heavy rain will be explored

as well. First, the Z_h and Z_{dr} membership functions for heavy rain compared to the Z_h and

Z_{dr} histogram plots from the April 10, 2009 hail case. The membership function is one

where the mode of the plot is found (Figure 6.4a). This suggests that heavy rain is what

is expected from the Z_h and Z_{dr} histograms from data associated with hail reports on

April 10, 2009. However, hail was observed with the data. Heavy rain could have been

observed as well, but from the reports, hail is the expected dominant hydrometeor type.

Clearly, since the mode of the histogram plots fits better with the membership function

for heavy rain, some adjustments may be needed for this membership function to

correctly classify hail. The Z_h and ρ_{hv} membership functions for heavy rain compared to

the Z_h and ρ_{hv} histogram plots from the April 10, 2009 case show that the mode is outside

of the expected values for rain (Figure 6.4b). The mode is near 0.925 and the

membership function is zero for values below 0.93 and is one for values above 0.97.

Only a few data points are found where the membership function equals one. This is
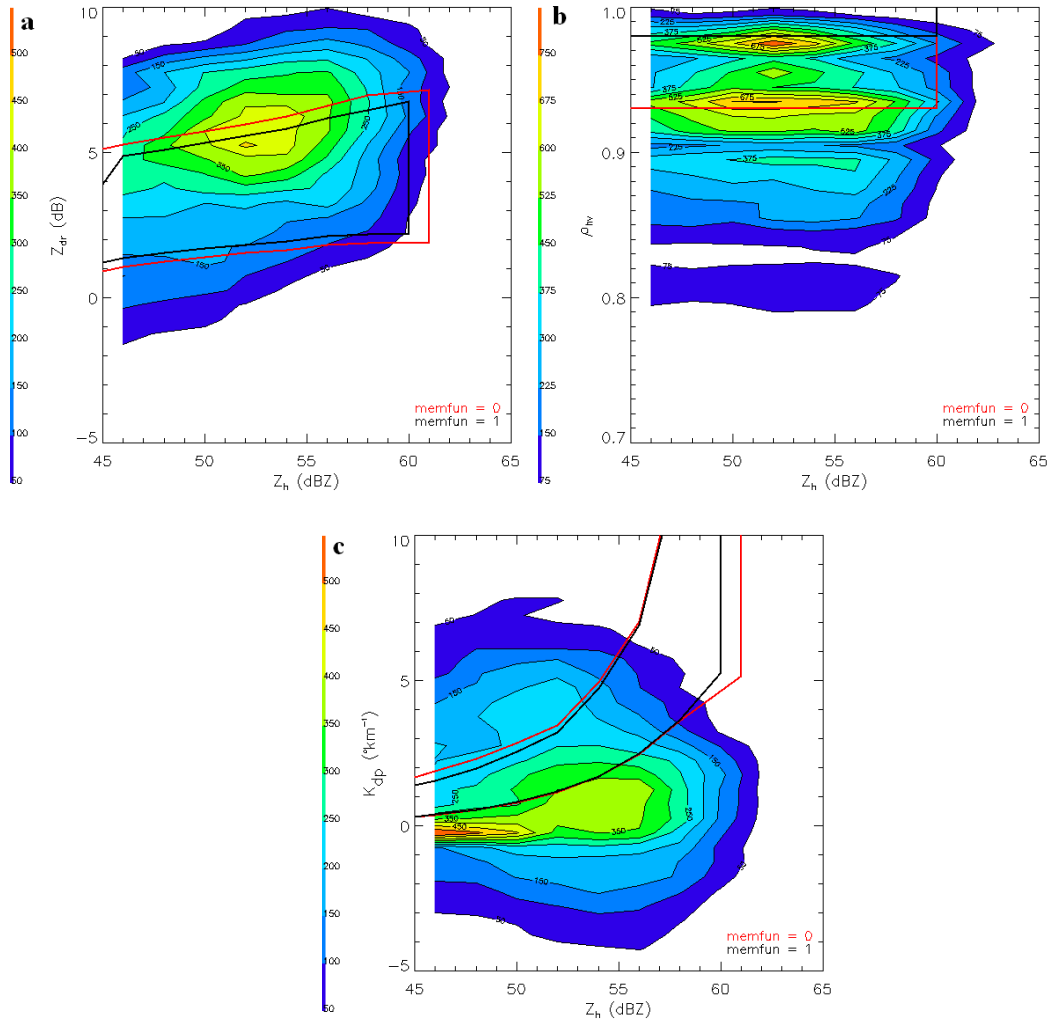
Figure 6.4: Same as in Figure 6.2 except heavy rain membership functions

expected since the histogram is of hail points and not heavy rain. The Z_h and K_{dp} membership functions for heavy rain are compared to the Z_h and K_{dp} histogram plots from the April 10, 2009 in Figure 6.4c. The membership function increase with increasing K_{dp} and incorporates some of the data in the histogram. However, the mode is outside of the range for heavy rain, which is what would be expected because the data in the histogram plots are from hail reports. The only membership function for heavy rain that fits well with the histogram plot around hail is the Z_h and Z_{dr} membership functions.

The rain and hail mixture was not a common choice for hydrometeor type from the C-band NCAR PID, but the membership functions will be compared to the histogram plots from April 10, 2009. The membership function of Z_h and Z_{dr} for rain and hail will be explored first. The plot indicates a narrow membership function only extending from 1 to 3 dB for Z_{dr} (Figure 6.5a). The problem with this membership function may be due to the limited area of Z_{dr} that is covered. However, the Z_h and ρ_{hv} membership functions for rain and hail is rather broad and includes the mode where the membership function is equal to one (Figure 6.5b). The membership function extends from 0.80 to 0.96 and covers a wide range of data points in the histogram. The Z_h and K_{dp} membership functions for rain and hail are rather narrow only extends from 0 to 2 °km^{-1} (Figure 6.5c). However, the mode of K_{dp} of 1 °km^{-1} between 52 – 57 dBZ falls within the membership function. The rain hail hydrometeor type may be less likely than the other hydrometeor types due to the small size of the membership functions of Z_h and Z_{dr} and Z_h and K_{dp} and the large range of values in the joint frequency histograms of the April 10, 2009 data set.
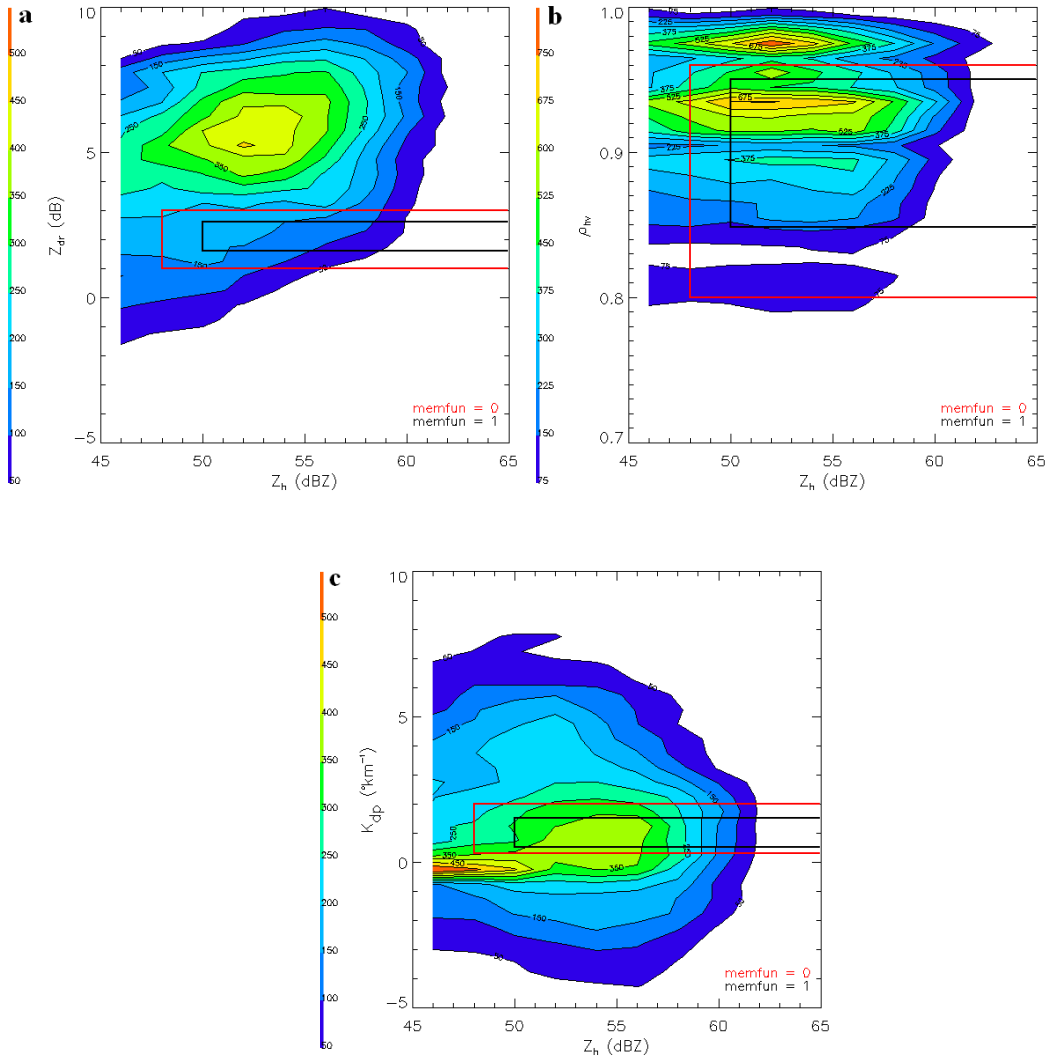
Figure 6.5: Same as in Figure 6.2 except rain-hail mixture membership functions.

6.2 Sensitivity Tests for Improving Melting Hail Detection at Low-Levels

As described in detail below, the 2-D membership functions of the C-band NCAR PID were modified based on the observations and, to a lesser extent, also the model results herein and from other studies (e.g., Marzano et al. 2005, Ryzhkov et al. 2009, Tabary et al. 2009) in order to improve the identification of hail at low levels in the April 10, 2009 hail event. Table 6.3 shows the observed percentage of each hydrometeor type in the C-band NCAR PID with modified membership functions. The most observed hydrometeor types by the algorithm are rain-hail mix (51.20 %), hail (25.27 %), graupel and rain (15.75 %), and heavy rain (4.05 %). The sample used for these results are data within 1 km of a hail report below 1 km from the April 10, 2009 hail event. Therefore, the most likely hydrometeor type for this sample should be hail or a rain hail mixture, and with modified membership functions this is true.

Due to the lack of points that were classified as rain hail mixture and hail from the original C-band NCAR PID, different membership functions were tried. Figure 6.6 shows the modifications made to the membership functions of rain hail mixture. The Z_h and Z_{dr} membership functions were modified to include higher values of Z_{dr} (3-8 dB) (Figure 6.6a). Modeling in Chapter 5 suggests that rain and melting hail mixtures can easily produce Z_{dr} of 4-6 dB. Therefore, an adjustment to the Z_h and Z_{dr} membership functions seems necessary. In addition, the modified Z_h and Z_{dr} membership functions are a much better fit to the data than the previous Z_h and Z_{dr} membership functions for rain hail mixtures. The Z_h and ρ_{hv} membership functions of rain hail mixture (Figure 6.6b) remained the same because observations in this study and other studies (Balakrishnan and Zrnic 1990b) demonstrate that ρ_{hv} is expected to be low (< 0.95) in rain hail mixtures and

Table 6.3: Percent of Occurrence of various hydrometeor types for all radar gates below

1 km in height and within 1 km of a hail report on April 10, 2009 using C-band NCAR

PID with modified membership functions

Hydrometeor ID	Percent of Occurrence (%)
Cloud	0.00
Drizzle	0.00
Light Rain	0.00
Moderate Rain	0.37
Heavy Rain	4.05
Hail	25.27
Rain Hail	51.20
Graupel and Small Hail	3.00
Graupel and Rain	15.75
Dry Snow	0.00
Wet Snow	0.00
Ice Crystals	0.00
Irregular Ice Crystals	0.00
Supercooled Liquid Drops	0.00
Flying Insects	0.00
Second Trip	0.00
Ground Clutter	0.36
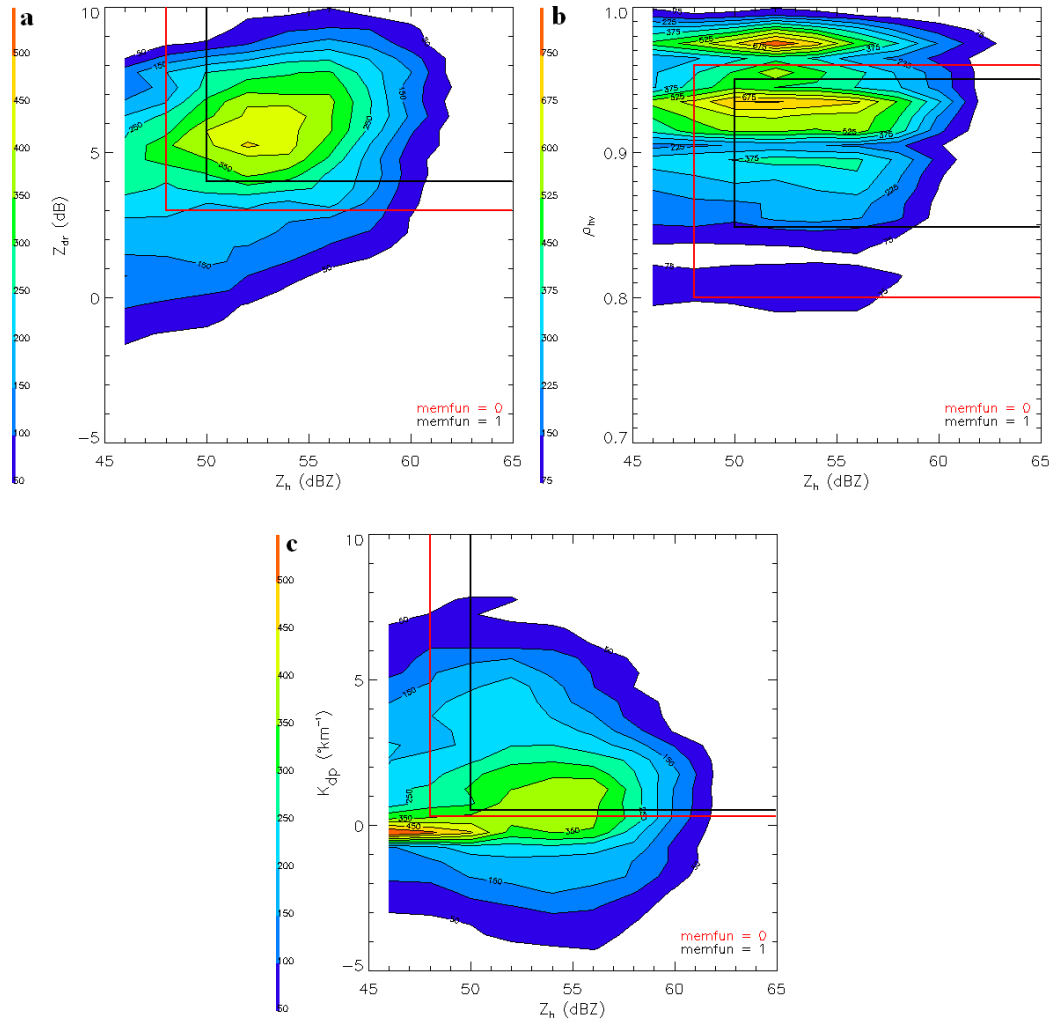
Figure 6.6: Same as in Figure 6.2 except modified membership functions for rain-hail mixture.

even more so when resonant particles are present (> 5 mm at the C-band). The membership function for Z_h and K_{dp} of rain hail mixture (Figure 6.6c) was changed to include larger values of K_{dp}. This adjustment is made because other modeling studies (e.g., Bringi et al. 1991) have shown that when rain is present K_{dp} can sometimes exceed 10 $^{\circ}$km^{-1} and other studies (e.g., Keenan 2003, Marzano et al. 2005) have used similar Z_h and K_{dp} membership functions for rain and hail mixtures at the C-band. These adjustments to the rain hail membership functions led to rain and hail mixtures being the most likely hydrometeor type 51.2 % of the time for the April 10, 2009 data set below 1 km. The increase in rain and hail detection is most likely due to the fact that the rain hail membership functions are a better fit to the data than previously.

Additionally, the membership functions were adjusted for hail (Figure 6.7). The Z_h and Z_{dr} membership functions were modified up slight to around 3-4 dB (Figure 6.7a). Modeling in Chapter 5 and other studies (e.g. Ryzhkov et al. 2009) indicate that pure hail at the C-band rarely exceeds 2-3 dB. In order for hail to produce higher Z_{dr} (> 3 dB), hail must fall wet and stable in the resonant sized region as seen in the modeling in Chapter 5. Therefore, the hail membership function only goes up to 3-4 dB. In addition, this membership function is similar to the suggestion made by Marzano et al. (2005) and Tabary et al. (2009) for Z_h and Z_{dr} membership functions for hail at the C-band. The Z_h and ρ_{hv} membership functions of hail (Figure 6.7b) remained the same because observations in this study and other studies (Balakrishnan and Zrnic 1990b) demonstrate that ρ_{hv} is expected to be low (< 0.95) when resonant particles are present (> 5 mm at the C-band). The membership functions for Z_h and K_{dp} for hail was adjusted slightly up to include the mode of the plot near Z_h of 53-57 dBZ and K_{dp} of 1 $^{\circ}$km^{-1}. In addition, the

149
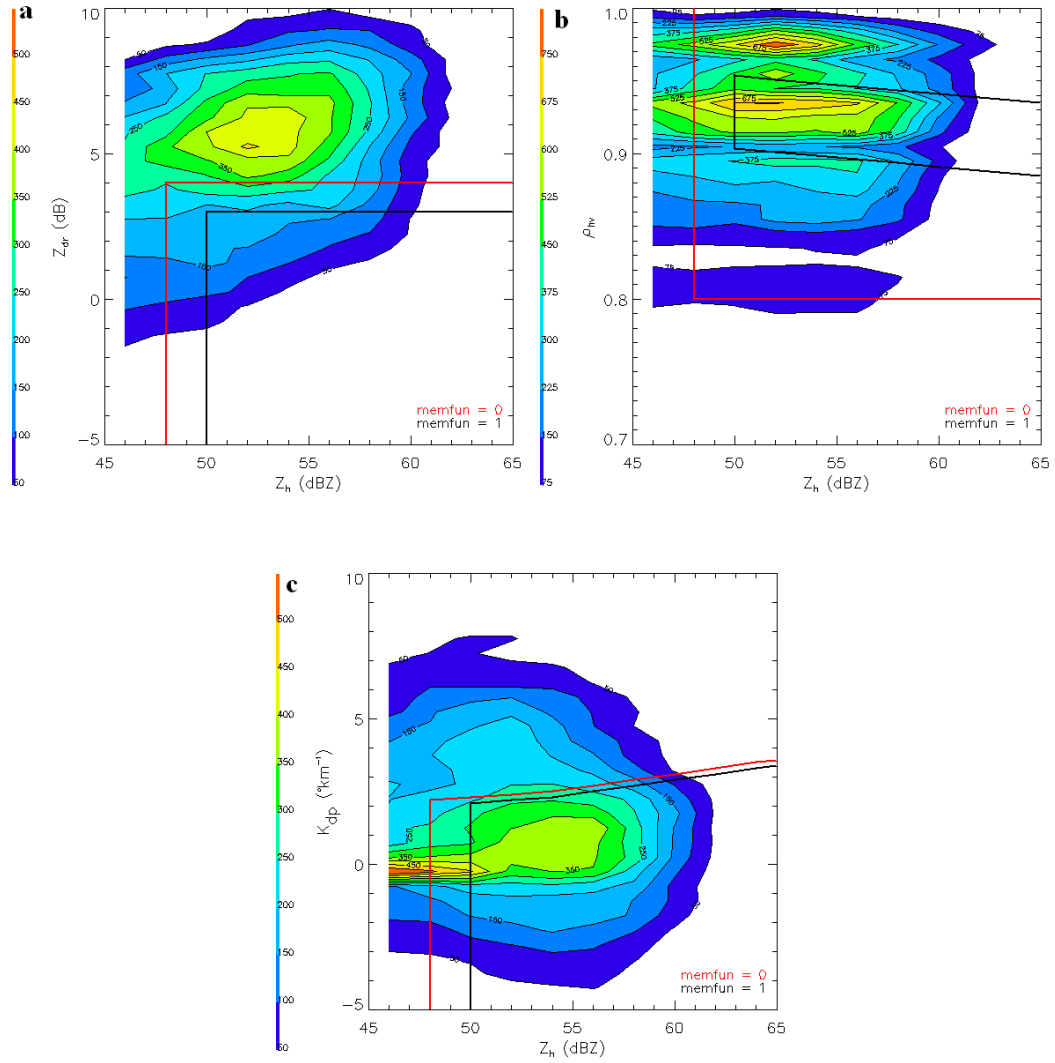
Figure 6.7: Same as Figure 6.2 except modified membership functions for hail.

modified Z_h and K_{dp} membership functions for hail includes all negative values of K_{dp} based on the suggestions of Marzano et al. (2005) and Tabary et al. (2009). Smyth et al. (1999) showed that hailstones with their major axis vertical in the resonant region can produce negative K_{dp} values. These adjustments to the membership functions for hail lead to hail being the most likely hydrometeor type 25.27 % of the time for the April 10, 2009 data set below 1 km. These modified membership functions seem to be a slight improvement and seem reasonable based on the observations and the modeling from this study and suggestions from other studies.

The final membership function that was modified is the membership function for heavy rain (Figure 6.8). There was only one membership function that was adjusted for and that is the Z_h and Z_{dr} membership function. The membership function was adjusted down slightly for Z_{dr} than in the previous heavy rain membership function. The adjustment was made because the rain case observed in Chapter 4 indicates that Z_{dr} of 4-5 dB is the maximum Z_{dr} that is observed in rain. Modeling studies at the C-band (e.g., Bringi et al. 1991) have shown that the maximum Z_{dr} for rain is observed around 4-5 dB. Additionally, other particle identification studies at the C-band (e.g., Keenan 2003, Marzano et al. 2005) use membership functions where the maximum value of Z_{dr} for heavy rain is 4-5 dB. However, the other two membership functions remained the same. These membership functions were similar to what was observed in the rain case in Chapter 4 and in modeling studies at the C-band (e.g., Bringi et al. 1991). These adjustments to the membership functions for heavy rain led to heavy rain being the most likely hydrometeor type 4.05 % of the time for the April 10, 2009 data set below 1 km. Overall, this is a large decrease compared to the previous membership functions. This
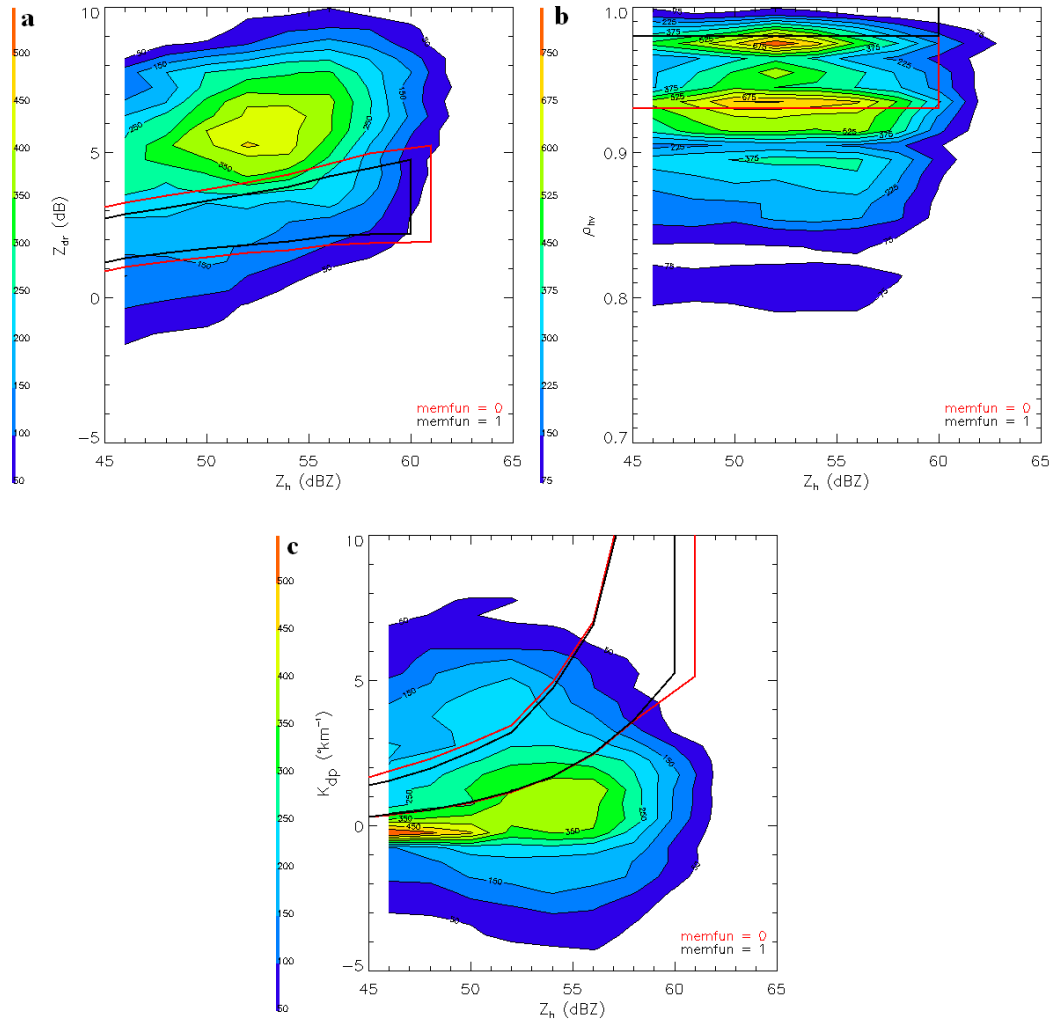
Figure 6.8: Same as Figure 6.2 except modified membership functions for heavy rain.

decrease could be due to the adjustment of the Z_h and Z_{dr} membership functions for heavy rain or due to the adjustment of the rain-hail membership functions because there is overlap between these two hydrometeor types.

Since there is significant overlap in Z_{dr} between heavy rain, rain hail mix, and hail, the final suggestion is to decrease the weighting function of Z_{dr}. Currently, the C-band NCAR PID is set up where the weighting functions of Z_h, Z_{dr}, temperature, and ρ_{hv} are twice the weighting functions of K_{dp}, standard deviation of Z_{dr}, standard deviation of velocity, and the standard deviation of Φ_{dp}. In this sensitivity test, the weighting functions of Z_{dr} and K_{dp} are switched. The original membership functions are used for each hydrometeor type (Figures 6.2-6.5). The results from this sensitivity test can be seen in Table 6.4. The results show that hail is the most likely hydrometeor type (30.56 %) followed by graupel and rain (23.40 %), heavy rain (19.17 %) and rain-hail mix (18.23 %). By decreasing the Z_{dr} and increasing the K_{dp} weighting function, hail is the most dominant hydrometeor type. This is most likely because the membership functions for hail of Z_h and K_{dp} and Z_h and ρ_{hv} are good fits to the April 10, 2009 hail report data set.

Overall, hail detection at the C-band using the NCAR PID is better at identifying hail above the 0 °C level as seen in Table 6.1. Therefore, the modifications to the membership and weighting functions were only tested on data well below the 0 °C level. From the clearly different results above and below the 0 °C level using the C-band NCAR PID, there may be a need for a different set of membership and weighting functions above and below the 0 °C level for hydrometeor identification at the C-band due to resonant sized melting hailstones and raindrops below the 0 °C level. These

Table 6.4: Percent of Occurrence of various hydrometeor types for all radar gates below

1 km in height and within 1 km of hail report on April 10, 2009 using C-band NCAR PID

with modified weighting functions

Hydrometeor ID	Percent of Occurrence (%)
Cloud	0.00
Drizzle	0.00
Light Rain	0.03
Moderate Rain	0.33
Heavy Rain	19.17
Hail	30.56
Rain Hail	18.23
Graupel and Small Hail	7.79
Graupel and Rain	23.40
Dry Snow	0.00
Wet Snow	0.00
Ice Crystals	0.00
Irregular Ice Crystals	0.00
Supercooled Liquid Drops	0.00
Flying Insects	0.00
Second Trip	0.00
Ground Clutter	0.49

sensitivity tests are just preliminary suggestions about the adjustments to the C-band NCAR PID. In order to accurately access the PID's effectiveness, a much more robust study would have to be executed with a dense network of rain gauges, disdrometers, and hail pads, which is out of the scope of this study. In addition, these PID modifications would have to be run on a variety of events, not just hail events, to make sure hail and rain hail mix is not being overly classified. However, the observations in Chapter 4 and the modeling in Chapter 5 have led to suggestions about modifications of the PID for hail detections. These modifications show that they are slightly better at detecting hail and rain hail mix at low levels than the current version of the PID.

CHAPTER 7

SUMMARY AND DISCUSSION

The primary objectives of this study were to

1. Identify and document the C-band polarimetric signatures of hail with an emphasis at low levels associated with storm reports.

2. Model hail and melting hail from reasonable assumptions to attempt to reproduce the C-band polarimetric signatures of hail at low levels.

3. Examine the current version of the NCAR PID for C-band and evaluating its effectiveness for detecting hail at low levels.

The sample size for this study is significant with 172 hail reports from 46 thunderstorms for nine different events. The reports ranged from a variety of seasons (January-August) and hail sizes (0.6-7.6 cm). This large sample size provided sufficient data to accurately document the C-band polarimetric signatures of hail, especially at low levels. Assumptions about hail and melting hail outlined in Chapter 2 provided the information necessary to model the C-band polarimetric signatures of hail and melting hail. The NCAR PID was used in the study to evaluate its ability to detect hail at the C-band. The current version of the algorithm is from Deierling et al. (2008).

The high Z_{dr} (3-8 dB) is similar to what has been observed in other C-band studies (e.g., Meischner et al. 1991, Ryzhkov et al. 2007, Kumjian and Ryzhkov 2008). However, these studies did not systematically investigate the specific conditions around a large number of confirmed hail reports. This study has expanded on previous studies for C-band signatures of hail (e.g., Meischner et al. 1991, Ryzhkov et al. 2007, Kumjian and Ryzhkov 2008) by carefully examining the C-band polarimetric signatures in close proximity to confirmed hail reports. These studies suggest that resonant effects produced by hailstones causes enhanced Z_{dr} at the C-band. In addition, these studies suggest that melting hailstones can help to enhance these resonant effects and make the hailstone appear to the radar as a giant oblate raindrop. In this study, all hailstones observed were above 5 mm and well into the resonant region at the C-band. Therefore, resonance most likely played a role in producing the high Z_{dr} (3-8 dB) signature that could have been enhanced by melting hailstones. In all the events analyzed, a significant shift can be seen from near 0 dB Z_{dr} to positive values of 3-8 dB below the melting level. This shift in Z_{dr} below the melting level is likely associated with the water torus that forms on the outside of the hailstone as it begins to melt. Rasmussen and Heymsfield (1987a) note that a water torus can act to stabilize the hailstone's fall mode such that its major axis is in the horizontal with fairly limited canting about the orientations.

In addition, these results of high Z_{dr} (3-8 dB) are similar to what have been observed by other studies that modeled melting hail at the C-band using the Rasmussen and Heymsfield (1987a) melt model (Vivekanandan et al. 1990, Meischner et al. 1991, Ryzhkov et al. 2009). However, Vivekanandan et al. (1990) and Meischner et al. (1991) model small melting hail (initial diameter < 1.0 cm) that completely or are almost

completely melted before reaching the ground. These two studies show that as melting occurs for these resonant sized particles (> 5mm at the C-band), a peak Z_{dr} of 8-9 dB can be observed as they become increasingly oblate due to the accumulation of melt water on the surface in the resonant sized region. Ryzhkov et al. (2009) uses the Rasmussen and Heymsfield (1987a) melt model to model hail up to 30 mm. Ryzhkov et al. (2009) concludes that larger melting hail (> 20 mm) contributes very little to all polarimetric variables and smaller size melting hail (< 20 mm) has the biggest impact on polarimetric variables, especially Z_{dr}. The simulations in Ryzhkov et al. (2009) assume that large (> 20 mm) melting hailstones at the C-band shed their melt water. As a result, the large hailstones tumble (cant) significantly about the horizontal and produce low Z_{dr} (< 2 dB). However, all of these melting hail modeling studies are strongly dependent upon the assumptions about the characteristics and fall mode of melting hail. In particular, Ryzhkov et al. (2009) assumes that melting hailstone larger than 1.4 cm will shed their melt water and tumble produce near 0 dB Z_{dr} at the C-band. In this study it has been observed that ARMOR range gates containing hail (0.64 − 10.80 cm) are typically characterized by high Z_{dr} (3-8 dB) near the surface. The analysis of Z_{dr} versus height in Chapter 4 shows that as the hailstones melt below the 0 °C line, Z_{dr} increases with means, medians, and modes from 3 to 8 dB near the surface. This increase can be attributed to melting that stabilizes the fall mode of large oblate hailstones (> 1.5 cm) that can produce 2-3 dB or even larger Z_{dr} (up to 10 dB) for monodisperse distributions modeled in Chapter 5. The modeling in Chapter 5 additionally showed that large melting hailstones, which are stably oriented in the horizontal and whose size distribution is described by a gamma distribution with a large shape parameter (> 10), can also produce high Z_{dr}

(> 6 dB). Modeling a mixture of large tumbling hailstones (D_0 of 1.5 to 2.5 cm), smaller melting stable oriented hailstones (D_0 of 0.6 to 0.9 cm), and rain produced a Z_{dr} of 3-4 dB if the contributions of the large tumbling hailstone to the reflectivity is small (reflectivity fraction < 0.3). Another potential explanation is that smaller hailstones melt first below the 0 °C line. As this occurs, more melting hailstones will fall in the enhanced resonant region of 5-8 mm at the C-band. Over time more and more of these stably oriented melting hailstones will fall into this resonant sized region (5-8 mm at the C-band) and may be able to outweigh the effects of larger tumbling hailstones and produce the large Z_{dr} (3-8 dB). Clearly, a better understanding of melting hailstone characteristics is needed to arrive at more concise conclusions about the microphysical reasoning for high Z_{dr} at the C-band.

Studies have shown that K_{dp} should be near 0 $°\text{km}^{-1}$ in hail because hail is isotropic (e.g., spherical) (Balakrishnan and Zrnic 1990a). In the empirical results section, K_{dp} is observed to be near 0 $°\text{km}^{-1}$ above the melting level, but below the melting level K_{dp} increasingly broadens ranging from -5 to 8 $°\text{km}^{-1}$ (Figure 4.12f). Smyth et al. (1999) suggest that oblate hail can cause non-zero values of K_{dp} in hail due to both positive intrinsic propagation phase and improperly removed backscatter phase during resonance, further complicating the matter at the C-band. Therefore, the nosiness of K_{dp} (ranging from -5 to 8 $°\text{km}^{-1}$) below the melting level can be attributed to potential errors in removing backscatter phase for resonant particles (e.g., hailstones and melting hailstones). Additionally, positive K_{dp} could also be observed in rain is also in the sample. Studies have shown (e.g., Bringi et al. 1991, Aydin and Giridhar 1992) that these positive values of K_{dp} (> 2 $°\text{km}^{-1}$) at high Z_h (> 45 dBZ) in this analysis fit well with

values that have been found for rain at the C-band ($> 2 \; °\mathrm{km}^{-1}$). There is no way to know in this study if rain is present in the sample because precipitation gauges and hail pads were not used. The influence of rain in the sample is one of the setbacks in this study. If this study was able to make a distinction between gates that contained rain and gates that contain hail, it could have potential impacts on being able to more accurately adjust the membership and weighting function for the C-band NCAR PID for hail identification. However, since a dense network of precipitation gauges and hail pads is not used it can be assumed that hail, melting hail, and rain are present in the sample in this study.

Lastly, ρ_{hv} is most often observed to be low (< 0.95) with the 75th percentile line in the composite analysis remains constantly near 0.96 (Figure 4.12c). Other studies have shown that ρ_{hv} values as low as 0.94-0.95 can be associated with large (> 5 mm) raindrops (Carey et al. 2000, Keenan et al. 2000, Zrnic et al. 2000). Therefore, the ρ_{hv} below 0.95 is most likely due to factors other than rain. Balarkrishnan and Zrnic (1990b) explain that possible reasons for a lowering in ρ_{hv} can be explained by irregular shaped hydrometeors (e.g., lumps and lobes), resonant sized particles, and a mixture of hydrometeor types (like hail and rain) that includes a variety of hydrometeor sizes, shapes, and fall speeds. Since resonance is more enhanced at the C-band than the S-band, a significant drop is ρ_{hv} can be observed for particles that are in the resonant region (> 5 mm). In addition, participants in the April 10, 2009 survey reported that many of the observed hailstones exhibited lumps and lobes that also could have contributed to lower values of ρ_{hv}. There could have also been a mixture of hydrometeors (e.g., rain, hail, and melting hail) in the radar volumes with a variety of shapes, sizes, and fall speeds that

could have lead to low ρ_{hv} (< 0.95). A more reasonable assumption is that a combination of these factors contributed to the lowering of ρ_{hv} (< 0.95).

Analysis of the polarimetric signatures associated with confirmed hail reports at the C-band reveal similar results to those more broadly presented in Meischner et al. (1991), Ryzhkov et al. (2007), and Kumjian and Ryzhkov (2008) for a few case studies. The overall composite analysis of the hail reports in Chapter 4 analyzed by joint frequency histogram below 1 km and statistical analysis of the 25th, 50th, and 75th percentile lines indicate the C-band polarimetric signatures of hail. The analysis reveals that the C-band polarimetric signatures of hail in northern Alabama are overwhelmingly characterized by high Z_h (> 50 dBZ), high Z_{dr} (3-8 dB), slightly positive K_{dp} (0-4 $°km^{-1}$), and low ρ_{hv} (0.85-0.95). The typical hail signature at the S-band can be classified as high Z_h (> 50 dBZ), near zero Z_{dr} ($-2 - 1$ dB) (e.g., Aydin et al. 1986, Bringi et al. 1986, Zrnic et al. 1993, Hubbert et al. 1998), slightly positive K_{dp} ($-0.5 - 1.5$ $°km^{-1}$) (e.g., Balakrishnan and Zrnic 1990a, Hubbert et al. 1998, Straka et al. 2000), and low ρ_{hv} (< 0.95) (e.g., Balakrishnan and Zrnic 1990b, Zrnic et al. 1993, Hubbert et al. 1998). From the empirical analysis in Chapter 4, the C-band polarimetric variable K_{dp} and ρ_{hv} in hail produce similar polarimetric signatures observed by most other studies at the S-band. One of the nuances of K_{dp} is that it is proportional to the frequency. Therefore, K_{dp} at the C-band would be roughly two times higher than the S-band for the same particle conditions. However, Z_{dr} for hail at the C-band, which is typically very large, is significantly different than the "hail hole" signature often observed in hail at the S-band. Therefore, the method used for detecting hail at the S-band using Z_{dr} cannot be transferred and applied at the C-band. One of these methods, H_{dr} (Aydin et al. 1986), was

presented in Chapter 4. The H_{dr} method was found to not be useful at the C-band because an overwhelming majority of hail points were characterized as rain by the H_{dr} method (Figure 4.1a). Therefore, this method cannot be transferred and applied for hail detection at the C-band.

Studies suggest that if hailstones are sufficiently large (> 1.5 cm) at the C-band, then Z_{dr} will be more like the "hail hole" signature observed at the S-band because these large drops will shed their melt water and randomly tumble appearing to the radar as an effective sphere (e.g., Vivekanandan et al. 1990, Meischner et al. 1991, Bringi and Chandrasekar 2001 p.451-452, Ryzhkov et al. 2009). To test this hypothesis, the hail reports were broken up into large and small categories. The large hailstones consisted of reports with hailstones over 4.45 cm while the small group consisted of hailstones smaller than this size. The statistical results reveled that the larger hailstone exhibited slightly higher Z_{dr} for small hail over all Z_h bin sizes. These comparisons were made by examining the 25th, 50th, and 75th percentile of small and large hail. From this analysis, this hypothesis is rejected. However, this study cannot be certain that rain and other smaller hail were present in the 1 km radius of the large hail reports. Nonetheless, if large rain drops and smaller hail are causing the large Z_{dr} and large hail is not because it is tumbling as suggested by Kumjian and Ryzhkov (2008) and Ryzhkov et al. (2009), then these small particles must be signifigantly and sufficiently more numerous than the large hail in order to dominate the reflectivity and hence the Z_{dr}, as shown in Chapter 5.

The observations chapter also explored a couple of potential "hail holes." One of these hail holes did not meet the storm report criteria outline in Chapter 3 while the other did. The potential "hail hole" that did not meet the storm criteria exhibited lower Z_{dr}

(~ 2 dB for corrected and 0 dB for uncorrected Z_{dr}) associated with high Z_h (> 50 dBZ) near the surface (Figure 4.20). This storm report should not be regarded with the highest of confidence due to the inaccuracy in the report. However, this example does produce a clear lowering in Z_{dr}. The lower Z_{dr} could be due to tumbling hail that appears to the radar as an effective sphere but there are other potential explanations for the signature as well. The signature could exist because the differential attenuation correction algorithm is under correcting Z_{dr}. Borowska et al. (2009) compared S-band and C-band polarimetric radars and concluded that strong attenuation and differential attenuation at the C-band can cause the Bringi et al. (2001) attenuation algorithm to under correct for attenuation and differential attenuation. Therefore, if under correcting is occurring in this case, then the corrected Z_{dr} would be higher and resemble the high Z_{dr} (3-8 dB) more than the "hail hole" signature. The storm report that did meet the criteria to be used in the study exhibited large values of Φ_{dp} (> 150°) (Figure 4.21). Additionally, the corrected Z_{dr} becomes negative on the backside of the cell. This is a classic example where differential attenuation is large and the Bringi et al. (2001) algorithm has likely failed and led to Z_{dr} being under corrected. In some instance, it appears that the C-band signatures of hail may resemble those of the S-band. However, other factors may contribute to these C-band signatures being similar to the S-band such as under correction of differential attenuation. More research on differential attenuation correction at the C-band in melting hail like Tabary et al. (2009) and Borowska e al. (2009) is required to make further progress on this open question. After studying the correction methods, more work is needed to understand the extent and frequency with which under-correction might impact hail identification at the C-band. Additionally, the overwhelming majority of data

analyzed in Chapter 4 suggests that the C-band signature of hail is characterized most of the time by the high Z_{dr} (3-8 dB) signature.

The next goal of the study is to try and reproduce the high Z_{dr} (3-8 dB) using the T-matrix and Mueller matrix. Using these methods a number of assumptions have to be made about the hydrometeor that is being modeled. If the following assumptions were used, then melting hailstones are able to produce high Z_{dr} (3-8 dB):

- Melting hailstones fall with their major axis horizontal.

- Melting hailstones are fairly oblate with axis ratios near 0.6.

- Melting hailstones fall rather stable and do not tumble or wobble randomly.

If these criteria are true, then high Z_{dr} can be reproduced for monodisperse, exponential, and gamma hailstone size distributions. The monodisperse distribution produces a maximum Z_{dr} at a median volume diameter of 1.4 cm (Figure 5.1). This is well outside the peak of resonance found in other studies of 5-8 mm for the C-band (e.g., Zrnic et al. 2000). However, there are different peaks of resonance with 5-8 mm being the first peak in resonance. Assuming a monodisperse distribution may add more emphasis to secondary peaks of resonance that may occur in the 1.4 cm range. The exponential distribution exhibits a peak of Z_{dr} in the typical resonance region between 5-8 mm (Figure 5.2). This is most likely due to the fact that the exponential distribution assumes a high concentration of particles on the lower end of the distribution (e.g., 5-8 mm); therefore, these sizes are even more enhanced when the median volume diameter is within the range of 5-8 mm and leads to the highest Z_{dr} being produced in this range of median volume diameters. The gamma distribution is highly dependent upon the value of μ that is used. As μ increases, the maximum Z_{dr} shifts towards higher values of median

volume diameter and the emphasis of the distribution shifts towards high median volume diameters (Figure 5.4). The distribution also becomes more like the monodisperse distribution as μ increases. Overall, it is easy to reproduce the high Z_{dr} signature using melting hail if certain assumptions are made about the hailstones fall mode, shape, size, and distribution.

Ryzhkov et al. (2007) Kumjian and Ryzhkov (2008), and Ryzhkov et al. (2009) suggest that the high Z_{dr} (3-8 dB) signature at the C-band occur because rain and melting hail mask the effects of large tumbling hail. To test this hypothesis, a mixture of rain, small melting hail, and large tumbling hail assuming an exponential distribution was examined to compare the reflectivity fraction of large hail to the resulting Z_{dr} using the T-matrix and Mueller matrix. The results showed that if large tumbling hail is dominant in reflectivity, then Z_{dr} will be near 0 dB. If the large (tumbling) hail reflectivity fraction is higher than 0.5, the resulting Z_{dr} is less than 2 dB (Figure 5.5). This simple test of the reflectivity fraction of large hail suggests that if large hail is dominant in the reflectivity, then large hail will dominate Z_{dr} and produce near zero Z_{dr}. Ryzhkov et al. (2009) modeled combination of rain, hail, and melting hail using the 2D nonhydrostatic mixed-phase spectral bin Hebrew University of Jerusalem Cloud Model and was able to produce Z_{dr} of 6 dB at the C-band in this mixture. The Ryzhkov et al. (2009) study attributes the large Z_{dr} to the contributions of the smaller melting hailstones. However, this study was only able to produce Z_{dr} of 3-4 dB in a mixture of large tumbling hail, smaller stable melting hail, and rain when the reflectivity fractions of large hail was less than 0.3. In addtion, the results in this study and Ryzhkov et al. (2009) are dependent upon the correct assumptions about the characteristics and fall mode of large melting hail.

The last and final goal of the study is to evaluate the overall performance of the current NCAR PID and suggest potential improvements for hail detection at the C-band. For this study, the focus for hail detection was below 1 km, well below the melting level and the location where hail detection is important to the general public. The initial version of the NCAR PID (Deierling et al. 2008) was tested, and it detected hail or rain hail mix for 39.07 % of the time for the April 10, 2009 data set below 1 km (Table 6.1). The data set is taken from within 1 km of a hail report; therefore, the combination of hail and rain hail mix should be classified as a majority of the points in the data set. The membership functions for Z_h and Z_{dr} and Z_h and K_{dp} were adjusted for hail, rain hail mix, and heavy rain based on observations in this study and Marzano et al. (2005). Additionally, the membership functions for Z_h and K_{dp} were adjusted for hail and rain hail mix based on observations in this study and Marzano et al. (2005). The adjustments to the membership functions led to hail and rain hail mix being detected for 76.47 % of the data points (Table 6.2). These results seem more reasonable than the previous membership functions. The second adjustment that was tested is the weighting functions of the original membership functions. Changing the weighting functions in the C-band NCAR PID changes the aggregation score for the most likely hydrometeor type. For this sensitivity test, the weighting functions of Z_{dr} and K_{dp} were switched because the Z_h and K_{dp} membership functions seemed to be better fit to the April 10, 2009 data set. This sensitivity test led to 49.73 % of the points in the data set being classified as either hail or rain hail mix (Table 6.3). Overall, the most realistic results came from the sensitivity test of adjusting the membership functions to better fit the April 10, 200 data and from the suggestions by Marzano et al. (2005). The original membership functions are not a good

fit to the data set that is used in this study. The data set should be representative of the C-band polarimetric signatures of hail at the surface. However, there is no way to be sure that rain or other hydrometeor types other than hail are present. This study would suggest that the membership functions for the PID be adjusted towards the new membership functions for hail and rain hail mix. However, a more robust and complete study using these membership functions will need to explore their effectiveness at identifying hail and hail/rain mixture without adversely affecting other categories (like heavy or moderate rain) in numerous meteorological situations and precipitation types.

Overall, this study shows that the C-band polarimetric signatures of hail produce similar results with the variables K_{dp} and ρ_{hv} and different results with the variable Z_{dr} when compared to the S-band. At the C-band, hail is identified by areas of high Z_h (> 50 dBZ) and high Z_{dr} (3-8 dB) while at the S-band, hail is identified by areas of high Z_h and low Z_{dr} (-2 − 1 dB). Additionally, these high Z_{dr} (3-8 dB) signatures can be reproduced using the T-matrix and Mueller matrix for melting hail. However, certain assumptions must be made about the melting hailstones shape, size, orientation, fall mode, and concentrations outlined in this chapter. The final step was to evaluate the current version of the NCAR PID for the C-band. The original version had some issues with detecting hail and rain and hail mixtures because of the uncertainty that exists of what a C-band hail signature should look like. Adjustment to membership functions for hail and rain hail mixtures provided the best solutions for improving hail detection near the surface. Ultimately, this study helps to classify the C-band signatures of hail, shows that the signatures can be reproduced using the T-matrix and Mueller matrix, and

suggests new ways to modify the NCAR PID for hail detection based on previous studies

(e.g., Marzano et al. 2005) and observations and modeling of hail in this study.

CHAPTER 8

CONCLUSIONS AND FUTURE WORK

In this study, a dual approach of empirical observations and radar modeling were used to examine the C-band polarimetric signatures of hail and melting hail. The ARMOR observations of hail in Chapter 4 show that the C-band signatures of hail are characterized by high Z_h (> 50 dBZ), high Z_{dr} (3-8 dB), positive K_{dp} (0-4 °km^{-1}), and low ρ_{hv} (0.85-0.95) at low-levels. Therefore, the hypothesis that C-band polarimetric signatures of hail are typically consistent with the "hail hole" signature of high Z_h (> 50 dBZ) and low Z_{dr} (-1 to 1 dB) (e.g. Aydin et al. 1986, Bringi et al. 1986) at low-levels can be rejected through the observations of nine events in Chapter 4. This result suggests that S-band techniques for identifying hail using Z_{dr} cannot be directly transferred and applied at the C-band without modifications. However, the C-band observations of K_{dp} and ρ_{hv} for hail are similar to those found at the S-band (e.g., Balakrishnan and Zrnic 1990a,b, Zrnic et al. 1993, Hubbert et al. 1998). However, K_{dp} is noisy in some cases (e.g., April 10, 2009) and may be due to the insufficient filtering of the backscatter differential phase (δ). In this study, a couple of potential "hail hole cases were presented. However, each case had a potential issue that casts some doubt on the veracity of the C-band hail hole. The first case fell outside of the storm report criteria

169

outlined in Chapter 3 and should not be regarded with the highest of confidence. The second case appeared to have difficulty with correcting for differential attenuation. Therefore, there were no clear examples of the "hail hole" signature at the C-band presented in this study. However, this study has shown that potential "hail hole" cases can exist at C-band.

It is theorized in this study along with others (e.g., Vivekanandan et al. 1990, Meischner et al. 1991, Ryzhkov et al. 2007) that the high Z_{dr} signature exist due to melting, resonant-sized, stably and horizontally oriented (i.e. with major axis in the horizontal) hailstones and raindrops that are present at low-levels. Resonance has been shown to cause increase values of Z_{dr} for particles over 5 mm (e.g., Vivekanandan et al. 1990, Meischner et al. 199, Zrnic et al. 2000). In addition, melting may play a role in setting up the right conditions for resonance including the necessary size, shape, fall mode, and dielectric. Therefore, the high Z_{dr} (3-8 dB) most likely is produced by the resonant-sized, stably oriented and melting hailstones and raindrops observed in this study. Future work is needed in the form of more hail events at the C-band to observe and more thoroughly document the C-band signature of hail.

The second part of this study involved the modeling of rain, hail, and melting hailstones using the T-matrix and Mueller matrix. The modeling objective was to try and reproduce the high Z_{dr} (3-8 dB) signatures that are observed at the C-band. The modeling in Chapter 5 showed that high Z_{dr} (3-10 dB) can be reproduced in monodisperse distributions of melting hail with median volume diameter of 0.5 – 1.9 cm with a low standard deviation of the canting angle (5°), the major axis falling horizontal, an axis ratio of 0.6, and a water coat thickness of 0.5 mm. Additionally, high Z_{dr} (3-6 dB) can be

observed for the same conditions for an exponential distribution with median volume diameters of 0.5-1.6 cm. The gamma distribution is highly dependent upon the shape parameter. Increasing the shape parameter ($10 \leq \mu \leq 20$) led to an increase in the peak Z_{dr} (6-7 dB) for a larger median volume diameter ($1.0 - 1.1$ cm). A mixture of rain, large (tumbling) hail, and melting (stable) hail was modeled as well. The simulations showed that if the large tumbling hail is dominant in the reflectivity, then Z_{dr} will be near 0 dB. However, a mixture of stable melting hail and large raindrops were modeled that showed Z_{dr} in this mixture could easily be 5-6 dB. Therefore, in order to reproduce the Z_{dr} values observed in Chapter 4, the melting hailstones of all sizes had to fall stable with small axis ratios and with their major axis horizontal. Studies have shown that small (< 1.5 cm) melting hail can fall stably if a sufficient water torus is present (e.g., Rasmussen and Heymsfield 1987a, Vivekanandan et al. 1990, Meischner et al. 1991). Vivekanandan et al. (1990) and Meischner et al. (1991) suggest that large hail (> 1.5 cm) will shed their melt water and tumble. However, in this study it has been observed that large hail (> 1.5 cm) can be associated with large Z_{dr} at the surface. Modeling in this study has shown that large (> 1.5 cm) stable hailstone can produce 2-3 dB for exponential and gamma size distribution. Additionally if a monodisperse distribution is assumed large (> 1.5 cm), melting stable hailstones can produce Z_{dr} up to 10 dB. Rasmussen and Heymsfield (1987a) state that is has not been conclusively determined if melting hail does or does not tumble. It cannot be conclusively determined if large hail (> 1.5 cm) do or do not tumble in this study. Therefore, it is unclear if the large Z_{dr} is produced through a mixture of large (> 1.5 cm) and small (< 1.5 cm) hail mixed with rain or if the smaller stable hail (< 1.5 cm) mixed with rain dominate the signature when large (> 1.5 cm)

hailstones are present. For future work, the Rasmussen and Heymsfield (1987a) melt model or similar hail melting model would need to be used to better understand the evolution of the water torus as the hailstone falls below the melting level. In addition, a better understanding of the characteristic and falling behavior of hailstone, especially melting hailstones, is needed to be able to make the correct assumptions for modeling the melt behavior of hailstones.

The third part of this study employed the C-band NCAR PID to evaluate its usefulness at detecting hail at low-levels. Overall, the current version of the C-band NCAR PID led to only 39.07 % of the April 10, 2009 data set near the surface being detected as hail or rain/hail mix. The suggestions made by Marzano et al. (2005) led to a 76.47 % of the April 10, 2009 data set near the surface being detected as hail or rain/hail mix. In addition, the weighting functions of Z_{dr} and K_{dp} were swapped in the original C-band NCAR PID because the K_{dp} membership functions seemed to be a better fit to the data set and led to 48.79 % of the April 10, 2009 data set near the surface being detected as hail or rain/hail mix. Overall, both suggestions led to a better detection of hail at the surface. The better detection for the modified NCAR PID is most likely due to Z_{dr} being effectively changed to account for the large Z_{dr} (3-8 dB) that occurs for large melting resonant sized hailstones below the melting level. The C-band NCAR PID worked well for hail and graupel identification above the melting level. Therefore, the use of different membership functions for above and below the melting level may be useful for indentifying hail at low-levels. However, in order to completely evaluate the performance of the C-band NCAR PID in hailstorms, a dense network of precipitation

gauges, disdrometers, and hail pads in numerous hailstorms and meteorological conditions would be needed.

Overall, this study has documented the C-band polarimetric signature of hail by examining the signature near high quality hail reports and shown that there are clear differences in Z_{dr} between the C-band and the S-band. This observed high Z_{dr} (3-8 dB) hail signature was to be reproduced by using radar modeling of melting hail and mixtures of melting hail and rain. The C-band NCAR PID was evaluated to show that hail detection improvements can still be made at the C-band. A few suggestions have been made for improvements of hail detection that may be found useful in future studies.

APPENDIX

RANGE SENSITIVITY TEST

The radar data associated with each hail report were taken from range gates within 1 km of each report. Studies have looked at the widths of hail shafts and swaths. Changnon (1992) looked at the spatial scale of hail swaths and found that the average swath in Illinois was 4.5 km and the average width was 1.3 km with an average duration of 8.8 minutes. This study determined the spatial scale of the hail swath from crop damage reports to insurance companies and from radar data. In addition to this study, other studies have observed from S-band dual polarimetric radar the "hail hole" signature on the order of 1 km wide or larger (e.g., Bringi 1986, Hubbert et al. 1998). From these studies and radar observations, it seems that a 1 km area radius around each hail report should contain data that are most representative of a C-band polarimetric radar signature of hail and that provides a sufficient sample size of range gates for this study. In this appendix, sensitivity tests are performed on the data from April 10, 2009 to examine the sensitivity of the results in the hail signature to changes in the analysis radius. For the test, the analysis radius is decreased by 50 % to 0.5 km and increased by 50 % to 1.5 km.

Table A.1 shows the difference between the mean from 1 km to 0.5 km for each polarimetric variable within each 2 dB reflectivity bin. It can be seen that the differences

in the means in Table A.1 are not significant for any bin interval. The maximum absolute

maximum differences are -0.55 dB for Z_{dr}, 0.61 °km^{-1} for K_{dp}, and -0.01 for ρ_{hv}. The

maximum differences in the mean Z_{dr} and K_{dp} occur at large Z_h bin size (63-65 dB). This

bin does not contain a large amount of data (see Figures A.1 and A.2). Differences in the

means between the two tests may not be statistically significant (Figure A.1). Figure A.1

shows the joint frequency histograms of Z_h and polarimetric data within 500 m of a hail

report on April 10, 2009. All the data points are also below 1 km because this is

representative of the C-band polarimetric hail signatures at the surface. Figure A.2 is the

same as Figure A.2 except that Figure A.2 is the joint frequency histogram of Z_h and

polarimetric data within 1 km of a hail report. It can be seen that both figures are similar

and the only differences exist in the amount of data. Of course Figure A.1 contains less

data because the radius of analysis 500 m is smaller compared to 1 km for Figure A.2.

However, statistically the plots have similar modes, medians, percentiles (25th and 75th),

and means (Figures A.1 and A.2, Table A.1). Overall, there are no clear differences

between the polarimetric signatures diagnosed within 500 m and 1 km of a hail report.

The next sensitivity test is to try a longer radius (1.5 km). Table A.2 shows the

difference between the mean radius from 1 km to 1.5 km for each polarimetric variable at

each 2 dB reflectivity bin. The maximum absolute magnitude of the differences are

0.37 dB for Z_{dr}, -0.30 °km^{-1} for K_{dp}, and -0.01 for ρ_{hv}. These maximum mean differences

are smaller than what are seen in Table A.2. Figure A.3 is the same as Figures A.1 and

A.2 except it is the joint frequency histogram of Z_h and polarimetric data within 1.5 km of

a hail report. Comparing Figures A.2 and A.3, they are both similar and no real

differences are seen. The only obvious differences is that Figure A.3 contains more data

Table A.1 The difference between mean polarimetric quantities (Z_{dr}, K_{dp}, and ρ_{hv}) within

1 km and 0.5 km of a hail report as a function of Z_h bin.

Z_h Bins (dBZ)	Z_{dr} Mean Difference (Z_{dr} mean (1 km) - Z_{dr} mean (0.5km)) dB	K_{dp} Mean Difference (K_{dp} mean(1km) - K_{dp} mean (0.5 km)) $^\circ km^{-1}$	ρ_{hv} Mean Difference (ρ_{hv} mean (1 km) - ρ_{hv} mean (0.5km))
45-47	-0.33	0.43	0.00
47-49	-0.42	0.41	0.00
49-51	-0.26	0.44	0.00
51-53	0.12	0.42	0.00
53-55	0.18	0.27	0.00
55-57	-0.11	0.17	0.00
57-59	-0.09	0.22	-0.01
59-61	-0.02	0.27	0.00
61-63	-0.30	0.13	0.00
63-65	-0.55	0.61	0.00

Table A.2: The difference between mean polarimetric quantities (Z_{dr}, K_{dp}, and ρ_{hv}) within 1 km and 1.5 km of a hail report as a function of Z_h bin.

Z_h Bins (dBZ)	Z_{dr} Mean Difference (Z_{dr} mean (1 km) - Z_{dr} mean (1.5km)) dB	K_{dp} Mean Difference (K_{dp} mean(1km) - K_{dp} mean (1.5 km)) $^\circ$km^{-1}	ρ_{hv} Mean Difference (ρ_{hv} mean (1 km) - ρ_{hv} mean (1.5km))
45-47	0.00	0.01	0.00
47-49	0.21	0.11	0.00
49-51	0.36	0.10	-0.01
51-53	0.37	0.14	0.00
53-55	0.28	-0.01	0.00
55-57	0.13	-0.01	0.00
57-59	0.01	-0.09	0.00
59-61	0.14	-0.18	0.00
61-63	0.37	-0.30	0.00
63-65	0.21	-0.29	-0.01
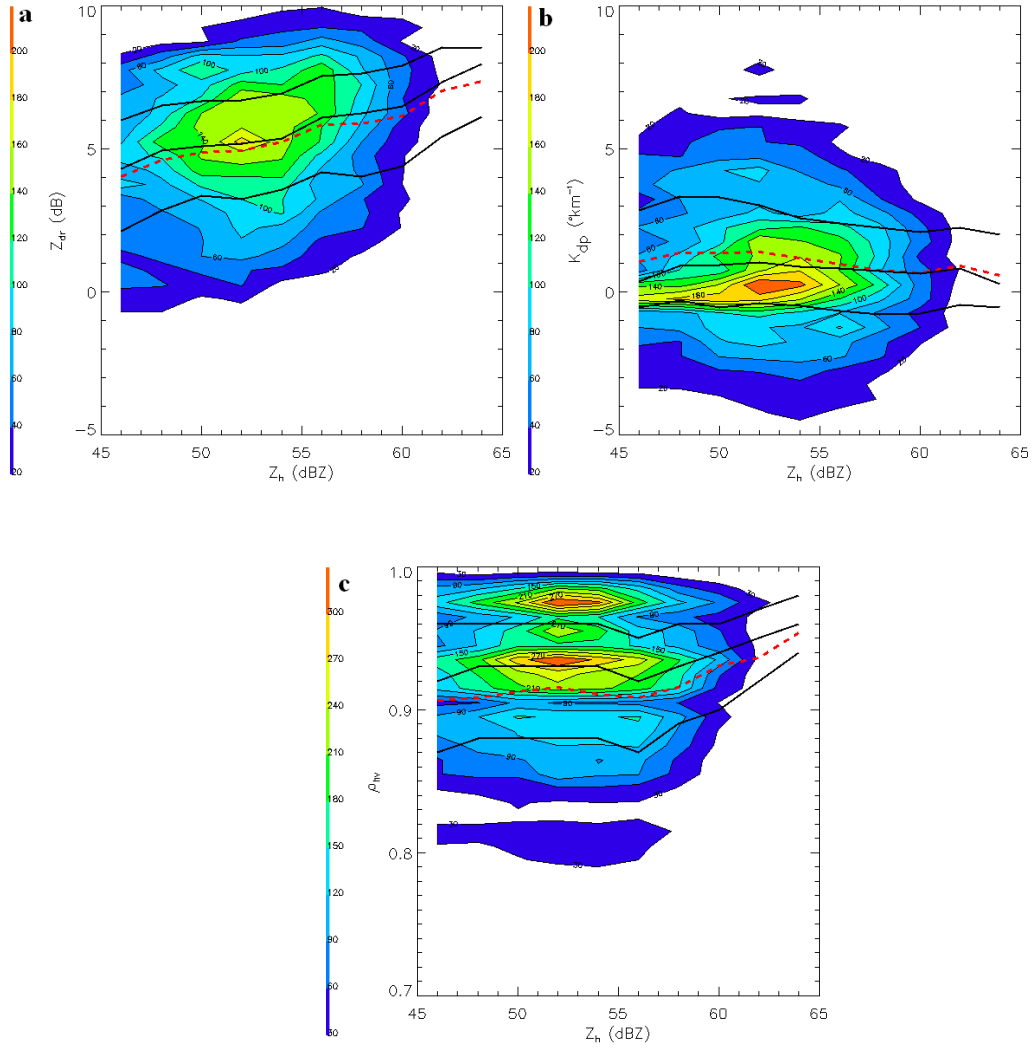
Figure A.1: Joint frequency histograms of Z_h and (a) Z_{dr} (b) K_{dp} (c) ρ_{hv}. All data is below 1 km and within a 500 m radius of a hail report from April 10, 2009. The bottom red line on each plot is the 25th percentile line, the middle red line on each plot is the 50th percentile line, and the top red line on each plot is the 75th percentile line. The Z_h data is in 2 dBZ bins, the Z_{dr} is in 0.5 dB bins, the K_{dp} data is in 0.5 °km^{-1} bins, and the ρ_{hv} data is in 0.05 bins.
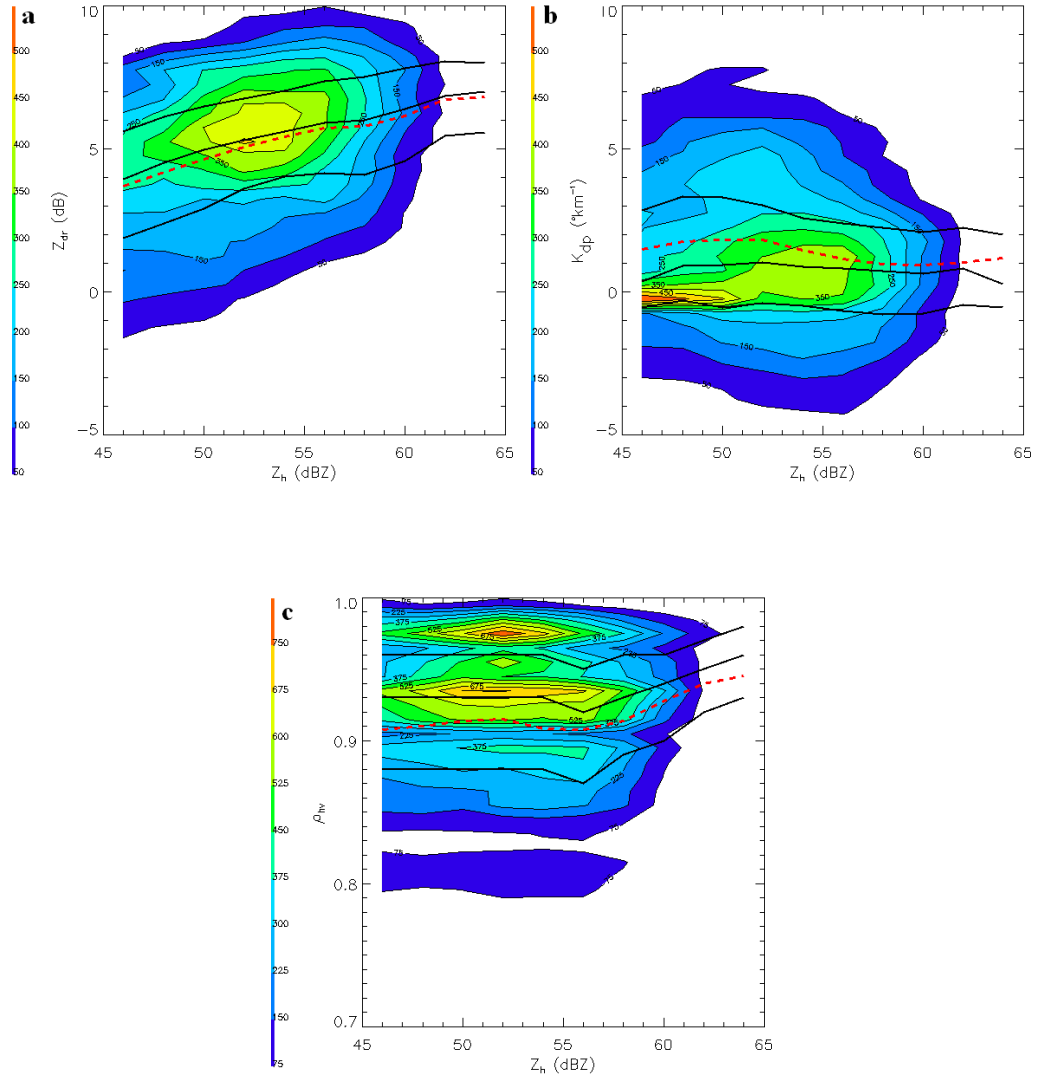
Figure A.2: Same as Figure A.1 except radius is 1 km.
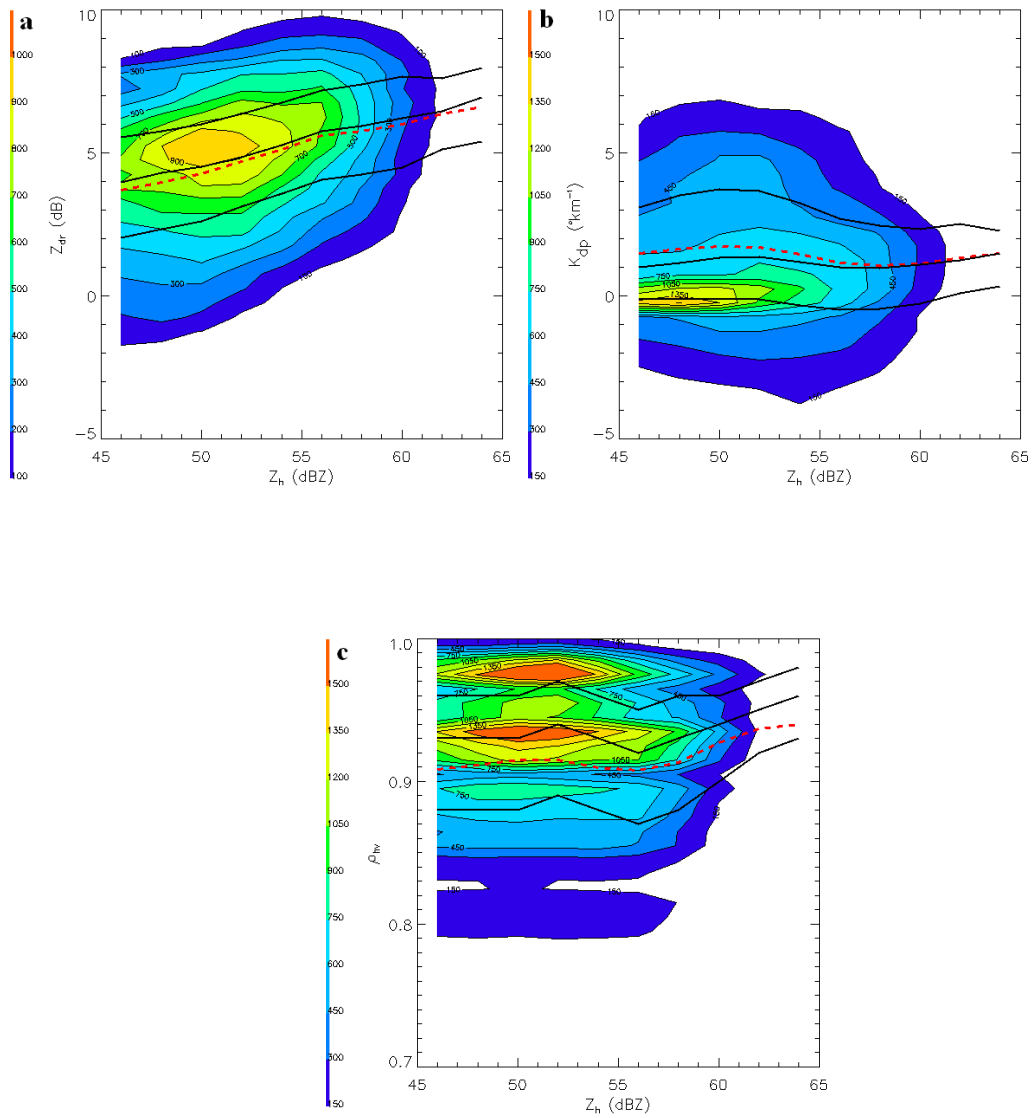
Figure A.3: Same as Figure A.1 except radius is 1.5 km.

than Figure A.2 because of the 1.5 km radius. Statistically, the plots are similar as can be seen in Table A.2. There appear to be small differences in the modes between 1 km and 1.5 km radius lengths as the modes for 1.5 km occur at slightly lower Z_h due to the increased radius. Overall, these differences between the polarimetric signatures between 1 km and 1.5 km are small and do not seem to be statistically important.

In this study, the preferred radius to examine data from a hail report is 1 km. Other studies have shown through observations (Changnon 1992) and polarimetric radar (e.g., Bringi et al. 1986, Hubbert et al. 1998) that a good approximation of a hail shaft width is on the order of 1 km. This section has shown that the polarimetric variables show no clear variations in data within a 0.5, 1.0, and 1.5 km radius from a hail report. Since there is no sensitivity in polarimetric signatures to the radii shorter (0.5 km) and longer (1.5 km) than 1 km and other studies suggest order of 1 km is a good approximation for the size of a hail shaft, 1 km radius was used as the distance that is most representative of a hail signature.

REFERENCES

Adler, R. F., M. J. Markus, and D. D. Fenn, 1985: Detection of severe Midwest thunderstorms using geosynchronous satellite data. *Mon. Wea. Rev.*, **113**, 769-781.

Andsager, K., K. V. Beard, and N. F. Laird, 1999: Laboratory measurements of axis ratios for large raindrops. *J. Atmos. Sci.*, **56**, 2673-2683.

Atlas, D. and F. H. Ludlam, 1961: Multi-wavelength radar reflectivity of hailstorms. *Quart. J. Roy. Meteor. Soc.*, **87**, 523-534.

Auer, A. H., Jr., 1994: Hail recognition through the combined use of radar reflectivity and cloud-top temperatures. *Mon. Wea. Rev.*, **122**, 2218-2221.

Auer, A. H., Jr., and J. D. Marwitz, 1972: Hail in the vicinity of organized updrafts. *J. Appl. Meteor.*, **11**, 748-751.

Aydin, K. T., T. Seliga, and V. Balaji, 1986: Remote sensing of hail with dual linear polarization radar. *J. Climate Appl. Meteor.*, **25**, 1475-1484.

Aydin, K., Y. Zhao, and T. A. Seliga, 1989: Rain-induced attenuation effects on C-band dual polarization meteorological radars. *IEEE Trans. Remote Sens.*, **25**, 57-66.

Aydin, K., Y. Zhao, and T. A. Seliga, 1990: A differential reflectivity hail measurement technique: Observations during the Denver hailstorm of 13 June 1984. *J.   Atmos. Oceanic Technol.*, **7**, 104-113.

Aydin, K. and Y. Zhao, 1990: A computational study of polarimetric radar observables in hail. *IEEE Trans. Remote Sens.*, **28**, 412-422.

Aydin, K. and V. Giridhar, 1992: C-Band dual polarization radar observable in rain. *J. Atmos. Oceanic Technol.*, **9**, 383-390.

Balakrishnan, N. and D. S. Zrnic, 1990a: Estimation of rain and hail rates in mixed-phase precipitation. *J. Atmos. Sci.*, **47**, 565-583.

Balakrishnan, N. and D. S. Zrnic, 1990b: Use of polarization to characterize precipitation and discriminate large hail. *J. Atmos. Sci.*, **47**, 1525-1540.

Baldini, L., E. Gorgucci, and J. Vivekanandan, 2004: Hydrometeor classification methodology for C-Band polarimetric radars. *ERAD*, 62-66.

Beard, K. V. and C. Chuang, 1987: A new model for the equilibrium shape of raindrops. *J. Atmos. Sci.*, **44**, 1509-1524.

Borowska, L., A. V. Ryzhkov, D. S. Zrnic, P. Zhang, D. Hudak, P. Neilley, M. Knight, R. D. Palmer, B. L. Cheong, A. Battaglia, and C. Simmer: Attenuation of radar signal in melting hail at C-band. *34th Conference on Radar Meteorology*, Williamsburg, VA, 5-9 October 2009.

Bringi, V. N., J. Vivekanandan, and J. D. Tuttle, 1986: Multiparameter radar measurements in Colorado convective storms. Part II: Hail detection studies. *J. Atmos. Sci.*, **43**, 2564-2577.

Bringi, V. N., V. Chandrasekar, N. Balakrishnan, and D. S. Zrnic, 1990: An examination of propagation effects in rainfall on radar measurements at microwave frequencies. *J. Atmos. Oceanic Technol.*, **7**, 829-840.

Bringi, V. N., V. Chandrasekar, P. Meischner, J. Hubbert, and Y Golestani, 1991: Polarimetric radar signatures of precipitation at S- and C-band. *IEEE Trans. Remote Sens.*, **138**, 109-119.

Bringi, V. N., T. D. Keenan, and V. Chandrasekar, 2001: Correcting C-Band radar Reflectivity and differential reflectivity data for rain attenuation: A self-consistent method with constraints. *IEEE Trans. Remote Sens.*, **39**, 1906-1915.

Bringi, V. N. and V. Chandrasekar, 2001: Polarimetric Doppler weather radar: Principles and applications. Cambridge University Press, Cambridge.

Carbone, R. E., D. Atlas, P. Eccles, R. Fetter, and E. Mueller, 1973: Dual wavelength radar hail detection. *Bull. Amer. Meteor. Soc.*, **54**, 921-924.

Carey, L. D., S. A. Rutledge, D. A. Ahijevych, and T. D. Keenan, 2000: Correcting propagation effects in C-Band polarimetric radar observations of tropical convection using differential propagation phase. *J. Appl. Meteor.*, **39**, 1405-1433.

Cecil, D. J., 2009: Passive microwave brightness temperatures as proxies for hailstorms. *J. Appl. Meteor. Clim.*, **48**, 1281-1286.

Changnon, S. A., 1999: Data and approaches for determining hail risk in the contiguous United States. *J. Appl. Meteor.*, **38**, 1730-1739.

Cheng, L. and M. English, 1983: A relationship between hailstone concentration and size. *J. Atmos. Sci.*, **40**, 204-213.

Deierling, W., J. Latham, W. A. Petersen, J. Latham, S. Ellis, and H. J. Christian, 2008: The relationship between lightning activity and ice fluxes in thunderstorms. *J. Geophys. Res.*, **113**, D15210.

Depue, T. K., P. C. Kennedy, and S. A. Rutledge, 2007: Performance of the hail differential reflectivity (H$_{dr}$) polarimetric radar hail indicator. *J. Appl. Meteor and Climat.*, **46**, 1290-1301.

Donaldson, R. J., 1961: Radar reflectivity profiles in thunderstorms. *J. Meteor.*, **18**, 292-305.

Donavon, R. A. and K. A. Jungbluth, 2007: Evaluation of a technique for radar identification of large hail across the upper Midwest and central Plains of the United States. *Wea. Forecasting*, **22**, 244-254.

Eccles, P. J. and D. Atlas, 1973: A dual-wavelength hail detector. *J. Appl. Meteor.*, **5**, 847-854.

Edwards, R. and R. L. Thompson, 1998: Nationwide comparisons of hail size with WSR-88D vertically liquid integrated water and derived thermodynamic sounding data. *Wea. Forecasting*, **13**, 277-285.

Gatlin, P. N., W. A. Petersen, L. D. Carey, and S. R. Jacks: The NEXRAD rainfall estimation processing system: A radar tool to improve rainfall estimation across the Tennessee River Valley. *34th Conference on Radar Meteorology*, Williamsburg, VA, 5-9 October 2009.

Greene, D.R. and R. A. Clark, 1972: Vertically integrated liquid water-a new analysis tool. *Mon. Wea. Rev.*, **100**, 548-552.

Gorgucci, E., G. Scarschilli, and V. Chandrasekar, 1994: A robust estimator of rainfall rate using differential reflectivity. *J. Atmos. Oceanic Technol.*, **11**, 586-592.

Gorgucci, E., G. Scarschilli, and V. Chandrasekar, 1996: Error structure of radar rainfall measurements at C-band frequencies with dual-polarization algorithm for attenuation correction. *J. Geophys. Res.*, **101**, 461-471.

Gorgucci, E., G. Scarschilli, and V. Chandrasekar, 1999: A procedure to calibrate multiparameter weather radar using properties of the rain medium. *IEEE Trans. Remote Sens.*, **37**, 269-276.

Gorgucci, E., G. Scarschilli, and V. Chandrasekar, 2000: Practical aspects of radar rainfall estimation using specific differential propagation phase. *J. Appl. Meteor.*, **39**, 945-955.

Herzegh, P. H. and A. R. Jameson, 1992: Observing precipitation through dual-polarization radar measurements. *Bull. Amer. Meteor. Soc.*, **73**, 1365-1374.

Hildebrand, P. H., 1978: Iterative correction for attenuation of 5 cm radar in rain. *J. Appl. Meteor.*, **17**, 508-514.

Hillaker, H. J. and P. J. Waite, 1985: Crop-hail damage in the Midwest corn belt. *J. Climate Appl. Meteor.*, **24**, 3-15.

Hitschfeld, W. and J. Bordan, 1954: Errors inherent in the radar measurement of rainfall at attenuating wavelengths. *J. Meteor.*, **11**, 58-67.

Höller, H., V. N. Bringi, J. Hubbert, M. Hagen, and P. F. Meischner, 1994: Life cycle and precipitation formation in a hybrid-type hailstorm revealed by polarimetric and Doppler radar measurements. *J. Atmos. Sci.*, **51**, 2500-2522.

Hubbert, J., V. Chadrasekar, V. N. Bringi, and P. Meischner, 1993: Processing and interpreting of cohert dual-polarized radar measurements. *J. Atmos. Oceanic Technol.*, **10**, 155-164.

Hubbert, J. and V. N. Bringi, 1995: An iterative filtering technique for the analysis of copular differential phase and dual-frequency radar measurements. *J. Atmos. Oceanic Technol.*, **12**, 643-648.

Hubbert, J., V. N. Bringi, L. D. Carey, and S. Bolen, 1998: CSU-CHILL polarimetric radar measurements from a severe hail storm in eastern Colorado. *J. Atmos. Sci.*, 749-775.

Jameson, J. R., 1983: Microphysical interpretation of multi-parameter radar measurements in rain. Part II: Estimations of raindrop size distribution parameters by combined dual-wavelength and polarization measurements. *J. Atmos. Sci.*, **40**, 1803-1813.

Keenan, T. D., L. D. Carey, D. S. Zrnic, and P. T. May, 2000: Sensitivity of 5-cm wavelength   polarimetric radar variables to raindrop axial ratio and drop size distribution. *J. Appl. Meteor.*, **40**, 526-545.

Keenan, T. D., 2003: Hydrometeor classification with a C-Band polarimetric radar. *Aust. Meteor. Mag.*, **52**, 23-31.

Kennedy, P. C., S. A. Rutledge, W. A. Petersen, and V. N. Bringi, 2001: Polarimetric radar observations of hail. *J. Appl. Meteor.*, **40**, 1347-1366.

Knight, C. A. and N. C. Knight, 1970: The falling behavior of hailstones. *J. Atmos. Sci.*, **27**, 672-680.

Knight, N. C., 1986: Hailstone shape factor and its relation to radar interpretation of hail. *J. Climate Appl. Meteor.*, **25**, 1956-1958.

Kumjian, M. R. and A. V. Ryzhkov, 2008: Polarimetric signatures in supercell thunderstorms. *J. Appl. Meteor. Clim.*, **47**, 1940-1961.

List, R., U. W. Rentsch, A. C. Byram, and E. P. Lozowski, 1973: On the aerodynamics of spheroidal hailstone models. *J. Atmos. Sci.*, **30**, 653-661.

Liu, H. and V. Chandrasekar, 2000: Classification of hydrometeors based on polarimetric radar measurements: Development of fuzzy logic and neuro-fuzzy systems, and in-situ verification. *J. Atmos. Oceanic Technol.*, **17**, 140-164.

Mather, G. K., D. Treddenick, and R. Parson, 1976: An observed relationship between the height of 45-dBZ contours in storm profile and surface hail reports. *J. Appl. Meteor.*, **15**, 1336-1340.

Matson, R. J. and A. W. Huggins, 1980: The direct measurement of sizes, shapes, and kinematics of falling hailstones. *J. Atmos. Sci.*, **37**, 1107-1125.

Meischner P. F., V. N. Bringi, D. Heimann, and H. Höller, 1991: A squall line in southern Germany: Kinematics and precipitation formation as deduced by advanced polarimetric and Doppler radar measurements. *Mon. Wea. Rev.*, 678-701.

Oguchi, T., 1983: Electromagnetic wave propagation and scattering in rain and other hydrometeors. *IEEE Proc.*, **71**, 1029-1078.

Petersen, W. A., and Coauthors, 1999: Mesoscale and radar observations of the Fort Collins flash flood of 28 July 1997. *Bull. Amer. Meteor. Soc.*, **80**, 191-216.

Petersen, W. A., K. R. Knupp, D. J. Cecil, and J. R. Mecikalski, 2007: The University of Alabama Huntsville THOR Center instrumentation: Research and operational collaboration. 33rd International Conference on Radar Meteorology, American Meteorological Society, Cairns, Australia, August 6-10, 2007.

Rasmussen, R. M., V. Levizzani, and H. R. Pruppacher, 1984: A wind tunnel and theoretical study on the melting behavior of atmospheric ice particles. III: Experiment and theory for spherical ice particles of radius > 500 μm. *J. Atmos. Sci.*, **41**, 381-388.

Rasmussen, R. M. and A. J. Heymsfield, 1987a: Melting and shedding of graupel and hail. Part I: Model physics. *J. Atmos. Sci.*, **44**, 2754-2763.

Rasmussen, R. M. and A. J. Heymsfield, 1987b: Melting and shedding of graupel and hail. Part II: Sensitivity study. *J. Atmos. Sci.*, **44**, 2764-2782.

Ray, P. S., 1972: Broad-band complex refractive indices of ice and water. *Appl. Opt.*, **11**, 1836-1844.

Rinehart, R. E. and J. D. Tuttle, 1982: Antenna beam patterns and dual-wavelength processing. *J. Appl. Meteor.*, **21**, 1865-1880.

Rinehart, R. E., 2004: Radar for Meteorologists 4th Edition. Rinehart Publications, Columbia, MO.

Ryzhkov, A. V. and D. S. Zrnic, 1995: Comparisons of dual-polarization radar estimators of rain. *J. Atmos. Oceanic Technol.*, **12**, 249-256.

Ryzhkov, A. V. and D. S. Zrnic, 1998: Discriminating between rain and snow with a polarimetric radar. *J. Appl. Meteor.*, **37**, 1228-1240.

Ryzhkov, A. V., S. E. Giangrande, V. M. Melnikov, and T. J. Schuur, 2005: Calibration issues of dual polarization radar measurements. *J. Atmos. Oceanic Technol.*, **22**, 1138-1155.

Ryzhkov, A. V., D. S. Zrnic, P. Zhang J. Krause, H. S. Park, D. Hudak. J. Young, J. L. Alford, M. Knight, and J. W. Conway: Comparison of polarimetric algorithms for hydrometeor classification at S and C bands, *33rd Conference on Radar Meteorology*, Caims, Queensland, 5-10 August 2007.

Ryzhkov, A. V.: Polarimetric characteristics of melting hail at S and C bands. *34th Conference on Radar Meteorology*, Williamsburg, VA, 5-9 October 2009.

Seliga, T. A. and V. N. Bringi, 1976: Potential use of radar differential reflectivity measurements at orthogonal polarizations for measuring precipitation. *J. Appl. Meteor.*, **15**, 69-76.

Seliga, T. A., K. Aydin, and H. Direskeneli, 1986: Disdrometer measurements during an intense rainfall event in central Illinois: Implications for differential radar reflectivity radar observations. *J. Climate Appl. Meteor.*, **25**, 835-846.

Smyth, T. J., T. M. Blackman, and A. J. Illingworth, 1999: Observations of oblate hail using dual polarization radar and implications for hail-detection schemes. *Quart. J. Roy. Meteor. Soc.*, **125**, 993-1016.

Straka, J. M. and D. S. Zrnic: An algorithm to deduce hydrometeor types and contents from multiparameter radar data. *26th Int. Conf. on Radar Meteorology*, Norman, OK, Amer. Meteor. Soc., 513-516.

Straka, J. M., D. S. Zrnic, and A. V. Ryzhkov, 2000: Bulk hydrometeor classification and quantification using polarimetric radar data: Synthesis of relations. *J. Appl. Meteor.*, **39**, 1341-1372.

Tabary, P., G. Vulpiani, J. J. Gourley, A. J. Illingworth, R.J. Thompson, and O. Bousquet, 2010: Unusually high differential attenuation at C-Band: Results from a two-year analysis of the French Trappes polarimetric radar data. *J. Appl. Meteor. Clim.*, **48**, 2037-2053.

Testud, J., E. L. Bouar, E. Obligis, and M. Ali-Mehenni, 2000: The rain profiling algorithm applied to polarimetric weather radar. *J. Atmos. Oceanic Technol.*, **17**, 322-356.

Thwaites, S., J. N. Carras, and W. C. McKlin, 1977: The aerodynamics of oblate hailstones. *Quart. J. Roy. Meteor. Soc.*, **103**, 803-808.

Trapp, R. J., D. M. Wheatly, N. T. Atkins, and R. W. Przybylinkski, 2005: Buyer beware: Some words of caution on the use of severe wind reports in postevent assessment and research. *Wea. and Forecasting*, **21**, 408-415.

Ulbrich, C. W., 1983: Natural variations in the analytical form of the raindrop size distribution. *J. Climate Appl. Meteor.*, **22**, 1764-1775.

Vivekanandan, J., V. N. Bringi, and R. Raghavan, 1990: Multiparameter radar modeling and observations of melting ice. *J. Atmos. Sci.*, **47**, 549-564.

Vivekanandan, J., W. M. Adams, and V. N. Bringi, 1991: Rigorous approach to polarimetric radar modeling of hydrometeor orientation distributions. *J. Appl. Meteor.*, **30**, 1053-1063.

Vivekanandan, J, S. M. Ellis, R. Oye, D. S. Zrnic, A. V. Ryzhkov, and J. Straka, 1999: Cloud microphysics retrieval using S-Band dual-polarization radar measurements. *Bull. Amer. Meteor. Soc.*, **80**, 381-388.

Wakimoto, R. M. and V. N. Bringi, 1988: Dual-polarization observations of microburst associated with intense convection: The 20 July storm during the MIST project. *Mon. Wea. Rev.*, **116**, 1521-1539.

Waterman, P. C., 1971: Symmetry, unitarity, and geometry in electromagnetic scattering. *Phys. Rev D*, **3**, 825-839.

Witt, A, M. D. Eilts, G. J. Stumpf, J. T. Johnson, E. D. Mitchell, and K. W. Thomas, 1998: An enhanced hail detection algorithm for the WSR-88D. *Wea. Forecasting*, **13**, 286-303.

Yuter, S. A. and R. A. Houze, 1995: Three-dimensional kinematics and microphysical evolution of Florida cumulonimbus. Part II: Frequency distribution of vertical velocity , reflectivity, and differential reflectivity. *Mon. Wea. Rev.*, **123**, 1941-1963.

Zeng, Z., S. E. Yuter, and R. A. Houze, Jr., 2001: Microphysics of the rapid development of heavy convective precipitation. *Mon. Wea. Rev.*, **129**, 1882-1904.

Ziegler, C. L., P. S. Ray, and N. C. Knight, 1983: Hail growth in an Oklahoma multicell storm. *J. Atmos. Sci.*, **40**, 1768-1791

Zrnic, D. S., V. N. Bringi, N. Balakrishnan, K. Aydin, V. Chandrasekar, and J. Hubbert, 1993: Polarimetric measurements in a severe hailstorm. *Mon. Wea. Rev.*, **121**, 2223-2238.

Zrnic, D. S. and A. V. Ryzhkov, 1996: Advantage of rain measurements using specific differential phase. *J. Atmos. Oceanic Technol.*, **13**, 454-464.

Zrnic, D. S., T. D. Keenan, L. D. Carey, and P. May, 2000: Sensitivity analysis of polarimetric variables at a 5-cm wavelength radar in rain. *J. Appl. Meteor.*, **39**, 1514-1526.